

Using Walls to Navigate the Room: Egocentric Representations of Borders for Spatial Navigation

Dissertation
zur Erlangung des Doktorgrades
der Naturwissenschaften

vorgelegt beim Fachbereich Biowissenschaften
der Johann Wolfgang Goethe -Universität
in Frankfurt am Main

von
Joeri van Wijngaarden
aus Rotterdam, Niederlande

Frankfurt (2021)

(D 30)

vom Fachbereich Biowissenschaften der
Johann Wolfgang Goethe - Universität als Dissertation angenommen.

Dekan: Prof. Dr. Sven Klimpel

Gutachter: Prof. Dr. Manfred Kössl

Dr. Hiroshi Ito

Datum der Disputation: 12 / 05 / 2022

The work presented in *Chapters II - VI* of this dissertation was published in the journal *eLife* under the following citation:

van Wijngaarden, J. B. G., Babl, S. S., & Ito, H. T. (2020). Entorhinal-retrosplenial circuits for allocentric-egocentric transformation of boundary coding. *Elife*, 9, e59816. DOI: 10.7554/eLife.59816

ACKNOWLEDGEMENTS

First and foremost, I would like to express my gratitude and appreciation for the support of my direct supervisor, Dr. Hiroshi Ito. Coming fresh from a computational group into his new laboratory, Hiroshi has taught me everything required to successfully participate in experimental neuroscience. From the first handling of a rat in a research setting, to the twisting of tetrode wires and building of drives, to performing delicate neurosurgeries for the implantation of electrodes into specific areas in the brain. He has always stimulated my personal development as a scientist, pushing towards excellence for the sake of new discovery, while staying critical both of our own work and that of others around us. He has been a tremendous support that made this research possible, and I will be forever grateful for his teaching and guidance.

Secondly, I would like to thank all my fellow colleagues of the Ito lab that have joined over the years. This includes Zahra, Hye-A, Alessa, Raunak, Salma, Ana, Nori, Tobias, Jisoo, Robert, and Marjan, in no particular order. It has been a pleasure to start in a new research group, and be part of its growth and development through the many contributions of each individual member. The critical discussions in our weekly meetings have helped shape our projects into the success stories that we have today, of which I'm sure many more will follow in the future.

Another critical pillar of support has come from the auxiliary facilities provided at the Max Planck Institute for Brain Research. Most notably, this includes the animal facilities with animal caretakers and veterinarians who have, day-in day-out, taken the burden of all animal care

out of our hands and onto their shoulders. Their essential work and efforts are what makes our science possible. My gratitude also extends to the mechanical workshop, in particular Fabian Bayer for the design and construction of all experimental mazes, as well as the scientific computing and IT department for setting up and maintaining all computational and digital infrastructure on which this research was built.

Further special mentions go out to Dr. Keisuke Yonehara and Dr. Martin Vinck, both members of my Thesis Advisory Committee. Their advice and suggestions have played an important role throughout the years to steer my project in the right direction and guide my overall project planning. I am especially thankful to Martin for the many offline discussions of my research and his suggestions of methodology to tackle critical issues. This was all facilitated by the current and previous coordinator of our IMPRS graduate program, Dr. Arjan Vink and Dr. Irina Epstein, who welcomed me into the Institute and created a stimulating environment by organizing the educational content and hosting invited speakers around our research.

Finally, I would like to thank my friends and family for their warm support throughout my time in Germany. Especially my parents, Frank and Adri, who always encouraged me from back home as I moved across borders. My partner Sara for her cheering and patience as I tumbled along my path, and my close friends who live in different countries but stayed with me and gave the support I needed along the way.

Table of Contents

ACKNOWLEDGEMENTS.....	i
ABSTRACT.....	1
ZUSAMMENFASSUNG.....	5
<i>Chapter I</i>	
An introduction to spatial navigation	13
The context of spatial navigation behaviour.....	15
Neural correlates of spatial navigation.....	19
The architecture and role of the Retrosplenial Cortex.....	21
Aim of the thesis.....	26
<i>Chapter II</i>	
A new class of border cells in the Retrosplenial Cortex	29
INTRODUCTION.....	31
RESULTS.....	33
RSC cells fire near the maze perimeter at specific distances.....	33
Border cells form new firing fields nearby added walls but not objects	40
Border cells retain their tuning in darkness and are not driven directly by whisker sensation	46
DISCUSSION	52
<i>Chapter III</i>	
Egocentric direction tuning of border cells.....	55
INTRODUCTION.....	57
RESULTS.....	59
RSC border cells show egocentric direction tuning properties independent of the global HD signal.....	59
Egocentric directional tuning in RSC is biased to the contralateral side of the recorded hemisphere	64
DISCUSSION	68

Chapter IV

Circuit dynamics and manipulations with the medial Entorhinal Cortex..... 71

 INTRODUCTION.....73

 RESULTS.....76

 Inhibition of MEC input disrupts border coding in RSC but not vice versa76

 RSC border coding is more local and correlated with the animal’s future motion..... 88

 DISCUSSION 94

Chapter V

Conclusions & future perspectives.....97

 CONCLUSIONS..... 99

Chapter VI

Methods & Analyses..... 105

 Subjects.....107

 Surgery, virus injection, and drive implantation..... 108

 Spike sorting and cell classification..... 110

 RSC border cells 111

 MEC border cells..... 111

 Head-direction cells 112

 Border rate maps..... 113

 Self-motion maps..... 114

 Decoding analysis..... 115

 Behavioural methods..... 116

 Histological procedures..... 118

 Statistical procedures 119

Chapter VII

Supplementary Information 121

 LITERATURE CITED123

 LIST OF FIGURES 131

 ABBREVIATIONS USED133

 CURRICULUM VITAE.....135

Abstract

Spatial navigation forms one of the core components of an animal's behavioural repertoire. Good navigational skills boost survival by allowing one to avoid predators, to search successfully for food in an unpredictable world, and to be able to find a mating partner. As a consequence, the brain has dedicated many of its resources to the processing of spatial information. Decades of seminal work has revealed how the brain is able to form detailed representations of one's current position, and use an internal cognitive map of the environment to traverse the local space. However, what is much less understood is how neural computations of position depend on distance information of salient external locations such as landmarks, and how these distal places are encoded in the brain.

The work in this thesis explores the role of one brain region in particular, the retrosplenial cortex (RSC), as a key area to implement distance computations in relation to distal landmarks. Previous research has shown that damage to the RSC results in losses of spatial memory and navigation ability, but its exact role in spatial cognition remains unclear. Initial electrophysiological recordings of single cells in the RSC during free exploration behaviour of the animal resulted in the discovery of a new population of neurons that robustly encode distance information towards nearby walls throughout the environment. Activity of these border cells was characterized by high firing rates near all boundaries of the arena that were available to the animal, and sensory manipulation experiments revealed that this activity persisted in the absence of direct visual or somatosensory detection of the wall.

It quickly became apparent that border cell activity was not only modulated by the distance to walls, but was contingent on the direction the animal was facing relative to the boundary. Approximately 40% of neurons displayed significant selectivity to the direction of walls, mostly in the hemifield contra-lateral to the recorded hemisphere, such that a neuron in left RSC is active whenever a wall occupies proximal space on the right side of the animal. Using a cue-rotation paradigm, experiments initially showed that this egocentric direction information was invariant to the physical rotation of the arena. Yet this rotation elicited a corresponding shift in the preferred direction of local head-direction cells, as well as a rotation in the firing fields of spatially-tuned cells in RSC. As a consequence, position and direction encoding in RSC must be bound together, rotating in unison during the environmental manipulations, as information about allocentric boundary locations is integrated with head-direction signals to form egocentric border representations.

It is known that the RSC forms many anatomical connections with other parts of the brain that encode spatial information, like the hippocampus and para-hippocampal areas. The next step was to establish the circuit mechanisms in place for RSC neurons to generate their activity in respect to the distance and direction of walls. A series of inactivation experiments revealed how RSC activity is inter-dependent with one of its communication partners, the medial entorhinal cortex (MEC). Together they form a wider functional network that encodes precise spatial information of borders, with information flowing from the MEC to RSC but not vice versa. While the conjunction between distance and heading direction relative to the outer walls was the main driver of neural activity in RSC, border cells displayed further behavioural correlates related to

movement trajectories. Spiking activity in either hemisphere tended to precede turning behaviour on a short time-scale in a way that border cells in the right RSC anticipated right-way turns ~300 ms into the future.

The interpretation of these results is that the RSC's primary role in spatial cognition is not necessarily on the early sensory processing stage as suggested by previous studies. Instead, it is involved in computations related to the generation of motion plans, using spatial information that is processed in other brain areas to plan and execute future actions. One potential function of the RSC's role in this process could be to act correctly in relation to the nearby perimeter, such that border cells in one hemisphere are involved in the encoding of walls in the contralateral hemifield, after which the animal makes an ipsilateral turn to avoid collision. Together this supports the idea that the MEC→RSC pathway links the encoding of space and position in the hippocampal system with the brain's motor action systems, allowing animals to use walls as prominent landmarks to navigate the room.

Zusammenfassung

Räumliche Navigation repräsentiert eine essentielle Komponente des tierischen Verhaltensrepertoires. Ausgeprägtes Orientierungsvermögen erhöht die Überlebensfähigkeit, indem sie ein Tier dazu befähigt, Fressfeinde zu vermeiden, erfolgreiche Nahrungssuche in einer dynamischen Umwelt ermöglicht und die Paarung mit Artgenossen erleichtert. Konsequenterweise verwenden Gehirne einen substantiellen Teil ihrer Ressourcen auf die Prozessierung räumlicher Informationen. Jahrzehntelange Grundlagenforschung hat zu einem zunehmend detaillierterem Verständnis geführt, wie das Gehirn die eigene Position in der Welt repräsentiert und interne kognitive Karten zur Navigation verwendet. Immer noch weitgehend ungeklärt ist hingegen, wie die neuronale Berechnung örtlicher Positionen von der Entfernung relevanter externer Positionen wie Orientierungspunkten abhängt, und welche Entsprechung solche weiter entfernten Orte auf neuronaler Ebene haben.

Die hier vorgestellte Arbeit exploriert im Speziellen die Rolle des retrosplenialen Cortex (RSC) als Schlüsselareal für distanzbasierte Berechnung in Relation zu distalen Orientierungshilfen. Bisherige Erkenntnisse weisen darauf hin, dass Läsionen des RSC zu einem Verlust von räumlichem Gedächtnis und Navigationsfähigkeit führen. So zeigen menschliche Patienten mit RSC-Läsionen verschiedenartige Störungen des Gedächtnisses bis zur Amnesie und leiden teilweise unter topographischer Orientierungslosigkeit, d.h. dem Verlust der Fähigkeit, sich in bekannten Umgebungen zurechtzufinden sowie wohlbekannte Orientierungshilfen zu verwenden um zu einem Ziel zu navigieren. Erstaunlicherweise sind solche Patienten weiterhin in der Lage bekannte Orientierungshilfen in ihrer

Nachbarschaft, wie etwa Ihnen bekannte Restaurants oder Bushaltestellen, zu erkennen, sie scheitern jedoch daran, diese als räumliche Information zu verwenden, um ihren Weg zu finden. Trotz dieser deutlichen Hinweise auf die Wichtigkeit des RSC bleibt dessen genaue Rolle für räumliche kognitive Fähigkeiten jedoch weiterhin unklar.

EINE NEUE KLASSE VON *BORDER CELLS* IM RETROSPLENIALEN KORTEX

Um herauszufinden, wie Zellen im RSC räumliche Informationen prozessieren, führte ich eine Reihe von elektrophysiologischen Messungen durch, in denen Ratten eine offene Arena mit verschiedenen hervorstechenden Orientierungshilfen frei explorieren konnten, während gleichzeitig die Aktivität dutzender RSC Neurone mithilfe von *high-density tetrode microdrives* gemessen wurde. Initiale Einzelzellmessungen führten zur Entdeckung einer bisher nicht charakterisierten Population von Neuronen, die Distanzinformation in Relation zu nahegelegenen Wänden der Arena robust kodierten. Die Aktivität dieser *border cells* war charakterisiert durch hohe Frequenzen von Aktionspotentialen in Wandnähe, was Veränderungen der Arenawände von quadratischer zu kreisförmiger, dreieckiger und hexagonaler Geometrie nicht verändert wurde. Weiterhin resultierte das Hinzufügen einer neuen, zentral positionierten Wand in zusätzlichen rezeptiven Feldern auf beiden Seiten der neuen Wand, was nicht beobachtet wurde wenn ein zusätzliches Objekt zentral in der Arena platziert wurde. Dies deutete darauf hin, dass die beschriebene Zellaktivität spezifisch für Grenzwände ist, die die Bewegung des Tieres einschränken.

Ein möglicher Mechanismus, der die Aktivität von *border cells* in Relation zu Wänden erklären könnte, basiert auf direkter sensorischer Wahrnehmung; visuell für distale Wände und somatosensorisch, d.h. Schnurrhaar-basiert für proximale Wände. Jedoch dauerte die zuvor beschriebene *border cell* Aktivität während Messungen in kompletter Dunkelheit und in Abwesenheit direkter somatosensorischer Perzeption weiter an. Aufgrunddessen konnten lokale sensorische cues als direkte Triebfeder hinter der RSC *border cell* Aktivität ausgeschlossen werden. Stattdessen schien ein Mechanismus am wahrscheinlichsten, der eine interne Repräsentation der globalen räumlichen Geometrie einer Umgebung nutzt.

EGOZENTRISCHE RICHTUNGSKODIERUNG DURCH *BORDER CELLS*

Neuronen, die räumliche Informationen verarbeiten, müssen bestimmte Referenzpunkte in ihrer Aktivität miteinbeziehen. Für viele der in bisherigen Studien identifizierten funktionalen Zelltypen, wie derjenigen im Hippocampus, dient die äußere Umgebung diesem Zweck. Beispielsweise wird eine *place cell* in der CA1-Region des Hippocampus dann aktiviert, wenn eine Ratte sich an einem bestimmten Ort befindet, unabhängig von der Orientierung des Tieres oder seiner bisherigen Trajektorie. In Bezug auf die *border cells* des RSC wurde es rasch ersichtlich, dass ihre Aktivität nicht unabhängig war vom Blickfeld des Tieres. Tatsächlich war die Aktionspotentialfrequenz von Zellen bestimmt durch eine Kombination der Distanz des Tieres zu den Wänden und der Richtung des Tieres in Relation zum jeweiligen Hindernis.

Circa 40% der Neuronen waren zu einem signifikanten Ausmaß selektiv für die Ausrichtung der Wände, vor allem derjenigen, die sich kontralateral zur Hirnhälfte befanden, von der aufgenommen wurde, sodass ein Neuron im linken RSC aktiv wird sobald sich eine Wand in nächster Nähe zur rechten Seite des Tieres befindet. Es ist bekannt, dass das Hirn ein internes Richtungssignal aufrechterhält, das dem Tier Orientierung ermöglicht. Dies erfolgt durch die Aktivität von *head-direction cells*. Dabei handelt es sich um Neuronen, die verstärkt feuern when sich der Körper des Tieres in einer bestimmten Richtung orientiert (z. B. gen Osten oder Westen etc.). Solche *head-direction cells* sind auch in einem Teil des RSC zu finden, was zu der Frage führte, in welchem Ausmaß Richtungsinformation dieser spezifischen Domäne die egozentrische Richtungsselektivität der *border cells* des RSC beeinflusst.

Um diese Frage zu beantworten, wurden Experimente auf Basis eines *cue-rotation* Prinzips durchgeführt, die anfangs zeigten, dass die *border cells* des RSC unabhängig von einem globalen, internen Richtungssinn operieren. Die physikalische Drehung der Arena induzierte eine damit einhergehende Veränderung in der bevorzugten Richtung lediglich für *head-direction cells*, während *border cells* ihr ursprüngliches Aktivitätsverhalten beibehielten. Jedoch zeigte sich auf einer zweiten Ebene der Analyse, dass die Rotation der Arena auch zu einer Rotation der Aktivitätsmuster von ortskodierenden Zellen im RSC führte. Daraus folgt, dass Position und Richtung im RSC zusammen kodiert werden und auch ihre Kodierung sich gemeinsam durch Manipulation der Umgebung verändert, indem Informationen über allozentrische Hindernisinformationen mit Richtungsinformation des Tieres integriert wird, um Hindernisse egozentrisch zu repräsentieren.

Mehrere neuere Studien machten plausible, dass solche egozentrischen Repräsentationen im Hirn durch egozentrische sensorische Erfahrung aufgebaut werden, wie zum Beispiel durch visuelle Informationen, die über die Retina übertragen werden, taktile Informationen über die Haut oder propriozeptive Wahrnehmung über Skelettmuskeln. Die Ergebnisse des vorstehenden Absatzes jedoch demonstrieren, dass *border cell* Aktivität auch in Dunkelheit existiert und auch in Abwesenheit tatsächlicher Wände. Dies führt zu der Frage welche Netzwerkmechanismen dafür verantwortlich sind, dass RSC Neuronen in Abhängigkeit von der Distanz und der Ausrichtung von Wänden aktiv werden.

NETWERKDYNAMIK UND MANIPULATIONEN DES ENTORHINALEN KORTEX

Es ist bekannt, dass der RSC über viele anatomische Verbindungen mit anderen Hirnarealen verfügt, die wiederum räumliche Informationen kodieren, wie dem Hippocampus und dem parahippocampalen Komplexes. Diese Vielzahl an Verbindungen hat zu verschiedenen Theorien darüber geführt, was die Rolle des RSC in einer weiter gefassten hierarchischen Struktur des Hirns sein könnte. Damit einhergehend ist es nun mit der Entdeckung der neuartigen *border cells* des RSC weiterhin unbekannt, welche Hirnregionen notwendig sind, um die Informationen bereitzustellen, die den RSC dazu befähigen, Grenzen zu erkennen oder welche Hirnareale ihrerseits Informationen vom RSC beziehen.

Um die Rolle unterschiedlicher Arten von räumlichen Zellen im Hirn zu analysieren und zu erkennen, inwieweit diese Zellen miteinander kommunizieren, fokussiert sich der letzte Teil dieser Dissertation auf das

Zusammenspiel zwischen *border cells* im RSC und seinem hauptsächlichen Kommunikationspartner, dem medialen entorhinalen Kortex (MEC). Ihre Interaktion wurde mittels zweier Techniken untersucht, die über die letzten zehn Jahre entwickelt wurden, Optogenetik und Pharmakogenetik. Bei beiden handelt es sich um gezielte, nicht-invasive Techniken zur Manipulation von neuronalen Schaltkreisen, die es ermöglichen, einzelnen Zellen im bestimmten Hirnarealen zu aktivieren oder zu inhibieren. Dies ist auch in nicht narkotisierten Tieren während normalem Verhalten möglich. Pharmakogenetische Inaktivierung des MEC führte zu einer Störung im Aktivitätsmuster von *border cells* des RSC, was die Annahme unterstützt, dass Informationen aus dem MEC für die akkurate Grenzrepräsentation im RSC notwendig sind. Dabei handelt es sich um einen unidirektionalen Informationsfluss, da Aktivitätsinhibierung des RSC keinen direkten Einfluss auf die neuronale Aktivität des MEC hatte. Optogenetische Inaktivierungsexperimente zeigten weiterhin, dass diese Störung verursacht wird durch die direkte Verbindung zwischen MEC und RSC und nicht durch eine dritte, vermittelnde Hirnregion.

Diese Reihe von Inaktivierungsexperimenten verdeutlichte die Interdependenz von RSC Aktivität und MEC. Zusammen formen sie ein funktionelles Netzwerk, das präzise räumliche Informationen begrenzender Elemente bereitstellt, wobei Informationen aus dem MEC zum RSC fließen, aber nicht umgekehrt. Obgleich die Verbindung zwischen Distanz und Bewegungsrichtung in Relation zu den begrenzenden Wänden den Haupttreiber der Aktivität von *border cells* des RSC darstellt, waren weitere Verhaltenskorrelate, die abhängig von der Bewegungstrajektorie des Tieres sind, charakteristisch für *border cells*. Eine Analyse, basierend auf Metriken der Informationstheorie, zeigte, wie Grenzinformationen

unterschiedlich in RSC und MEC repräsentiert ist und inwieweit diese Information direkten Bezug auf das Verhalten des Tieres hat. Neuronale Aktivität in beiden Hemisphären ging Wendeverhalten auf einer kurzen Zeitskala voraus, sodass *border cells* des RSC Wendungen zur rechten Seite ca. 300 ms voraussagen konnten. Diese antizipatorische Aktivität wurde im MEC nicht beobachtet, was demonstriert, dass beide Regionen unterschiedliche Aspekte von Grenzrepräsentationen kodieren, wobei der räumliche Input des MEC im RSC dazu benutzt wird, die nächsten Aktionen des Tieres zu ermöglichen.

ZUSAMMENFASSUNG & AUSBLICK

Diese Ergebnisse sind so zu interpretieren, dass die primäre Rolle des RSC im Rahmen räumlicher Kognition nicht notwendigerweise eine frühe Prozessierung sensorischer Informationen ist, sowie es bisherige Studien nahelegten. Stattdessen ist er involviert in neuronale Berechnungen im Kontext der Bewegungsplanung. Hierzu nutzt er räumliche Informationen aus anderen Hirnarealen, um zukünftige Aktionen zu planen und umzusetzen. Eine mögliche Funktion des RSC in diesem Prozess könnte es sein, korrektes Verhalten in Bezug auf nahegelegene Eingrenzungen sicherzustellen, sodass *border cells* in einer Hemisphäre zur Repräsentation von Wänden im kontralateralen Hemifeld beitragen. Das führt zu einem ipsilateralen Wendeverhalten des Tieres, um eine Kollision zu vermeiden. Insgesamt unterstützt dies das Konzept, dass die Bahn zwischen MEC→RSC Ortsinformationen und Position im hippocampalen System mit dem motorischen System des Hirns verbindet und es so dem Tier ermöglicht, Begrenzungen sowie auch prominente Orientierungspunkte in seiner Navigation zu integrieren.

Chapter I

An introduction to spatial navigation

THE CONTEXT OF SPATIAL NAVIGATION BEHAVIOUR

Navigation behaviour is critical for survival in nearly all animal species. It encompasses the search for food, either prey or vegetation, the avoidance of predators, and perhaps most importantly, the finding of a mating partner. As such, different species across the animal kingdom have developed a wide range of strategies to navigate their environment and adapted to their unique circumstances. In accordance with the science of evolution, proposed by Charles Darwin under the notion that properties which favour survival will propagate through a lineage, it is the individual most apt at avoiding being eaten that will tip the scale of survival in his favour (Darwin, 1859).

Optimal adaptation can be particularly found in extreme environments, where most others would not survive. One such example is the *Psychrolutes Microporosus*, a species of fish that was discovered on deep-sea expeditions, and lives at depths below 600 meters off the coast of Australia (**Figure 1**). They grow up to 30 cm in length, but have to cope with an extreme 100-fold increase of external pressure, and do so by having only soft body tissue with little to no muscle tone. As a result, they demonstrate perhaps one of the simplest forms of navigation, that is, they float passively in the dark waters without expending energy, and find both food and a mating partner by coincidence.

By contrast, most other vertebrates – those that live in shallow water, on land or in the air – take an active role in their environment. In its most basic form, this active exploration entails movement to a food source that is sensed directly. For example, one widely used animal model in biology and neuroscience is the *Caenorhabditis elegans*, a nematode roughly 1 mm in

length with a known genome (Eguen et al., 1998) and a nervous system that has been mapped completely (*e.g.*, a documented connectome) (White et al., 1986) (**Figure 1**). It has been studied primarily in the context of genetics and biological signalling pathways, but individual worms display a rich behavioural repertoire that includes locomotion and food-seeking behaviour. They combine environmental sensing with their previously learned experience that manifests as chemotaxis – movement towards a chemical stimulus – and dietary choices, where worms learn to hunt for high quality food (Shtonda and Avery, 2006).

While experience can shape and improve the effectiveness of food search in the nearby environment, advanced navigation strategies rely on more than current sensory information, and instead incorporate memories of important locations to guide behaviour. In other words, familiarity and an understanding of the surrounding context can provide an additional layer of information to support the decision-making process of where to go and at which time. To illustrate its value, we can look at several types of bird species and mammals that perform food caching, the act of moving food from one location to another to store for eating at a later time.

Many food sources do not provide a constant supply, but rather occur infrequently in concentrated stocks (*i.e.*, many nuts in a single tree) and often fluctuate between times of abundance and deficiency over the course of hours (*i.e.*, night versus day) up to months (*i.e.*, autumn versus winter). As a consequence, hoarding a stash of food over longer periods of time and spreading it across a large area proves to be a great strategy for survival (Smith and Reichman, 1984). However, this activity introduces the **challenge of retrieval**: re-finding one of many hiding locations in a variable

world, with food that spoils over time. Examples of excellent hoarders that solved this problem include Marsh tits (*Parus palustris*), a bird that can store and retrieve seeds across dozens of different sites over the course of a day (Shettleworth and Krebs, 1982), and the European Jay (*Garrulus g. glandarius*), which has been observed to retrieve stored food caches up to 72 days after hiding (Bossema, 1979) (**Figure 1**). Their ability to accurately re-find previously visited locations does not rely on the pursuit of established sensory cues (*e.g.*, an olfactory trace), since birds often ignore any artificially placed food stashes within 1 meter distance and recover sites in a similar sequence as they stored them (Cowie et al., 1981). Instead, recovery is critically dependent on spatial memories and the recognition of important landmarks, with caches generally stored more than 1 km distance from the food source.

An animal is thus required to locate a multitude of hiding places and know its own location relative to them. This **spatial awareness** – an understanding of spatial relationships between one’s current position and the surrounding area – sits at the core of many aspects of complex navigation. One of the first experimental demonstrations of these spatial cognitive abilities came from Edward Tolman, who designed the ‘sunburst’ maze to study rodent behaviour (Tolman et al., 1946). The maze provides a starting location for the rat in a circular room, which is then tasked to follow a path with several turns to reach a reward location. After several learning trials, a test phase starts in which the original path is blocked, but many alternative options are provided. These alternatives are all straight paths, but depart at different angles along the arena’s radius, and only one points towards the original goal location. The experiment showed that from all possible corridors, many animals proceeded to choose the correct option

that would lead them directly to the goal location, despite never having walked this route. They were thus able to calculate a new optimal trajectory in space based on previous experience and an understanding of the spatial layout. Since these early experiments, many advances have been made to understand behavioural components of navigation. But quickly one of the major questions became how the brain is able support this spatial cognition.

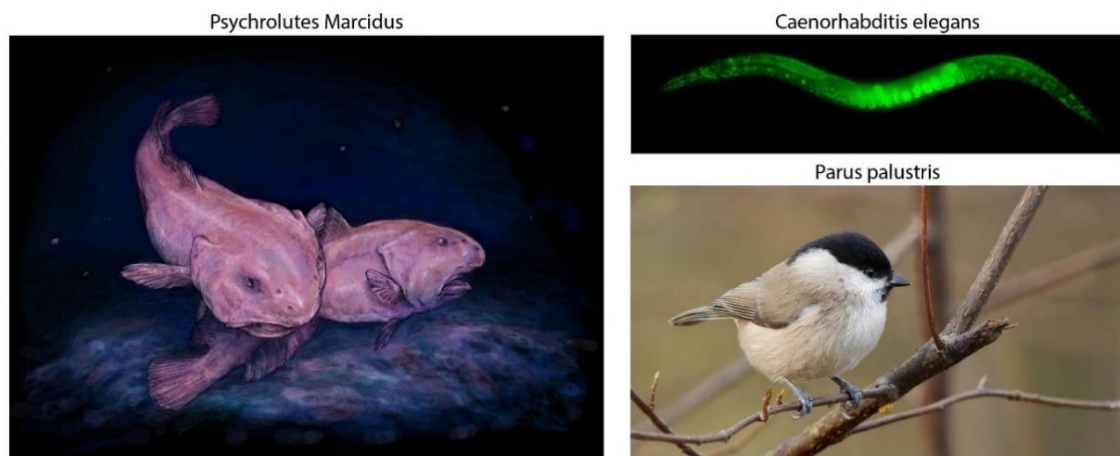


Figure 1. Depiction of animal species that are iconic for navigation behaviour in the wild. Left: Artist's impression of two deep-sea fish, *Psychrolutes Marcidus*, living 1000 m under sea level in complete darkness. Their body consists primarily of a gelatine mass to handle buoyancy under extreme pressure, and they eat whatever Crustaceans float by. Top right: *C. elegans* adult with GFP coding sequence inserted into a histone-encoding gene by Cas9-triggered homologous recombination. Worms display basic, experience-dependent food-seeking behaviour and dietary choice. Bottom right: Photo of a Marsh tit (*Parus palustris*), a bird known for their superb memory of hiding locations, storing food across many different caches spread throughout their territory.

Original sources (reproduced with permission):

- Rachel Koning, <https://commons.wikimedia.org/wiki/User:Rcaauwe>
- Dan Dickinson, https://commons.wikimedia.org/wiki/File:C._elegans.jpg
- Frank Vassen, <https://www.flickr.com/people/42244964@N03>

NEURAL CORRELATES OF SPATIAL NAVIGATION

There is a vast body of literature from the last 5 decades which uncovered the neural correlates that implement fundamental aspects of spatial coding, with a general consensus on the importance of the medial Temporal Lobe (MTL; see (Squire et al., 2004) for an extensive review). The MTL is a system of neural structures that includes the hippocampus (CA regions) and neighbouring perirhinal, entorhinal and parahippocampal cortices, and plays a central role in spatial processing (Moser et al., 2008) (**Figure 2A**).

The first description of a key functional cell type from the MTL to support spatial computations has been of the **place cell**, a neuron located in the hippocampus that is active only when the animal is in a specific place in the proximal environment, thus forming a representation of a single location, with neighbouring cells firing at different locations. (O'Keefe and Dostrovsky, 1971) (**Figure 2B**). The population activity of many place cells together can distinguish nearby positions with high precision at centimetre resolution, even in an open field away from salient objects or landmarks (Brown et al., 1998; Wilson and McNaughton, 1993), allowing animals to navigate to specific places in the environment (Morris, 1981). It has therefore been proposed that place cells in the hippocampus form the basic elements of a distributed, internal cognitive map (O'Keefe and Nadel, 1978).

A second important discovery has been of the **grid cell**, a functional cell type found in the medial Entorhinal Cortex (MEC) that forms grid-like hexagonal firing patterns throughout the available space (Hafting et al., 2005) (**Figure 2C**). Grid cells have varying properties of their firing fields, such as the spacing between fields or the pattern's orientation relative to an

external reference, giving population activity of grid cells full coverage of the arena. Their periodic firing as a function of space, independent of the running direction and speed of the animal, has been proposed to serve as an intrinsic metric for space that allows for distance-based computations (McNaughton et al., 2006).

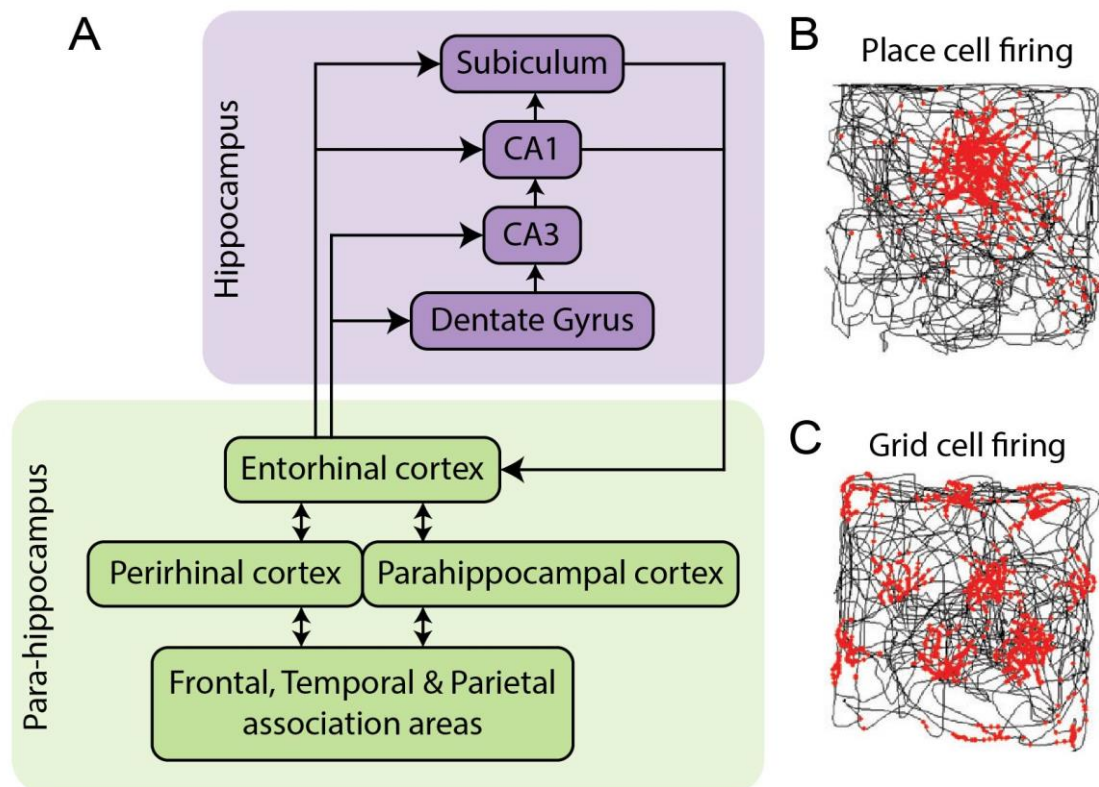


Figure 2. The medial temporal lobe is a key circuit involved in spatial cognition. (A) Functional circuit diagram of the MTL which includes the hippocampus (purple) and surrounding para-hippocampal (green) brain regions. Arrows indicate direct anatomical projections between areas. (B) Trajectory spike plot of a typical place cell, first recorded in the CA1 region of the hippocampus. Spike locations (red) are superimposed on the animal's trajectory in the recording enclosure (black). Most place cells have a single firing location. (C) Firing pattern of a grid cell, first recorded in the medial entorhinal cortex. Firing fields of a grid cell form a periodic triangular matrix tiling the entire environment available to the animal. Reproduced from (Moser et al., 2008)

The resulting accurate spatial coding of position in the brain, supported by place and grid cells, has been suggested to depend on the estimation of the distance and direction relative to landmarks, particularly walls or edges in a closed environment (Barry et al., 2006; O'Keefe and Burgess, 1996a). Grid cells for example show distortions in their firing fields near walls that are morphed (Krupic et al., 2018), while cell firing accumulates error in precision towards the arena centre which is corrected after touching walls (Hardcastle et al., 2015), indicating dependence of grid field alignment with the arena boundaries. This boundary information is encoded in two additional classes of cells, the **border cell** in the MEC and the **boundary-vector cell** in the Subiculum, both of which are active whenever the animal is in close proximity of the edge of the arena (Lever et al., 2009; Solstad et al., 2008).

However, much less is known about how the brain encodes landmarks beyond direct boundaries of an enclosed space, in particular across larger distances. Recent work by Kate Jeffery found a landmark-dominated direction signal in the Retrosplenial Cortex (RSC) of rats (Jacob et al., 2017), while an fMRI-study further implicated the RSC for landmark coding in humans (Auger et al., 2012), warranting closer examination of the RSC's relevance for landmark processing.

THE ARCHITECTURE AND ROLE OF THE RETROSPLENIAL CORTEX

Involvement of the Retrosplenial cortex in spatial memory and awareness becomes apparent when studying the impact of brain damage and its resulting loss of function, especially in humans. Naturally occurring ischaemic lesions due to stroke, and injury-induced tissue damage after accidents, are well documented in respect to neural function, and damage to the RSC in particular has been associated with specific spatial deficits (see

(Maguire, 2001) for a review). Patients with lesions to the RSC report several memory problems, including amnesia, and can suffer from **topographic disorientation**, the inability to orient yourself relative to familiar surroundings and to be incapable of using well-known landmarks to get to your destination. Surprisingly, patients are able to recognize landmarks in their neighbourhood, such as local restaurants or a bus stop, when they are directly in front of them, but are not able to use this spatial information to find their way. One such case, patient 2 in (Takahashi et al., 1997), was a 55-year old taxi driver who suffered an acute cerebral haemorrhage in the RSC while driving his car. Although he was very familiar with the city layout, when presented with a map of Kawasaki, he was perplexed when asked to point to the location of the city's principal buildings, and could not even answer whether to turn left or right to get from one place to another. Deficits like these can have dramatic impacts on daily life, as patients get lost among the many rooms in the hospital, and often end up confined to their home, being unable to move around without help.

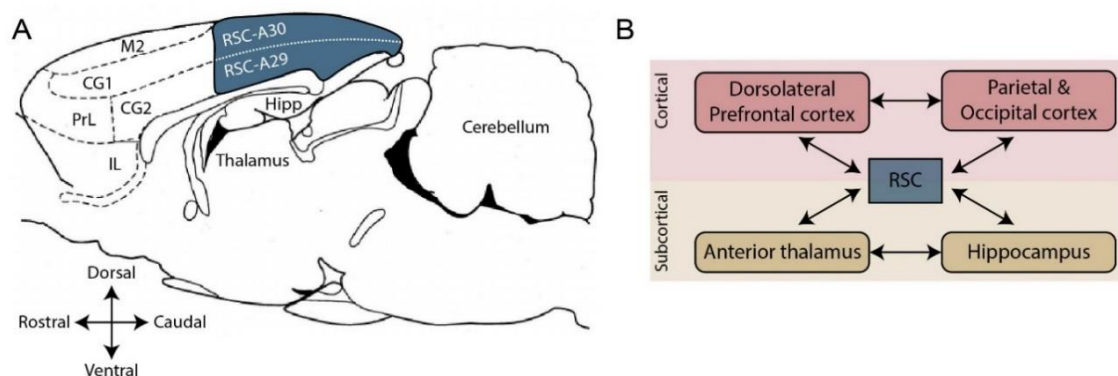


Figure 3. Anatomical location of the retrosplenial cortex.

(A) Schematic sagittal section of a rat's brain, with the retrosplenial cortex (RSC) marked in blue. The RSC can be subdivided further into a more dorsal, dysgranular part (A30) and a ventral granular region (A29). M2, motor cortex; CG, cingulate gyrus; PrL, prelimbic frontal cortex; IL, infralimbic frontal cortex; Hipp, hippocampus. (B) Functional circuit diagram showing the RSC is placed at an interface between the hippocampus / thalamus and associative and sensory cortical brain areas. Adapted from (Vann et al., 2009)

Anatomically, the RSC interfaces regions of the hippocampus and the MEC with different sensory and motor cortices (van Groen and Wyss, 1990, 1992; Van Groen and Wyss, 2003; Jones and Witter, 2007; Sugar et al., 2011) (**Figure 3**). Particularly in rats, the RSC is one of the largest cortical areas in the brain, covering more than half the length of the cerebrum and extending along the rostral-caudal axis. It comprises the posterior half of the cingulate cortex, together with the anterior cingulate cortex (ACC), and can be subdivided into two distinct regions. The medioventral side of RSC consists of a granular part with 6 clearly defined layers, referred to as area 29 in humans and primates, with further subdivisions into areas a (Rga) and b (Rgb) (van Groen and Wyss, 1990; Van Groen and Wyss, 2003). The dorsolateral part lacks a clearly defined layered structure, and is designated dysgranular area 30 (Rdg) (van Groen and Wyss, 1992). While both subregions share connectivity patterns with the (para) hippocampal regions, dysgranular area 30 is more interconnected with visual areas 17 and 18b, whereas granular areas 29a and 29b form more connections with different thalamic nuclei (Vogt and Miller, 1983).

Early single-unit electrophysiology in RSC identified a subset of ~10% of cells as **head-direction cells** (Chen et al., 1994), neurons that fire when the animal is facing a global direction, a cell type first found in the post-Subiculum (Taube et al., 1990) that subserves the animal's sense of direction (Taube, 2007). Further studies have described complex spatial modulation patterns for the remaining 90% of cells, with firing related to movement (Cho and Sharp, 2001) and position of the animal (Mao et al., 2017), or geometric shapes of the environment (Alexander and Nitz, 2015). But from these electrophysiological studies, no consistent picture has emerged as to what extent neuronal firing in RSC is related to external aspects of the

environment, nor how individual neurons convey information about these features to other brain regions.

Based on the region's connectivity, it has been suggested that one important role for the RSC could be to mediate between different types of spatial representations (Vann et al., 2009). Most functional cell types in the MTL with spatial tuning properties encode information independent of animal's viewpoint (*i.e.*, in an **allocentric reference frame**), that is, a rat can face different directions with different visual scenes in the same location, but the place or grid cell will fire indiscriminately (Hafting et al., 2005; McNaughton et al., 2006; O'Keefe and Nadel, 1978). Conversely, an animal's sensory experience is initially anchored to sensory organs mapped on the body (*i.e.*, in **egocentric coordinates**), for example, visual information on the retina, tactile sensation on the skin, or proprioceptive signals from skeletal muscles. This self-referenced sensory information, as well as an animal's navigation plans and their underlying sequence of motor actions, are processed in a viewpoint-dependent manner (Ekstrom et al., 2014; Georgopoulos, 1988).

One important computational step then becomes to transform information from one reference frame into another, such that sensory information about the environment can be used to update internal allocentric representations of space (**Figure 4**). Theoretical models have implemented this process using an RSC connectivity circuit (Bicanski and Burgess, 2018; Byrne et al., 2007; Clark et al., 2018), but direct evidence of such transformation in the brain is still missing.

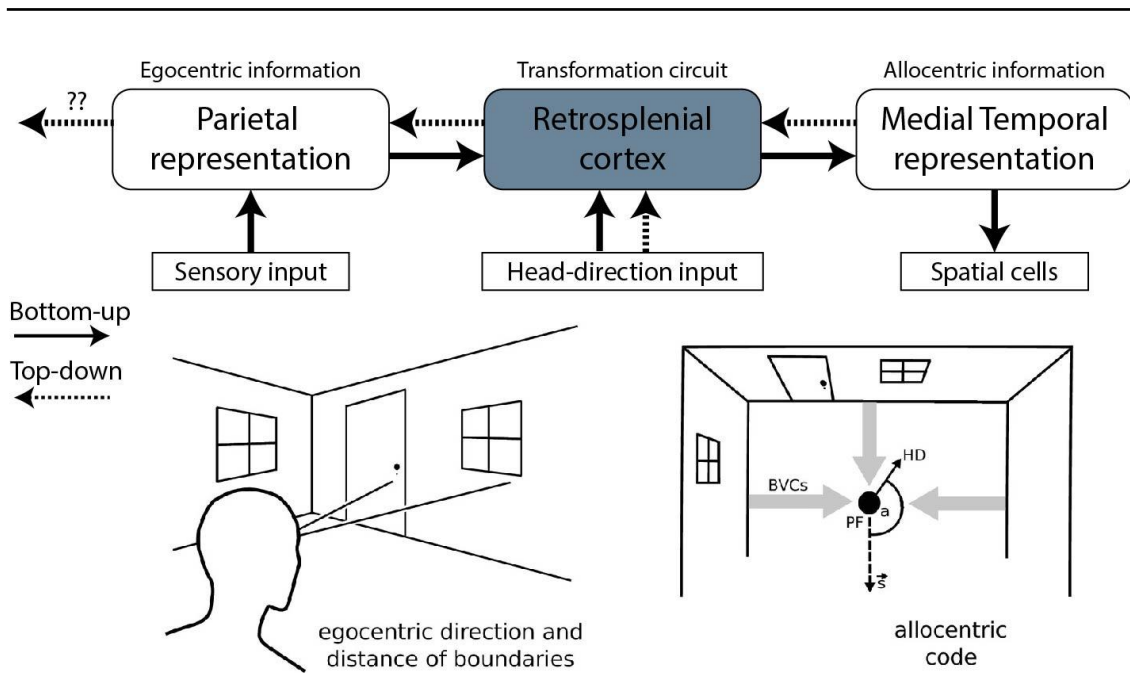


Figure 4. Schematic of a computational model that implements information transformation.

Processed sensory information reaches the parietal cortex to support an egocentric representation of the local environment. Retrosplenial cortex uses current head-direction (HD) information to perform the transformation from egocentric to allocentric coding. At a given location, the environment is then represented in allocentric coordinates through the activity of different allocentric cell types found in the MTL. A combination of boundary vector cells (BVC) and place cells with a given place field (PF) code for location in a viewpoint-independent manner. Black arrows indicate the flow of information during perception and memory encoding (bottom-up), while dotted arrows indicate the reverse flow (top-down). Adapted

AIM OF THE THESIS

Advanced spatial navigation strategies require internal spatial representations of one's own position, as well as information about the surrounding proximal and distal environment. The former has been studied extensively over the last decades, with most seminal work focused on the representation of current position in the hippocampal and parahippocampal brain regions (reviewed in Moser et al., 2008). The latter has received substantially less attention, in particular regarding the input pathways to the MTL for external contextual information such as landmarks. As a consequence, it remains unclear how distal landmarks are encoded in the brain, and how internal models of space are updated based on this distance and direction information.

It is on this premise that my dissertation attempts to make a meaningful contribution, by investigating the role of the Retrosplenial Cortex in encoding important landmark information, and its potential involvement in coordinate transformation between egocentric information in sensory regions and allocentric information processing in the MTL.

The work presented in *Chapter II* will address what are the basic firing properties of individual RSC neurons in an open field environment, by performing large-scale single-unit recordings during free exploration behaviour. It will focus on the discovery of a new type of border cell that encodes distance information throughout the environment, providing a detailed characterization of how these cells compute their information contingent on the animal's sensory experience. This is followed by an analysis of conjunctive coding properties of these cells in *Chapter III*, after finding that a subset of border cells further encode direction information of

boundaries from an egocentric perspective. Behavioural experiments show how this direction information interacts with the global head-direction signal that is present locally in the RSC. Having established firing characteristics of border cells in RSC, the following *Chapter IV* will address how the RSC communicates its spatial information with other brain areas of the MTL, in particular the medial Entorhinal Cortex, by using neural inactivation techniques such as opto- and chemogenetics. Together this provides a detailed picture of the extent and direction of communication between the RSC and MEC, helping us understand coordinate transformation of spatial information in the brain.

Chapter II

A new class of border cells in the Retrosplenial Cortex

The results and figures presented in the following chapter have been published previously in *eLife* under the following citation:

van Wijngaarden, J. B. G., Babl, S. S., & Ito, H. T. (2020). Entorhinal-retrosplenial circuits for allocentric-egocentric transformation of boundary coding. *Elife*, *9*, e59816. DOI: 10.7554/eLife.59816

INTRODUCTION

Rodents travel great distances in their natural habitat, establishing foraging paths on which they hunt and search for food. These paths often follow (natural) edges along the environment, providing safety and cover from their predators as opposed to exposure in open fields. It comes as no surprise then that in a laboratory setting, the open field arena was used for decades to induce anxious emotional states, as one of the most popular instruments to study animal psychology (Walsh and Cummins, 1976). Upon first exposure to the arena, animals display two types of behaviour that indicate their levels of anxiety and timidity, namely the amount of defecation (Hall, 1934) and thigmotaxis (Valle, 1970), also known as “wall hugging”. Rats in particular show stereotypical initial navigation behaviour, starting with freezing and reduced locomotion (often in corners), followed by careful exploration, spending up to 98 per cent of their time alongside walls (Valle, 1970). It is only after extensive habituation, coupled with scattering of food for motivation, that rats are nudged to leave the safe cover of walls.

Walls and edges thus play a prominent role in movement trajectories through space, and are one of the most behaviourally relevant features of the animal’s direct environment. Accordingly, there are dedicated representations of environmental boundaries present in the hippocampus and parahippocampal regions (Solstad et al., 2008; Stewart et al., 2014), with cells that increase their firing rate as animals traverse nearby the maze perimeter, implying a pivotal role of boundary information in generating accurate spatial representations in the brain. However, beyond their initial

phenomenological description, it remains unclear how such cells generate their border responses, to what extent they rely on direct sensory information, and how they differentiate walls from other features like distant landmarks.

Previous work proposed a complimentary role here for the Retrosplenial Cortex (Mitchell et al., 2018), as it is involved in visual processing of landmarks (Fischer et al., 2020) and receives direct input from sensory areas (Passarelli et al., 2018), while forming direct connections with many components of the (para) hippocampal brain structures (Honda and Ishizuka, 2015; Jones and Witter, 2007; Sugar et al., 2011).

The goal of this chapter then is to establish the spatial coding properties of neurons in the RSC during navigation behaviour, and explore under which environmental conditions this neural activity is generated. This characterization resulted in the discovery of a new population of neurons that robustly encode distance information towards nearby walls throughout the environment. These border cells fire consistently whenever the animal moves at specific distances from the walls, independent of arena shape or size. In order to separate them from the remaining population, I developed a novel template matching procedure using the Earth Mover's Distance (EMD), a distance metric from the mathematical theory of optimal transport, to classify cells based on their two-dimensional firing rate maps. This metric is then used to show that border responses are specific to boundaries that impede movement of the animal, while they are invariant to different objects introduced into the maze.

RESULTS

RSC CELLS FIRE NEAR THE MAZE PERIMETER AT SPECIFIC DISTANCES

To capture the activity of neurons in the Retrosplenial cortex, I performed electrophysiological experiments by making chronic implants of 28-tetrode microdrives in the RSC of rats (**Figure 5A**). This allowed for the simultaneous recording of single-unit activity from dozens of neurons over time, during which animals were able to freely move around their environment. Initial behaviour for the experiment consisted of free exploration of a squared open field arena, while rats foraged for scattered chocolate pellets after being maintained on a mildly food-restricted diet (**Figure 5B**). All animals were sufficiently habituated to the environment and procedures, and actively explored the entire arena (**Figure 5C**). The experimental setup was placed in the room with fixed landmarks to allow the animals to orient themselves relative to external features.

I recorded the activity of 5415 RSC neurons across eight animals ($n = 82$ sessions) and observed a subpopulation of cells that fired consistently at the edge of the arena (examples shown in **Figure 5C**). Across this subgroup, there was a variety of preferred firing distances from the wall, ranging from very near proximity up to a body-length (15-18 cm) away. Unlike traditional border cells found in MEC and subiculum (Solstad et al., 2008; Stewart et al., 2014), these border responses occurred throughout the environment on each of the four available walls. RSC border cells furthermore form multiple firing fields that are not necessarily directly connected to the wall.

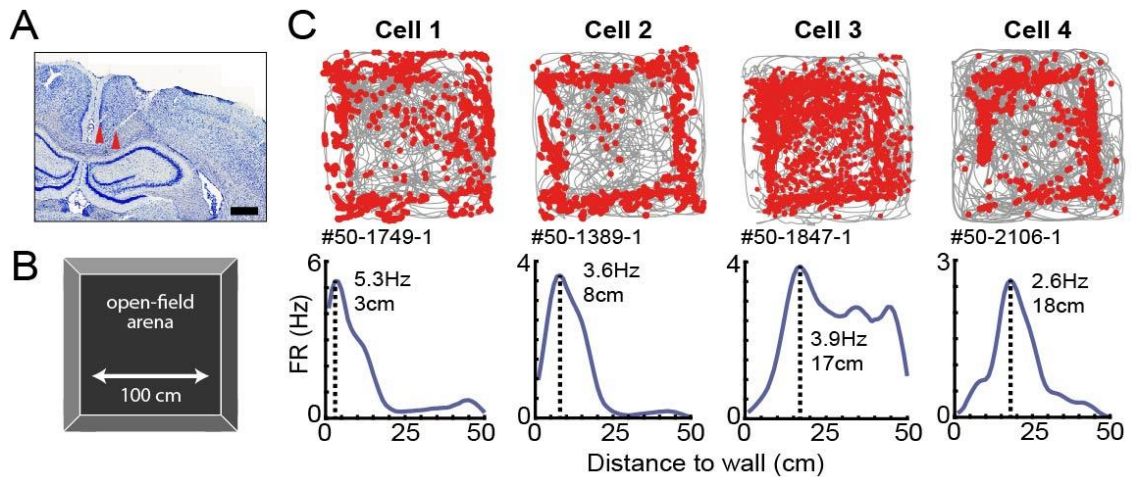


Figure 5. Response profiles of border cells in RSC.

(A) Location of tetrode tracts marked with red in an example Nissl-stained coronal section. Scale bar, 1000 μm . (B) Task behaviour consisted of free exploration in a squared 1 m² arena. (C) Trajectory spike plots (top row) and distance firing rate (FR) plots (bottom row) of four example cells that fired at different distances away from the wall, relative to the closest wall at any time. Grey lines indicate the animal's trajectory and red dots the rat's position when a spike occurred.

Typical border cell classification uses the original border score, developed by (Solstad et al., 2008), but applying it to this dataset only yielded a small fraction of border cells in RSC, as this score is based on the occupancy of a single firing field along a wall and is strongly biased to connected bins. Instead, I developed a new model-based approach using a template-matching procedure to classify these border cells in RSC, based on (Grossberger et al., 2018).

This method uses two-dimensional (2D) information of the firing rate maps and builds on the assumption that border cells have their spikes concentrated at the entire outer ring of the arena, incorporating geometric information into the classification procedure. The dissimilarity between a cell's spatial firing rate map and a 'boundary' template (**Figure 6E**) was assessed by the algorithm based on the Earth Mover's Distance (EMD, **Figure 6A-D**), a distance metric from the mathematical theory of optimal

transport (Hitchcock, 1941; Rubner et al., 1998). The EMD is a normalized score, calculated as the minimum cost required to match a cell's firing rate map with the template distribution by moving firing rate units, also known as the Wasserstein distance. While this metric is sensitive to a change in the geometric shape of rate maps, it is robust to small variations of preferred firing distances or pixel-by-pixel jittering, giving a single metric that can quantitatively assess changes in the cell's spatial tuning as a function of experimental manipulations, such as reshaping of the maze or adding an object or wall.

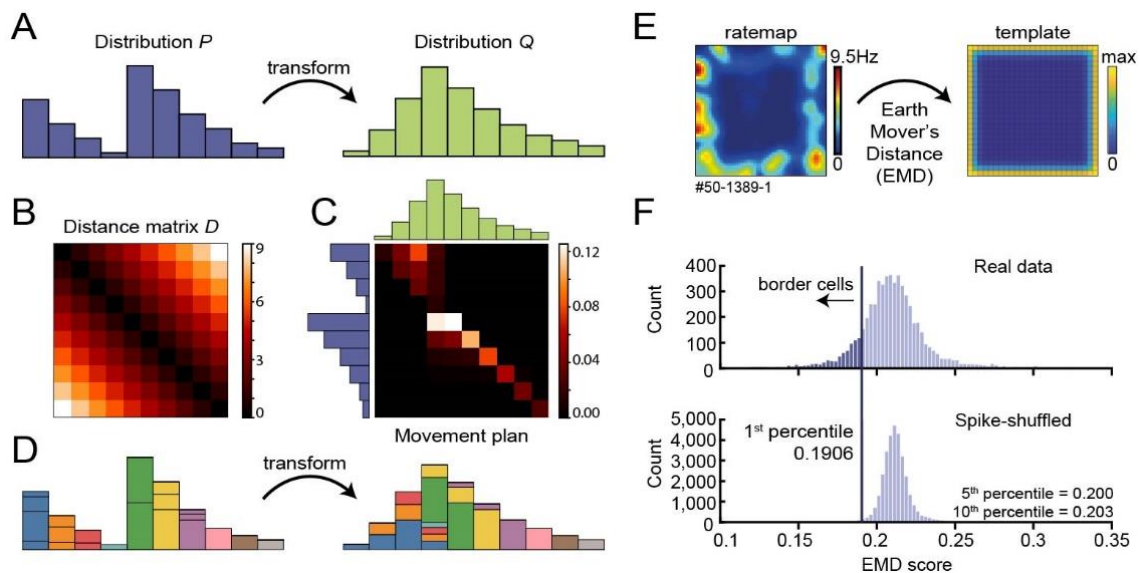


Figure 6. Border cell classification using the Earth Mover's Distance.

(A) The goal of the EMD algorithm is to transform one probability distribution P , into a second distribution Q , here in a single dimension. (B) The first step is to compute a distance matrix D between each possible combination of data bins. (C) A linear solver then finds the optimal movement plan to move units of 'earth' (coloured bins) across data bins with the minimum amount of effort. (D) A representation how different portions of mass from distribution P (left) are moved to create distribution Q (right) in the optimal solution. (E) Applying this algorithm to the neural data, a template-matching procedure was used to classify border cells by calculating the EMD score between each cell's spatial rate map and an ideal template (see Materials and methods in *Chapter VI*). (F) A cell was classified as a border cell when its EMD score fell below the 1st percentile of a shuffled null distribution, together with an average FR above 0.5 Hz. Visualization in (A-D) is based on: <https://github.com/vincentherrmann/wasserstein-notebook>

Border cells were defined as cells with a low dissimilarity EMD score below the 1st percentile of a spike-shuffled null distribution of 0.191, and an average firing rate (FR) above 0.5 Hz (examples shown in **Figure 8A**). Cells with a low EMD score are more similar to the chosen boundary template, and with increasing scores will diverge further away from the typical border cell (**Figure 7A**). In total, 485 out of 5415 RSC cells (9.0%) passed this criterion (**Figure 6E,F**), which is a 3.4-fold increase compared to only 142 cells that would have been found using the original border score (**Figure 7B**).

For the selected border cells, overall spiking rate was not related to their associated EMD score (Pearson's correlation: $r = 0.037$, $p=0.42$; **Figure 7C**), but a small correlation ($r = 0.17$, $p < 0.001$) existed between the EMD score and their preferred firing distance, where neurons with lower distance tuning have their activity concentrated closer to the walls (**Figure 7D**).

Across the population, selected border cells had a similar distribution of average firing rates compared to other cells recorded on the same tetrodes (border cells: $FR = 2.97 \pm 0.20$ Hz, others: $FR = 3.25 \pm 0.07$ Hz; Wilcoxon ranksum test: $z = 0.057$, $p=0.955$; **Figure 8B**). However, there were significantly higher spatial correlations between the first and last recording sessions (border cells: $r = 0.52 \pm 0.008$, others: $r = 0.20 \pm 0.003$; Wilcoxon ranksum test: $z = -24.50$, $p=1.60 \times 10^{-132}$; **Figure 8C**). Border cells were recorded across the granular and dysgranular regions of the RSC, and had waveform properties similar to the other cells recorded (**Figure 9A,B**).

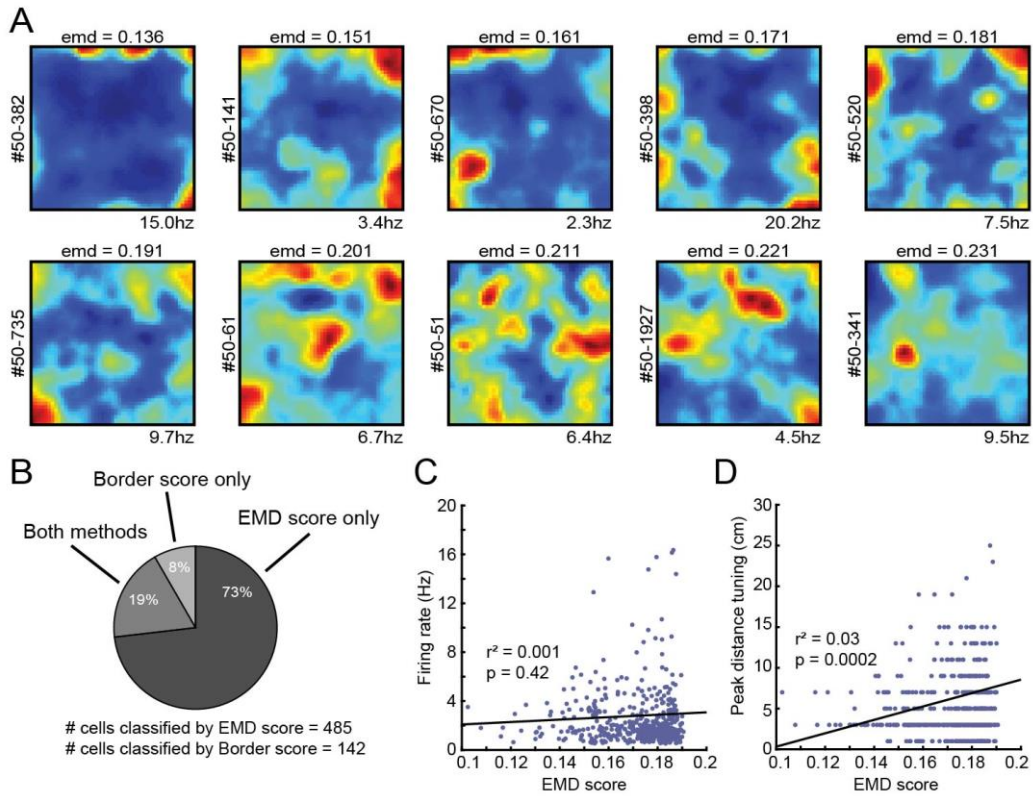


Figure 7. Classification results using the EMD and border score metrics.

(A) Spatial rate maps of separate neurons recorded in RSC of one individual animal with EMD scores at evenly spaced intervals (range: 0.14–0.23). Cells with a score below the value of 0.191 are considered to be border cells. (B) Distribution and overlap of border cell classification using the border score and EMD methods. (C) No significant correlation exists between a cell’s overall firing rate and its EMD score. (D) A small correlation ($r = 0.17$) exists between a border cell’s EMD score and its preferred firing distance, as cells with lower distance tuning are more similar to the boundary template.

Activity of neurons in RSC was additionally modulated by the running speed of the animal, with lower firing rates in the low-speed range, where border cells further showed reduced activity in the low-speed range compared to other recorded cells ($p < 0.05$ in the range of 0–12 cm/s; Wilcoxon ranksum test; **Figure 8D**).

$$r = \exp\left(\sum_i X_i^T w_i\right) / dt \quad (\text{Eq. 1})$$

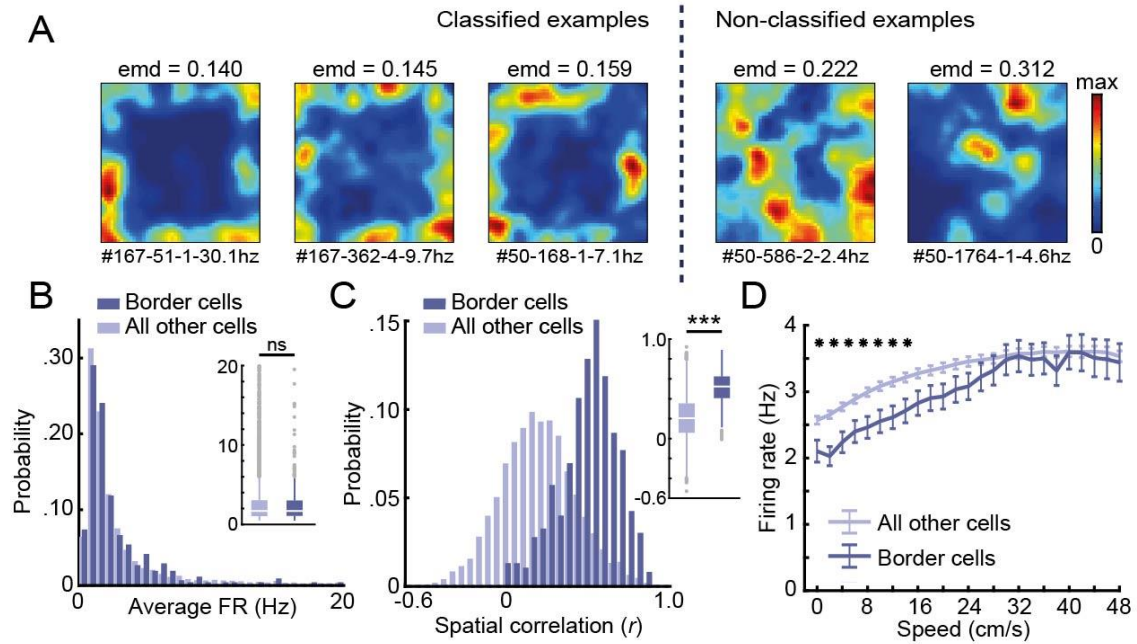


Figure 8. RSC border cell population characteristics.

(A) Colour-coded spatial rate maps of five example cells with different EMD scores, where warm colours indicate high firing. From left to right: three typical border cells, a non-uniform firing cell, and a cell with focused firing fields. (B) Distribution of average FR over the entire recording day shows no difference in overall activity between border cells and other recorded cells. (C) Distribution of spatial correlations between recorded sessions shows significantly higher spatial correlations for border cells compared to other recorded cells. (D) Both border cells and other cells recorded in RSC are modulated by running speed, with a ramping of firing rates as the running speed increases. * $p < 0.05$, *** $p < 0.001$, Wilcoxon ranksum test

To account for the possibility of border cell activity because of their speed modulation, and not border tuning, I further analysed the speed profiles of the animals. On average, an animal's running speed was uniform across space (**Figure 9E**), and unrelated to the distance to any boundary (non-significant in the range of 5–45 cm; Wilcoxon ranksum test against overall median; Bonferroni-corrected $\alpha = 0.005$; **Figure 9D**), and could thus not account for the cell's spatial tuning. Applying an unbiased classification approach based on linear-nonlinear models (Hardcastle et al., 2017) showed that running speed and wall-distance are two independent factors that explain the activity of RSC cells, confirming that RSC border and speed tuning are separately expressed features (**Figure 9C**).

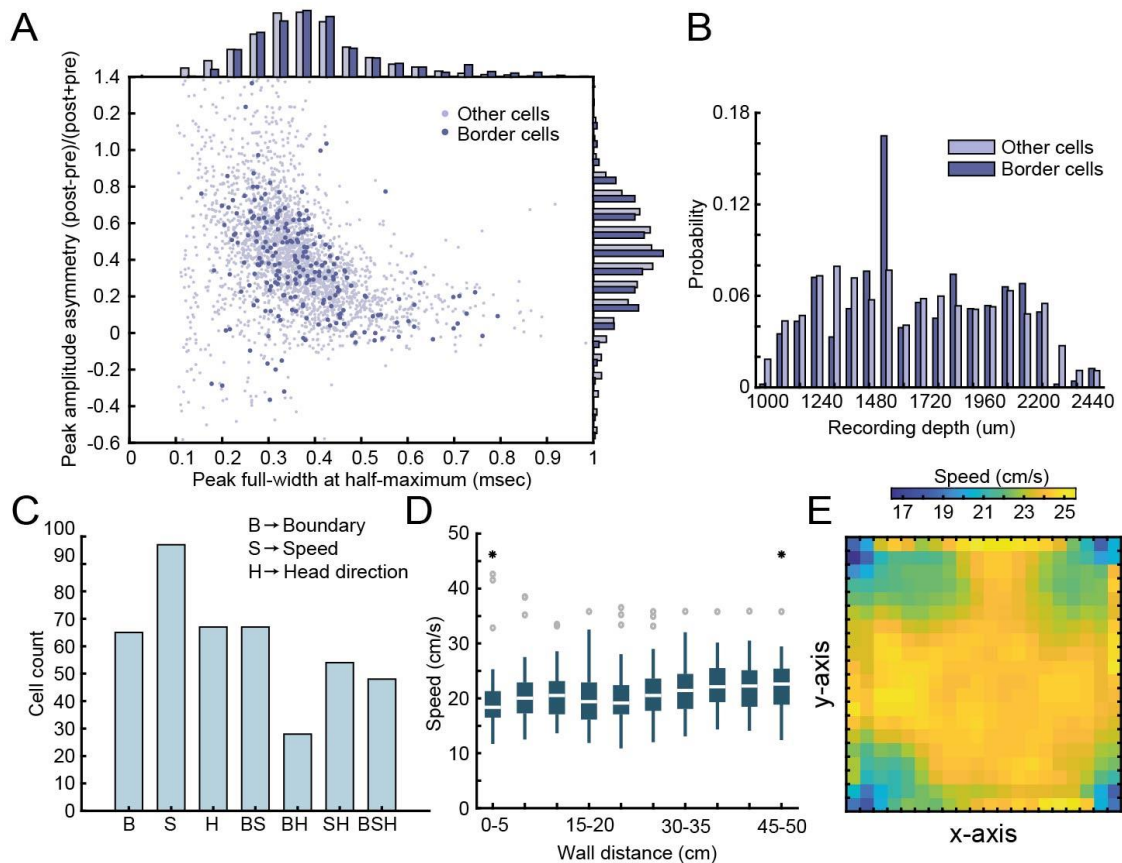


Figure 9. The dissociation between the animal's running speed and activity around borders.

(A) Waveform properties of RSC border cells versus other cells recorded on the same tetrodes show no major difference between both populations. (B) Border cells were recorded both in granular and dysgranular layers of RSC across the recording depths. (C) An unbiased classification approach was applied based on linear-nonlinear models (Hardcastle et al., 2017). Three variables, X_i , were included: B , a one-dimensional vector of distance to the closest boundary, S , the animal's running speed, and H , the animal's allocentric head-direction. Models were built with increasing complexity using a forward-search approach (e.g., starting with one variable, then adding more if the model's performance increases significantly, tested using ten-fold cross-validation). The model that best explained (e.g., had maximal log-likelihood) the cell's firing rate, r , using optimal weights, w_i , was then selected (Eq. 1). Results show that boundary, speed, and head-direction encoding in RSC are independent features, as they can be expressed in isolation, combined with a substantial number of neurons that display conjunctive coding. (D) There was no bias in the animal's behaviour around walls, as the running speed of the animals was uniformly distributed as a function of distance to the closest wall. (E) Speed of the animals was uniformly distributed across the 2D space of the arena. * $p < 0.05$, Wilcoxon signed-rank test

BORDER CELLS FORM NEW FIRING FIELDS NEARBY ADDED WALLS BUT NOT OBJECTS

To understand the generation of boundary coding in RSC, I quantified the impact of the change of environmental features on the activity of RSC border cells by using the EMD metric. The first question is whether the firing of these border cells is limited to walls, or if neurons also encode information about other features of the environment, such as local cues or objects (Hoydal et al., 2019; Jacob et al., 2017).

My first manipulation was to temporarily add a wall, protruding from one side into the centre of the maze (**Figure 10A,B**). Border cells formed new firing fields around the added walls accordingly, as their firing rate inside a region-of-interest (ROI; 15×5 spatial bins) around the wall increased significantly in the added wall sessions (Regular: FR = 1.19 ± 0.13 Hz; Added wall: FR = 1.58 ± 0.21 Hz; Wilcoxon signed-rank test: $z = -2.67$, $p=0.0076$; $n = 42$ border cells; **Figure 10C**). This was accompanied by a sharp drop in spatial correlations between rate maps of regular versus added wall sessions (Reg-Reg: $r = 0.51 \pm 0.04$, Reg-Wall: $r = 0.25 \pm 0.04$; Wilcoxon signed-rank test: $z = 4.43$, $p=9.31 \times 10^{-6}$; Bonferroni-corrected $\alpha = 0.025$; **Figure 10D**), while correlations remained high when comparing within session types (Wall-Wall: $r = 0.47 \pm 0.03$; Wilcoxon signed-rank test with Reg-Reg correlation: $z = 0.63$, $p=0.53$; Bonferroni-corrected $\alpha = 0.025$; **Figure 10D**).

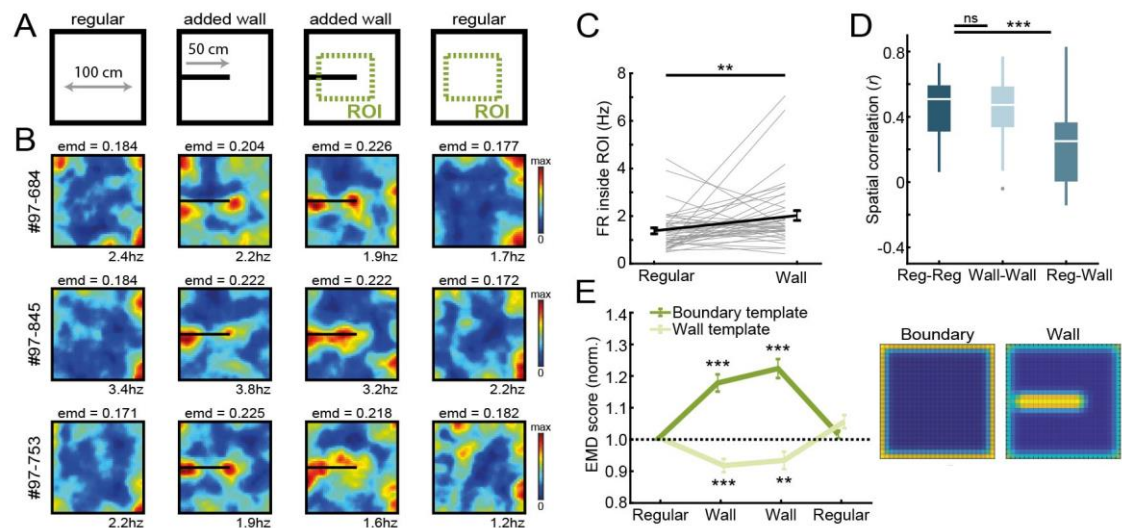


Figure 10. Single cell and population activity of border cells around an added wall. (A) An additional temporary wall was placed on the maze in the middle sessions. (B) Spatial rate maps of three typical border cells across regular and added wall sessions during one recording day. (C) Border cells formed new firing fields nearby the added wall, as cells significantly increased their firing rate in the region-of-interest (ROI) area around the central wall. (D) Spatial correlations between rate maps of regular and wall sessions were decreased, but remained high within session type. (E) Dissimilarity increased for the boundary template as cells formed fields around the added wall, whereas dissimilarity decreased for an added wall template. ** $p < 0.01$, *** $p < 0.001$, Wilcoxon signed-rank test

The EMD metric furthermore showed a significant increase in dissimilarity between rate maps of these added wall sessions and the original boundary template (Normalized boundary EMD score: R1, 1.0 ± 0 , W1, 1.178 ± 0.03 , W2, 1.223 ± 0.03 , R2, 1.016 ± 0.01 ; Friedman test: $X^2(3)=77.9$, $p=8.6 \times 10^{-17}$; Post-hoc Wilcoxon signed-rank test: R1-W1, $z = -5.35$, $p=9.0 \times 10^{-8}$, R1-W2, $z = -5.58$, $p=2.37 \times 10^{-8}$, R1-R2, $z = -1.27$, $p=0.20$; Bonferroni-corrected $\alpha = 0.017$; **Figure 10E**). In contrast, the dissimilarity between the same rate maps and an ‘added wall’ template decreased significantly (Normalized wall EMD score: R1, 1.0 ± 0 , W1, 0.918 ± 0.02 , W2, 0.934 ± 0.03 , R2, 1.057 ± 0.02 ;

Friedman test: $X^2(3)=33.7$, $p=2.3 \times 10^{-7}$; Post-hoc Wilcoxon signed-rank test: R1-W1, $z = -3.89$, $p=9.8 \times 10^{-5}$, R1-W2, $z = 2.59$, $p=0.0095$, R1-R2, $z = -2.22$, $p=0.027$; Bonferroni-corrected $\alpha = 0.017$; **Figure 10E**), indicating that firing fields of border cells incorporated boundary information of the added wall.

To investigate generalization to other environmental features, I further added additional objects to the arena and tested the specificity of border responses to the spatial layout (**Figure 11A,B**). The size of the object was 10 cm in diameter, and the animal could walk around or climb on top without it impeding the animal's movement completely. Contrary to an added wall, RSC border cells maintained tuning only to the outer walls and did not fire whenever objects were inside their receptive field (Circular ROI, eight bins in diameter; Regular: FR = 1.39 ± 0.26 Hz; Added object: FR = 1.42 ± 0.21 Hz; Wilcoxon signed-rank test: $z = -0.63$, $p=0.53$; $n = 23$ border cells; **Figure 11C**). EMD analyses however showed a significant increase in dissimilarity to the boundary template in the object sessions (Normalized boundary EMD score: R1, 1.0 ± 0 , O1, 1.097 ± 0.031 , O2, 1.079 ± 0.028 , R2, 1.024 ± 0.021 ; Friedman test: $X^2(3)=14.7$, $p=0.002$; Post-hoc Wilcoxon signed-rank test: R1-O1, $z = -2.74$, $p=0.006$, R1-O2, $z = -2.62$, $p=0.009$, R1-R2, $z = -1.00$, $p=0.32$; Bonferroni-corrected $\alpha = 0.017$; **Figure 11E**), indicating changes in the rate maps by the object. This change was not due to new firing fields around the object, however, because fitting an 'object' template did not lead to a decrease in dissimilarity during object sessions (Normalized object EMD score: R1, 1.0 ± 0 , O1, 1.026 ± 0.026 , O2, 0.995 ± 0.029 , R2, 0.990 ± 0.025 ; Friedman test: $X^2(3)=2.32$, $p=0.51$; **Figure 11E**).

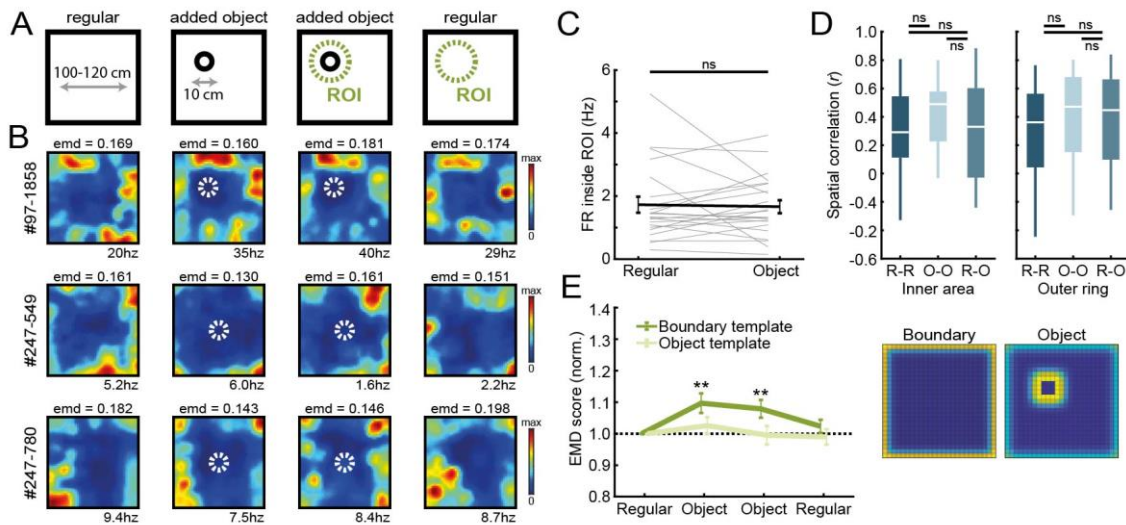


Figure 11. Single cell and population activity of border cells around objects.

(A) A new object was introduced either in the north-west corner or the centre of the maze. (B) Spatial rate maps of three example border cells across regular and object sessions. (C) Firing rate of border cells in a ROI around the added object remained unchanged between session types. (D) No significant drop was observed in spatial correlations of border cells by the addition of the object. Correlations were split between an outer ring (four rows) and the remaining inner area to isolate activity related to the outer walls versus the object. (E) There was an increase in EMD scores for the boundary template, whereas the spatial rate maps did not fit with the object template either, as their EMD scores remained unchanged. $**p < 0.01$, Wilcoxon signed-rank test

The maintenance of original firing fields was further confirmed by spatial correlations across session types that did not drop when comparing rate maps between regular and object sessions, neither for the outer rows of pixels adjacent to the walls (Reg-Reg: $r = 0.36 \pm 0.07$, Object-Object: $r = 0.47 \pm 0.07$; $z = -0.88$, $p = 0.38$; Reg-Object: $r = 0.45 \pm 0.07$; comparing with R-R: $z = -1.28$, $p = 0.20$; comparing with R-O: $z = 1.16$, $p = 0.25$; Wilcoxon signed-rank test; Bonferroni-corrected $\alpha = 0.017$; **Figure 11D**, right panel), nor the inner area surrounding the object (Reg-Reg: $r = 0.29 \pm 0.07$, Object-Object:

$r = 0.49 \pm 0.05$; $z = -1.58$, $p=0.11$; Reg-Object: $r = 0.33 \pm 0.07$; comparing with Reg-Reg: $z = -0.49$, $p=0.63$; comparing with Reg-Object: $z = 1.16$, $p=0.25$; Wilcoxon signed-rank test; Bonferroni-corrected $\alpha = 0.017$; **Figure 11D**, left panel).

To further confirm the specificity of border cell firing to the outer walls, I performed additional experiments across different shapes of the environment, as well as under novel conditions. Recordings performed in arenas with a hexagonal, circular, or triangular shape indeed showed the adaptation of firing fields of RSC border cells to the spatial layout of boundaries (**Figure 12A-C**), while cells showed activity already from the beginning of the session and did not need time for adaptation in a novel arena and experimental room (first-half familiar session, $FR = 1.98 \pm 0.42$ Hz; first-half novel session, $FR = 2.30 \pm 0.53$ Hz, $p=0.56$; second half novel session, $FR = 1.71 \pm 0.54$ Hz, $p=0.68$; Wilcoxon signed-rank test; $n = 14$ border cells; **Figure 12D,E**). Taken together, these results indicate that RSC border cells encode information that is specific to boundaries of the spatial layout where cell responses differentiate between the types of added features.

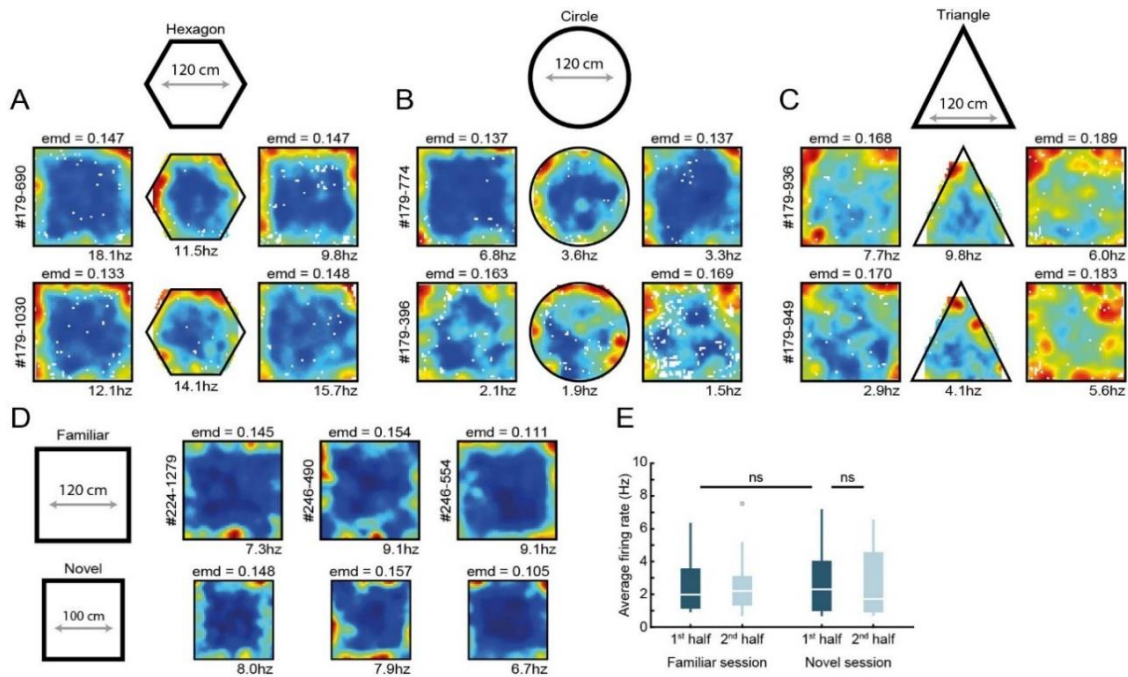


Figure 12. RSC border cell firing under novel conditions and different arena shapes. (A–C) Recordings were performed across different shapes of environments. Shown are rate maps of border cells that fired at the edge of a squared arena, and cells maintained their firing to the borders when the outer walls were changed to form a hexagonal (A), circular (B), or triangular (C) shape. (D) Several experimental sessions were performed under novel conditions, where animals had never visited neither this maze nor the recording room before. Shown are spatial rate maps of three typical RSC border cells with no qualitative differences between a familiar and novel maze. (E) Across the population, cells fired with a similar spiking rate already from the beginning of the session, with no significant differences between the familiar and novel sessions. Wilcoxon signed-rank test

BORDER CELLS RETAIN THEIR TUNING IN DARKNESS AND ARE NOT DRIVEN DIRECTLY BY WHISKER SENSATION

One way for border cells to compute information of boundaries is through direct sensory detection of the walls, for example, by whisking or visual observation (Raudies and Hasselmo, 2012). I investigated the importance of direct sensory input on border tuning by removing visual information of the boundary (**Figure 13A**). First, to assess the impact of visual information, I introduced an infrared position tracking system as opposed to regular light-emitting diodes (LED; see Materials and methods in *Chapter VI* for details) to ensure no visible light was present in the maze for animals to identify boundaries. I recorded the activity of RSC border cells in both dim-light and darkness conditions, but observed no significant changes in EMD dissimilarity scores across the sessions (Boundary EMD score: R1, 0.183 ± 0.001 , D1, 0.185 ± 0.003 , D2, 0.177 ± 0.003 , R2, 0.182 ± 0.002 ; Friedman test: $X^2(3)=1.23$, $p=0.75$; $n = 21$ border cells; **Figure 13B,D**). There were also no changes across spatial correlations between different session types (Reg-Reg: $r = 0.42 \pm 0.03$, Reg-Dark: $r = 0.38 \pm 0.03$; Wilcoxon signed-rank test $z = 0.61$, $p=0.54$; Dark-Dark: $r = 0.42 \pm 0.05$, Wilcoxon signed-rank test with Reg-Reg correlation, $z = 1.20$, $p=0.23$; Bonferroni-corrected $\alpha = 0.025$; **Figure 13C**), indicating that activity is not generated through visual sensory input.

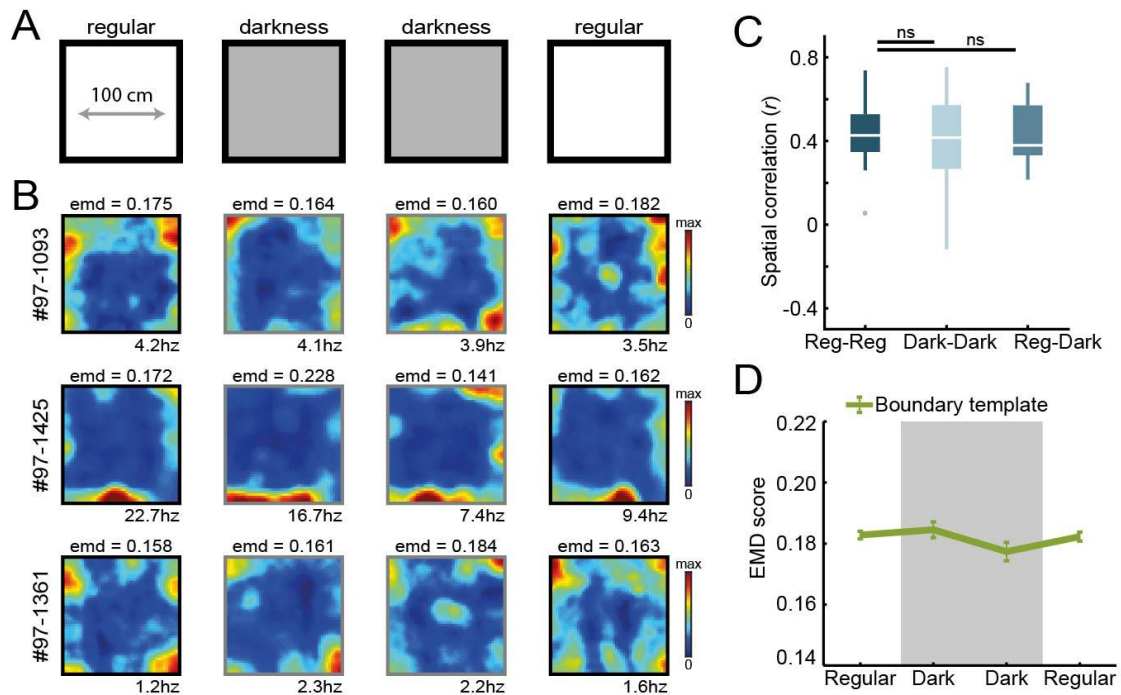


Figure 13. Border coding is maintained in darkness.

(A) Recordings were performed under no visible light in the middle sessions, and the animal's position was tracked in the infrared spectrum. (B) Spatial rate maps of three typical border cells recorded in light and dark conditions. (C) Spatial correlations between rate maps of regular and dark sessions remained high, indicating border cells still fired nearby boundaries in darkness. (D) There were no changes in EMD scores with the boundary template, confirming that cells maintained their tuning to the outer walls without direct visual detection. Wilcoxon signed-rank test

In order to examine the role of tactile sensation on boundary representations, I next removed all four outer walls that left a drop-edge above the floor, limiting movement of the animal in the absence of direct somatosensory information of a physical barrier (**Figure 14A**). The EMD scores showed that the majority of border cells were unaffected by the wall removal, with no significant changes in the drop-edge session (Unaffected cells: boundary EMD score: R1, 0.183 ± 0.002 , Drop, 0.186 ± 0.003 , R2, 0.183 ± 0.001 ; Friedman test: $X^2(2)=4.59$, $p=0.10$; $n = 17$ border cells; **Figure 14B,C**). However, a subset of cells had disrupted firing nearby the boundary edges ($n = 8/25$ affected cells, separated based on an increase in EMD that exceeded the 95th-percentile of a null distribution of change, computed using the differences between first and last regular sessions; boundary EMD score: R1,

0.169 ± 0.008, Drop, 0.202 ± 0.004, R2, 0.175 ± 0.006; Friedman test: $X^2(2)=11.0$, $p=0.004$; Post-hoc Wilcoxon signed-rank test: R1-Drop, $z = -2.95$, $p=0.003$, R1-R2, $z = 0$, $p=1.0$; Bonferroni-corrected $\alpha = 0.025$; **Figure 14C**).

A similar result emerged from the spatial correlations, where rate map correlations remained high when comparing regular and drop-edge sessions, but only for the unaffected cells that had stable EMD scores across session type (Unaffected cells: Reg-Reg, $r = 0.50 \pm 0.04$, Reg-Drop, $r = 0.45 \pm 0.04$; Wilcoxon signed-rank test: $z = 1.21$, $p=0.23$; Affected cells: Reg-Reg, $r = 0.57 \pm 0.05$, Reg-Drop, $r = 0.14 \pm 0.07$; Wilcoxon signed-rank test: $p=0.008$; **Figure 14D**).

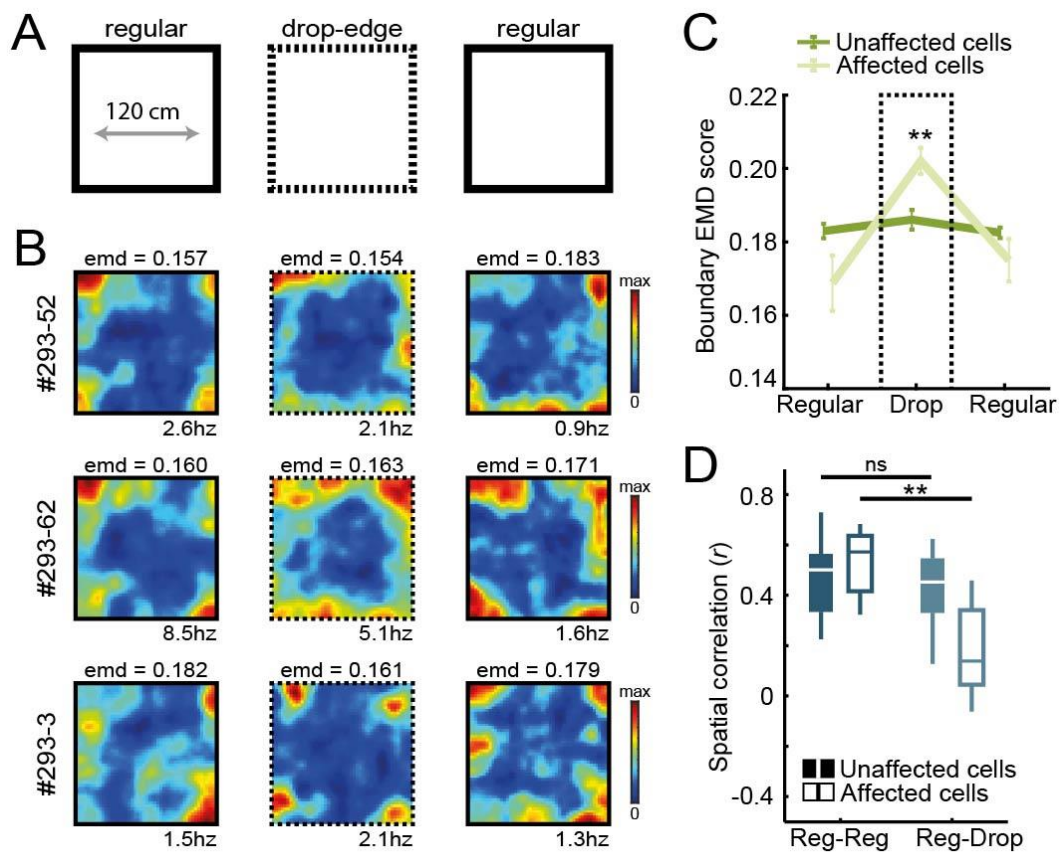


Figure 14. Border coding is maintained the absence of physical walls.

(A) All four outer walls were removed, leaving only a drop-edge to confine the arena. (B) Spatial rate maps of three example border cells across recording sessions. (C) Spatial rate maps were maintained for a majority of border cells (unaffected), but a subset of neurons showed disrupted firing near the drop-edge that resulted in an increase in the EMD score on the boundary template (affected). (D) Spatial correlations between rate maps of regular and drop-edge sessions remained high for the unaffected cells but decreased significantly for the affected cells. ** $p < 0.01$, Wilcoxon signed-rank test

To directly test the necessity of whisker-mediated tactile sensation, I trimmed the animal's whiskers after which they freely explored the arena (**Figure 15A,B**). I did not observe a significant change in the proportion of border cells in RSC after the trimming of whiskers (intact whiskers: 29/276 cells classified as border cells, boundary EMD score = 0.183 ± 0.002 ; trimmed whiskers: 23/285 cells classified as border cells, boundary EMD score = 0.186 ± 0.005 ; change in proportion of border cells: $z = 1.00$, $p=0.32$, binomial test; **Figure 15B**), nor did I see a change in the overall firing rates (before: $FR = 1.58 \pm 0.38$; after: $FR = 1.16 \pm 0.47$; Wilcoxon signed-rank test: $z = 1.04$, $p=0.30$; **Figure 15C**), suggesting that whisker sensation is not essential for boundary representation.

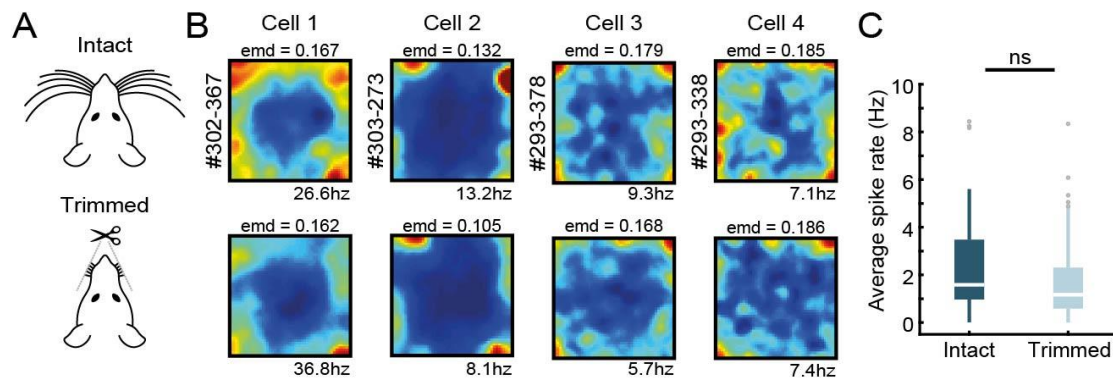


Figure 15. Control experiment to assess the role of somatosensory information in computing border information.

(A) Whiskers of rats were trimmed to the skin on the final recording day, with one behavioural session before and after trimming for each animal. (B) Example rate maps of RSC border cells before (top row) and after trimming (bottom row), with four examples of cells that were unaffected by trimming and maintained their boundary tuning in the absence of whiskers. No significant changes were observed in the proportion of border cells due to whisker trimming. (C) Whisker trimming had no significant effect on the overall firing rates of RSC border cells. Wilcoxon signed-rank test

I further recorded from cells located in the barrel field region of the somatosensory cortex (Slbf) in order to understand the nature of somatosensory information through whiskers (**Figure 16A–C**). Although I was able to identify a subpopulation of cells that fired nearby boundaries in the somatosensory cortex ($n = 23/173$ cells classified as border cells using the same criteria; **Figure 16D**), an important difference with RSC cells is that Slbf neurons fired consistently near added objects when introduced into the arena, highlighting the selective tuning of RSC border cells to boundaries but not objects (Normalized boundary EMD score: R1, 1.0 ± 0 , O1, 1.067 ± 0.01 , O2, 1.084 ± 0.01 , R2, 0.971 ± 0.01 ; Friedman test: $X^2(3)=47.1$, $p=3.3 \times 10^{-10}$; Post-hoc Wilcoxon signed-rank test: R1-O1, $z = -3.65$, $p=2.6 \times 10^{-4}$, R1-O2, $z = -3.89$, $p=9.9 \times 10^{-5}$, R1-R2, $z = 2.95$, $p=0.003$; Bonferroni-corrected $\alpha = 0.017$; Normalized object EMD score: R1, 1.0 ± 0 , O1, 0.977 ± 0.005 , O2, 0.967 ± 0.005 , R2, 1.015 ± 0.004 ; Friedman test: $X^2(3)=47.5$, $p=2.7 \times 10^{-10}$; Post-hoc Wilcoxon signed-rank test: R1-O1, $z = 3.50$, $p=4.7 \times 10^{-4}$, R1-O2, $z = 3.80$, $p=1.4 \times 10^{-4}$, R1-R2, $z = -3.16$, $p=0.002$; Bonferroni-corrected $\alpha = 0.017$; **Figure 16E**). Together, these results suggest that the activity of RSC border cells is not simply driven by the detection of boundaries through visual or tactile sensation, and their distinct firing around boundaries but not objects implies additional computations in the brain.

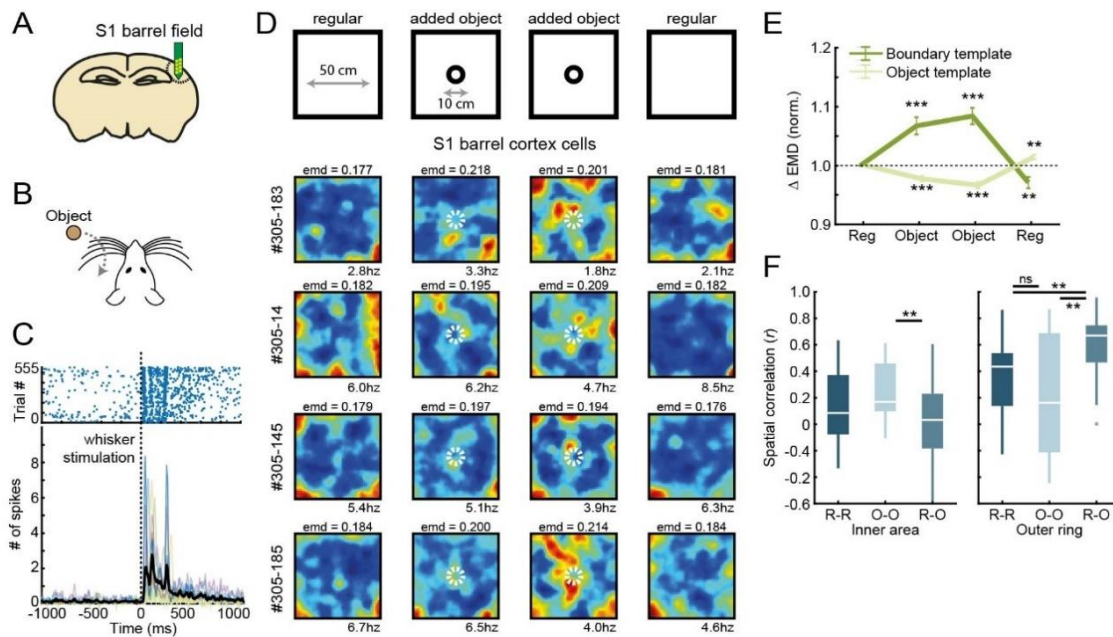


Figure 16. Control experiment to compare boundary coding in RSC with somatosensory coding in Slbf.

(A) Recordings were performed from neurons in the barrel field of the primary somatosensory cortex (Slbf) by implanting a 64-channel silicon probe. (B) In an anesthetized preparation, an object (sandpaper) was moved through the whiskers contralateral to the recorded hemisphere at 10 s intervals. The silicon probe was lowered until a substantial number of cells responded consistently to the whisker stimulation. (C) A subset of neurons fired reliably after whisker stimulation. Top: example raster plot of spikes from a representative whisker-responsive cell. Bottom: number of spikes for individual neurons (coloured lines) and the population-average (black line) shows that neurons fired 30–300 ms after the object moved through the whiskers. (D) Recordings were performed across four behavioural sessions, with an object introduced to the maze in the middle two sessions. Shown are rate maps of four example cells recorded from S1 barrel cortex that matched our border cell criteria, where cells fired around the edges of the arena but also formed firing fields around the object. (E) EMD scores confirm that Slbf cells fired around objects, as the boundary EMD scores increased significantly in the object session, while the object template EMD scores decreased accordingly. (F) Spatial correlations between rate maps of regular and object sessions decreased significantly when comparing the inner area of the rate map, consistent with the formation of firing fields around the object. ** $p < 0.01$, *** $p < 0.001$, Wilcoxon signed-rank test

DISCUSSION

Many spatial navigation strategies rely on salient features of the environment to create movement plans, for example, by planning trajectories relative to landmarks and considering the location of obstacles or blocked paths. To make this possible, the brain needs to form internal representations of these components, where the activity of neurons conveys spatial information about their characteristics such as their location, distance or direction. One of the most likely candidates to implement such representations is the Retrosplenial cortex (Mitchell et al., 2018; Vann et al., 2009). Single-unit recording studies have revealed some initial firing properties of cells, mostly complex spatial modulation patterns (Alexander and Nitz, 2015; Cho and Sharp, 2001), but thus far it remained unclear how individual neurons implement a variety of spatial coding principles to represent spatial information of external features.

The goal of this chapter was to establish how neurons in the RSC perform spatial computations, and what kind of spatial information can be found in their activity patterns. To do so, I performed a set of experiments where rats were allowed to freely explore an open arena with different salient features present, while simultaneously recording the activity of dozens of neurons in RSC by using high-density tetrode microdrives. My initial recordings revealed the presence of a new class of cells present in this brain region, the border cell. These cells displayed tuning for the distance of walls, with high firing rates as the animal was at specific distances away from a wall. Border tuning was present for all boundaries indiscriminately, with similar activity around any of the available walls, even as the arena shape was changed from a squared to a triangular or hexagonal arena. This is very different from two related cell types, the border cell in MEC (Solstad

et al., 2008) and boundary-vector cell in subiculum (Lever et al., 2009; Stewart et al., 2014), which are also active near walls but are anchored to a single border (e.g., firing nearby the east, but not northern wall).

To investigate whether activity of RSC border cells was specifically related to borders, and not due other behavioural or environmental variables, I performed a series of experiments that introduced different new elements into the arena. I found that cell firing was specific to boundaries that impede movement, as a new wall resulted in additional nearby firing fields on both sides, similar to how MEC border cells and subicular boundary-vector cells form fields on either side of an extra wall (Solstad et al., 2008; Stewart et al., 2014). Contrary to an additional wall, RSC border cells did not show a corresponding increase in their activity when an object was introduced into the maze. This finding is consistent with the distinction between border and object-vector cells found in MEC, where separate functional cell types encode positional information of both types of features independently (Hoydal et al., 2019).

One possible way for border cells to generate their activity in respect to a border is by direct sensory detection of the wall, either through visual observation from a distance or touch sensing using their whiskers at closer distances (Grant et al., 2009; Raudies and Hasselmo, 2012). To determine the importance of this sensory information, I manipulated the sensory experience of the animal by removing either of the two sensory modalities in isolation. Under the condition of no visible light, boundary coding was preserved for all RSC border cells, while in the absence of physical walls or the animal's whiskers, the majority of cells maintained their tuning. This result is also consistent with border cells in MEC, which maintain their boundary tuning without walls present, albeit with some degree of rotational mapping (Solstad et al., 2008), and boundary-vector cells in

subiculum, which preserve their activity patterns in darkness (Lever et al., 2009) and around a drop-edge (Stewart et al., 2014). From this we can conclude that RSC border cells, as well as those in MEC and subiculum, share most of their tuning properties under different environmental conditions, and are not simply driven by local sensory cues, but likely discriminate boundaries based on a global spatial layout of the environment.

One major difference between these different types of border cells however is their anchoring to the environment, or lack thereof, where only RSC border cells fire across the entire arena near all available walls. Rather than being anchored to a wall in any of the cardinal directions, in which case there is a fixed relationship between the position of the animal and a specific boundary, RSC border cells fire whenever any boundary is located within their receptive field at a specific distance relative to the animal. Another distinctive feature of RSC border cells is the small jittering in their firing rate map, where firing fields are not continuous alongside a wall, nor are they identical across different recording sessions for the same neuron. Neural activity is known to have high innate variability, for example, the visual cortex can show different responses to an identical visual stimulus (Arieli et al., 1996; Tomko and Crapper, 1974) which can be ascribed not only to differences in input that these cells receive, but to other modulatory factors such as arousal, attention and adaptation (Carandini, 2004; Goris et al., 2014; Shadlen and Newsome, 1994). But an alternative explanation for the variability in firing found in RSC border cells is that the 2-dimensional rate map that represents activity as a function of x- and y-position does not properly capture all tuning properties of these neurons. This latter possibility will be explored in the next Chapter.

Chapter III

Egocentric direction tuning of border cells

The results and figures presented in the following chapter have been published previously in *eLife* under the citation below. Experiments that provided results shown in **Figure 19** were performed in collaboration with Susanne Babl.

van Wijngaarden, J. B. G., Babl, S. S., & Ito, H. T. (2020). Entorhinal-retrosplenial circuits for allocentric-egocentric transformation of boundary coding. *Elife*, 9, e59816. DOI: 10.7554/eLife.59816

INTRODUCTION

Neurons that perform spatial computations need to anchor their activity in respect to some reference point. For many spatial cells that have been characterized in the hippocampus or parahippocampal brain areas, this is done relative to the external environment. For example, a place cell in the CA1 region of the hippocampus will be active whenever the rat is at a given x- and y-coordinate in an arena in a 2-dimensional plane (O'Keefe and Dostrovsky, 1971). Each time the animal visits that location, the cell will discharge many spikes such that characteristics of the place itself, the exact coordinates in the room, becomes the dominant behavioural state that drives place cell activity. A similar anchoring to the environment occurs for an animal's sense of direction (e.g., coding in an allocentric reference frame), where head-direction (HD) cells fire as a function of the cardinal direction the animal faces in the environment (Taube, 1998), independent of the animal's behaviour or location (i.e., when facing east rather than to the right) (Taube et al., 1990).

Conversely, many sensorimotor computations are anchored in respect to the body and not the environment (e.g., they are viewpoint-dependent or egocentric in nature). Imagine the scenario of sitting behind a desk and wanting to grab a cup of coffee; first the visual information arrives on the retina that allows you to locate the cup from your perspective. Then, a series of sensorimotor transformations occur that combine the visual and proprioceptive signals to generate a motor plan that results in extending your arm and grabbing the object on your left (Flanders et al., 1992; Fogassi and Luppino, 2005; Pouget and Snyder, 2000; Snyder et al., 2000).

Allocentric or egocentric reference frames are not restricted to either domain however, and spatial representations co-exist and interact in both (Klatzky, 1998; Redish and Touretzky, 1997; Touretzky and Redish, 1996). On a behavioural level, this can be observed in experiments where participants have no access to external environmental information, yet are able to solve a spatial navigation task using only egocentric movement information during blind walking (Loomis et al., 1992). On a neural level, several functional neuron types in the posterior parietal cortex carry navigation-relevant information in different coordinate systems, such as neurons encoding visual spatial locations in a head-centred coordinate space (Andersen et al., 1985) or cells that are tuned to specific modes of the animal's movement irrespective of its location or heading (Whitlock et al., 2012).

In the previous chapter it became clear that there are differences in anchoring between border cells of different brain regions, where RSC neurons do not differentiate between wall identities but instead fire throughout the entire arena. This chapter will examine in detail the reference frames that RSC border cells utilize by mapping their activity to an egocentric coordinate system, instead of using allocentric 2-D firing rate maps. This egocentric analysis revealed that a subset of border cells displayed conjunctive tuning properties, where not only distance to the wall is a driving factor, but their receptive fields contain additional direction components. Global arena rotation experiments then revealed that this direction selectivity operates independently from the global direction signal as encoded by head-direction cells locally, while large-scale recordings from both hemispheres uncovered that the preferred direction of border cells is largely skewed across the population, with a strong tendency for tuning to the contra-lateral side.

RESULTS

RSC BORDER CELLS SHOW EGOCENTRIC DIRECTION TUNING PROPERTIES INDEPENDENT OF THE GLOBAL HD SIGNAL

To understand how RSC border cell activity is anchored to the environment, I performed additional analyses on the data collected previously by remapping the neural activity from allocentric x- and y-coordinates onto an egocentric reference frame. The first observation was that spikes alongside a single wall are clustered in terms of the heading direction of the animal, where the rat was facing the same direction for all activity nearby that wall (e.g., facing the north-east direction nearby the north wall) (**Figure 17A**). Typical allocentric 2-D rate maps do not capture this direction component, as it simply averages all activity for each spatial bin. Instead, I developed a new coordinate system that is egocentric in nature by having the body of the animal always as a fixed centre point (**Figure 17B**).

At each timepoint, the nearest wall occupies a spatial bin in this body-centric border map, where coordinates in polar space indicate distance and direction of the wall relative to the animal. The resulting egocentric border rate maps revealed distinct firing fields at specific locations, as directionally-tuned border cells fired predominantly whenever the wall occupied proximal space at a particular angle from the animal's viewpoint (**Figure 17C**).

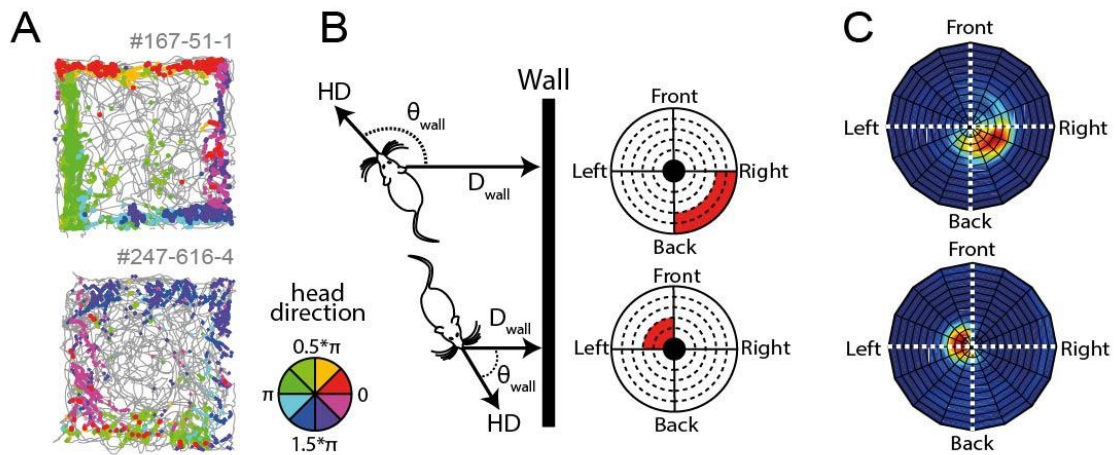


Figure 17. Egocentric direction tuning of RSC border cells.

(A) Example trajectory spike plots with spike locations color-coded according to the head-direction of the animal. Most spikes alongside a wall occur only when the animal was in a narrow range of directions. (B) Trajectory data was projected onto new body-centric border maps, where coordinates indicate the distance (D_{wall}) and direction (θ_{wall}) of the closest wall relative to the animal's position and head-direction (HD), respectively. (C) Rate maps in this border space for the same example cells as in (A).

When neurons display conjunctive coding properties, it's important to ensure this is not a result of merging two clusters together during the spike-sorting process. The semi-automatic spike-sorting algorithm Kilosort was used to assign spikes to individual clusters, with settings that promote over-clustering during the automated assignment (Pachitariu et al., 2016). This was followed by careful manual inspection of each cluster on its waveform and spiking properties, with particular care during the few merges that took place. Clusters were treated as individual neurons when their spikes formed well-isolated clusters in their loadings on Single Vector Decomposition (SVD) factors (**Figure 18G**). Those neurons that were classified as border cells with conjunctive tuning properties were well-isolated clusters in SVD space (**Figure 18G**) with waveforms indicative of pyramidal cells (**Figure 18F**), that displayed distinct firing fields in egocentric border space (**Figure 18D**), with no specific patterns in allocentric HD space (**Figure 18E**). These properties are indicative of neurons being sensitive to two different components of boundary information, namely the distance and direction relative to the animal.

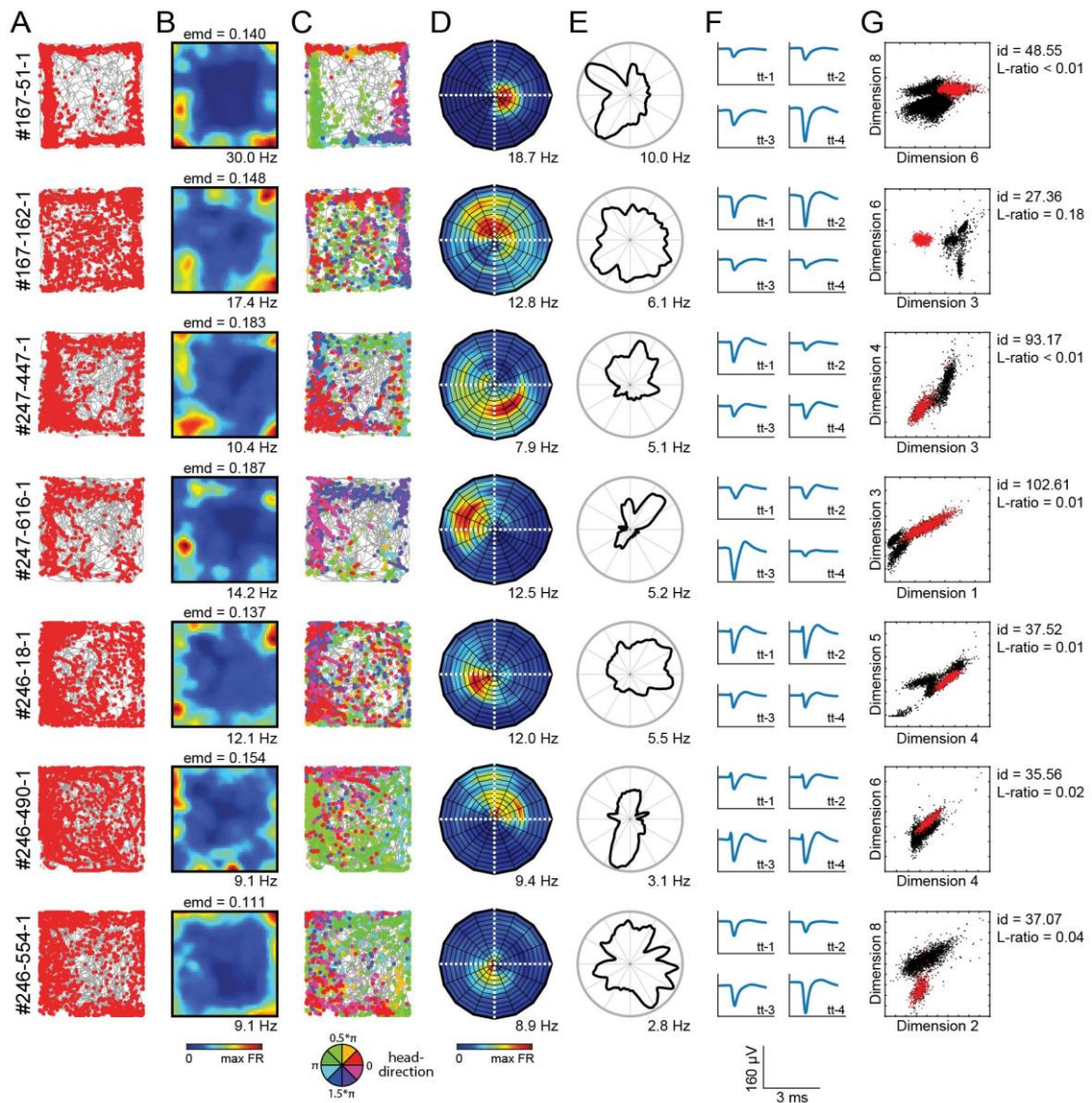


Figure 18. Neuron cluster properties along all behavioural axes.

Shown are example cells (one per row) with their firing properties across multiple behavioural variables, together with their cluster properties obtained during spike sorting. (A) Trajectory spike plots with the animal's trajectory (grey line) and his position in space (red dots) at the time of spiking. (B) Color-coded spatial rate map in allocentric space, with warm colours indicating higher firing rate. (C) Head-direction trajectory spike plots, with coloured dots indicating the head-direction of the animal at time of spiking. (D) Body-centric border rate maps, showing the firing rate with respect to the distance and direction of the boundary relative to the animal. (E) Firing rate as a function of global allocentric head-direction. (F) Cluster waveforms across four channels of the main tetrode where the cell was recorded. (G) Cluster factor loadings on two distinctive SVD factors used for cluster cutting during spike sorting in the Kilosort algorithm. Cluster quality metrics show isolation distance (id) and L-ratio (Schmitzer-Torbert et al., 2005).

I next sought to establish whether this egocentric constraint was imposed by the head-direction signal through the integration with spatial or sensory cues of the environment, as RSC receives inputs from the anterior limbic system that is a major source of head-direction signals, and a subpopulation of RSC cells are tuned to allocentric head-direction (Chen et al., 1994; Mitchell et al., 2018). If the egocentric boundary representation of RSC border cells is driven by internally generated global direction signals, realignment of the head-direction cells may affect the preferred tuning direction of RSC border cells. In order to manipulate the tuning of head-direction cells, four blue landmark LEDs were placed on one side of the maze while all other sensory cues were kept invariant across the environment. The entire experimental setup was then rotated 90° clockwise in the middle sessions (**Figure 19A**).

Head-direction cells that have their activity anchored to the salient landmark cues shifted their preferred tuning direction along with the arena rotation (example shown in **Figure 19B**), although across the population this shift was not a full 90° (A-A': median shift = 2.6°, $z = 1.23$, $p=0.23$; B1-B2: median shift = 0.8°, $z = 0.61$, $p=0.54$; A-B1: median shift = 62.9°, $z = 4.62$, $p=3.8 \times 10^{-6}$; A-B1 rotated: median shift = -27.3°, $z = -3.07$, $p=0.002$; Wilcoxon signed-rank test; Bonferroni-corrected $\alpha = 0.013$; $n = 28$ HD cells; **Figure 19E**). In contrast to head-direction cells, the border cells that had significant directional tuning did not shown any change in their preferred direction (two examples shown in **Figure 19C,D**), with no shifts across the population (A-A': median shift = 0°, $z = 0.14$, $p=0.89$; B1-B2: median shift = 0°, $z = -1.21$, $p=0.22$; A-B1: median shift = 0°, $z = 2.42$, $p=0.015$; A-B1 rotated: median shift = -68°, $z = -3.74$, $p=1.8 \times 10^{-4}$; Wilcoxon signed-rank test; Bonferroni-corrected $\alpha = 0.013$; $n = 31$ directionally-tuned border cells; **Figure 19E**).

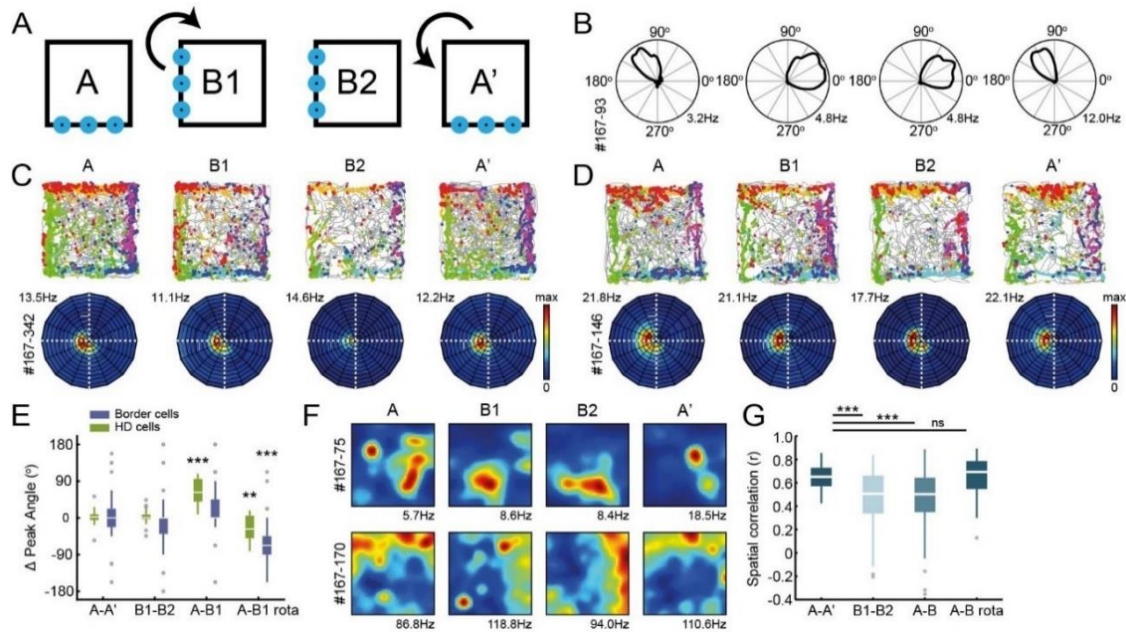


Figure 19. Egocentric direction tuning of RSC border cells functions independent of global head-direction signals.

(A) Behavioural rotation experiment, with blue LEDs placed as distal cues on one side of the maze, where the entire experimental set-up was rotated 90° clockwise in the middle sessions. (B) An example of an allocentric HD cell that was anchored to the environment, and shifted its tuning according to the rotation. (C-D) Two example border cells with trajectory spike plots (top row) and border rate maps (bottom row) showing egocentric border tuning was stable across rotation sessions. (E) Comparison of shifts in direction tuning for allocentric head-direction cells and egocentric border cells across the different sessions, where B1-rota is a rotated version of the rate map in the opposite direction of the physical rotation of the arena, matching the layout again as in A. (F) Two examples of spatially-stable cells, defined as having spatial correlations above the 99th percentile of a time-shuffled distribution, which rotated along with the cue. ** $p < 0.01$, *** $p < 0.001$, Wilcoxon signed-rank test

This result indicates that the direction tuning of RSC border cells is generated either through the local sensation of walls independent of the head-direction signal, or by the integration of allocentric boundary-position and head-direction coding that rotated together. The RSC's ability to discriminate between boundaries and objects, together with the

invariance of border tuning in the absence of visual or tactile signals, goes against the mechanism of local sensation. In support of the latter possibility, I explored how the cue rotation affected neurons in RSC that have position-selective firing, which were defined as cells with spatial correlations between rate maps of the first and last recording session above the 99th percentile threshold of a spike-shuffled distribution that were not border cells. These spatially modulated cells also shifted their firing patterns with the cue, as their rate maps rotated along with the arena (two example cells in **Figure 19F**; spatial correlations: A-A', $r = 0.63 \pm 0.018$, A-B, $r = 0.48 \pm 0.058$, Wilcoxon signed-rank test: $z = 3.52$, $p = 4.4 \times 10^{-4}$; A-B rotated, $r = 0.70 \pm 0.033$, Wilcoxon signed-rank test: $z = -1.07$, $p = 0.29$; $n = 32/384$ spatially stable cells; **Figure 19G**). It's likely that RSC border cells thus maintain their wall-tuning as a conjunctive code of position and head-direction information that rotated together with the environment.

EGOCENTRIC DIRECTIONAL TUNING IN RSC IS BIASED TO THE CONTRALATERAL SIDE OF THE RECORDED HEMISPHERE

After observing directional spike-trajectory plots and border rate maps of many RSC border cells it became clear that there was a strong overlap in tuning properties of neurons recorded in the same animal. For example, neurons shown in **Figure 19C,D** and the top two cells in **Figure 18C** are recorded in RSC in the right hemisphere of the same rat, with similar firing patterns nearby the walls (*e.g.*, all red/orange near the Northern wall, or light/dark blue near the Southern wall). To further investigate this pattern, I performed additional large-scale recordings across RSC in both left and right hemispheres. Due to the necessary angle of entry for tetrodes and the microdrive's inclination of 25° towards the midline (see

histology in **Figure 5A**), it was not possible to record from both hemispheres simultaneously, so this was done across different rats.

Among all recorded border cells that were identified with the EMD metric, 190 out of 485 neurons (39.2%) had significant egocentric directional tuning, with mean vector lengths (MVL) above the 95th percentile of a spike-shuffled distribution in all regular sessions (**Figure 20A,B**). The distribution of preferred directions of these egocentric border cells indeed showed a strong bias that was dependent on the hemisphere where cells were recorded from (Left hemisphere: mean direction = -114° , $z = 3.16$, $p=0.041$; $n = 41$ directionally-tuned border cells; Right hemisphere: mean direction = 41° , $z = 38.8$, $p=9.1 \times 10^{-19}$; $n = 149$ directionally-tuned border cells; Rayleigh test; comparing both distributions: two-sample Kuiper test, $k = 3.1 \times 10^3$, $p=0.001$; **Figure 20C**). The majority of border cells were tuned to the contralateral side of the recorded hemisphere, although not exclusively (**Figure 20C**).

There was a similarly skewed distribution in the distance tuning of cells, with cells firing predominantly when walls were in the very near proximity (**Figure 20D**), although some cells had fields at extended distances up to 20 cm away from the wall. One potential cause for this proximity bias could be the design of the original boundary template that has maximal weight only at the entire outer edge of the map, biasing selection to cells that follow that firing pattern. In order to account for this potential confound, I performed another classification procedure using additional templates with fields at increasing distances away from the wall (**Figure 20E**). Using this procedure, most original cells could still be captured using templates with fields up to 12 cm away, and although higher templates found some additional cells, no major new populations of border

cells were found using far-distance templates (**Figure 20E**). To find the distance limit at which cells would still be classified with the primary template, I further simulated a set of synthetic neurons that fired at specific wall distances using all behavioural data, and found that the boundary template was able to classify cells with firing fields up to 18 cm away from the walls (**Figure 20F**). Together these results confirm that the majority of RSC border cells exhibit distance tuning at the proximity of walls.

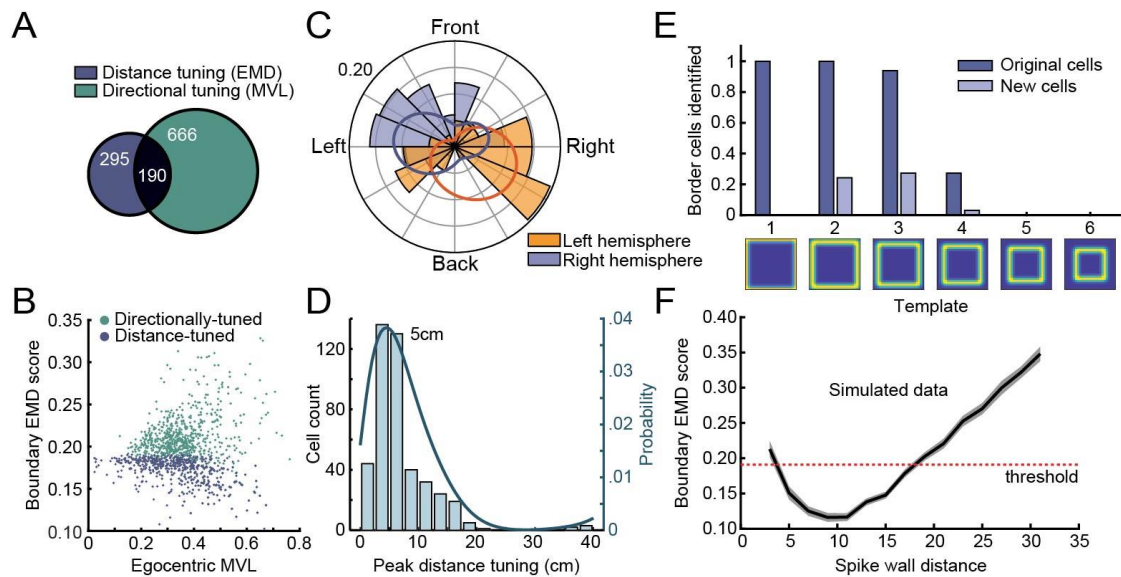


Figure 20. Directional and distance tuning properties of RSC border cells.

(A) Venn diagram showing the overlap between cells that display distance tuning (classified using the EMD scores) and cells with egocentric directional tuning to walls (classified using the egocentric boundary MVL). (B) Distribution of MVL values and EMD scores for cells that are significantly tuned to the distance or direction to the boundaries. (C) Preferred directional tuning of all recorded border cells with significant directional tuning, split according to the location of the electrode in either the left or right hemisphere. (D) Preferred distance tuning of all RSC border cells. (E) EMD classification of RSC border cells with a subset of data and different templates, each with firing fields at increasingly further distances from the wall (4 cm bins). Most original cells could be captured using templates with fields up to 12 cm away (template 3), and although higher templates found several additional cells, no major new populations of border cells were found using far-distance templates. (F) Simulated EMD scores of rate maps with synthetic spikes at specific distances away from the wall, simulated at 2 cm intervals using all behavioural sessions. Mean across cells (thick line) \pm SEM (shaded)

The hemisphere-specific tuning bias implies that boundary representations in RSC may be generated by direct sensory signals, or reflect the command of motor actions, in both of which it arises along the right-left body axis. The previous chapter has shown that boundary coding in RSC is unlikely to depend on direct sensory inputs, but this is further confirmed by the fact that a loss of tactile sensation through whisker trimming had no effect on the extent of directional tuning of border cells (before trimming: 7/49 cells had significant directional tuning, MVL = 0.538 ± 0.06 ; after trimming: 10/49 cells were significantly tuned, MVL = 0.502 ± 0.08 ; change in MVL: $t(6) = 1.80$, $p=0.12$, t-test; change in cell proportion: $z = 1.05$, $p=0.29$, binomial test; **Figure 15**), nor did recording in complete darkness affect the directional tuning of cells (light conditions: 5/21 cells had significant directional tuning, MVL = 0.326 ± 0.07 ; darkness: 4/5 cells maintained their tuning, 2/16 cells were tuned only in darkness, MVL = 0.318 ± 0.05 ; change in MVL: $t(4) = -0.51$, $p=0.64$, t-test; change in cell proportion: $z = 0.33$, $p=0.75$, binomial test; **Figure 13**), implying that this bias is not a direct consequence of the lateralized nature of sensory input.

DISCUSSION

Spatial navigation depends on a wide-range of functional cells types found in the brain, including cells that encode elements of one's current position, different aspects of motion, as well as parts of the external environment. Broadly speaking, these different types of cells can be segregated into two groups, where the brain forms spatial representations in two distinct references frames that are either viewpoint-dependent (i.e., egocentric) with activity anchored to the body, or viewpoint-independent (i.e., allocentric) with tuning that is anchored to the external world.

The brain is known to encode boundary information through the activity of allocentric border cells in MEC (Solstad et al., 2008) and boundary vector cells in Subiculum (Lever et al., 2009; Stewart et al., 2014), but the results described in this chapter are the first demonstration of boundary coding in an egocentric manner through the direction-selectivity of border cells in RSC. These neurons were first classified based on their firing in proximity of all walls of the environment, but remapping of their activity onto egocentric border axes showed distinct firing fields at a specific angle from the animal's facing direction. From all recorded border cells, approximately 40% displayed significant selectivity to the direction of walls that was predominantly contra-lateral to the electrode, such that a neuron in left RSC is active whenever a wall occupies proximal space on the right side of the animal. Using a cue-rotation paradigm, I was able to show that this direction selectivity of RSC border cells does not result from the input of local head-direction cells, as these HD cells rotated their preferred direction tuning along with the environment while border cell tuning remained unchanged.

It remains unclear then what are the exact circuit mechanisms in place that provide these border cells their tuning properties. During the execution of these experiments, several related reports came out that proposed an answer. A series of papers described egocentric tuning properties and anchoring to local features of the environment across different brain regions, starting with egocentric tuning to objects in the lateral entorhinal cortex (Wang et al., 2018), then selectivity for the direction to the centre of the maze in the postrhinal cortex (LaChance et al., 2019), and finally directional selectivity for walls in parahippocampal regions (Gofman et al., 2019), the dorsomedial striatum (Hinman et al., 2019) and also RSC (Alexander et al., 2020). These authors proposed that all egocentric representations are generated based on egocentric sensory information, and originate from early cortical and thalamic processing to provide egocentric spatial information to the hippocampus and MEC. While there is indeed network connectivity in place to support this process, their reasoning is based on work that is phenomenological in nature, and no concrete evidence yet exists for this sensory hypothesis.

My earlier experiments have shown already that RSC border cells likely discriminate boundaries based on a global spatial layout of the environment, and maintain both their distance and direction tuning to walls in the absence of direct sensory detection. However, the next chapter will address the open question whether RSC neurons indeed provide their egocentric spatial information to related allocentric cells in the parahippocampal regions.

Chapter IV

Circuit dynamics and manipulations with the medial Entorhinal Cortex

The results and figures presented in the following chapter have been published previously in *eLife* under the citation below. Experiments that provided results shown in **Figure 21-Figure 25** were performed in collaboration with Hiroshi Ito.

van Wijngaarden, J. B. G., Babl, S. S., & Ito, H. T. (2020). Entorhinal-retrosplenial circuits for allocentric-egocentric transformation of boundary coding. *Elife*, 9, e59816. DOI: 10.7554/eLife.59816

INTRODUCTION

Borders and walls make up the most stringent restriction for possible trajectories through space, in particular in an open field environment used in many spatial navigation experiments. The study of spatial representations in the brain that support navigation has produced a large number of spatially tuned cells, but it was clear already early on that borders play an important role in these spatial computations. For example, place cells were able to maintain their place fields relative to a fixed cue card in the event of isotropic scaling of a cylindrical arena, although a number of cells also completely remap the location of their field (Muller and Kubie, 1987). In case of anisotropic scaling of a squared arena along one axis, place cells have been shown to morph their firing field alongside the same axis (O'Keefe and Burgess, 1996b). These experiments led to computational models that predicted the presence of border cells, neurons that provide distance and direction information of borders to spatial cells in the hippocampus and parahippocampal regions (Barry et al., 2006; Hartley et al., 2000). The models demonstrated that border distance input allows for place cells to fire in locations away from walls, without depending on the integration of movement information, and could account for the scaling of field properties after environmental reshaping.

Two groups subsequently described the presence of this cell type in the brain, first the border cell in the medial entorhinal cortex that is active nearby specific walls in any orientation of the animal (Solstad et al., 2008), and secondly the boundary vector cell that carries both distance and direction information to an allocentric wall (Lever et al., 2009). Since their discovery, borders have been shown experimentally to play an important

role also for the activity of grid cells, for example, borders can serve as an error-correction mechanism where the precision of grid cell spiking decreases as a function of time since last encountering a wall (Hardcastle et al., 2015). The location of a grid cell's firing fields (e.g., the grid phase) has furthermore been shown to be tethered to boundaries in case of global arena rescaling (Keinath et al., 2018), while local modification of walls affects grid cell firing by causing local transformations of the grid field map (Krupic et al., 2018).

Authors of these studies hypothesized that this influence of the arena's borders comes from direct interactions between the border and grid cells in MEC, but no direct evidence of this interplay yet exists. In fact, many questions remain regarding the circuit mechanisms that underly the activity of border cells in the brain, both in MEC, subiculum and now also in RSC. Anatomical tracing studies have shown that all three regions are interconnected with direct, bi-directional connections between each of them (Ding, 2013; van Groen and Wyss, 1990, 1992; Van Groen and Wyss, 2003; Jones and Witter, 2007; Sugar et al., 2011), but is not known how these border cells across regions interact, nor whether there is any functional interdependence.

In order to dissociate the contribution of the different types of border cells in the brain, and to establish the extent of communication between them, this Chapter will uncover part of the border coding network by studying the interplay between border cells in MEC and RSC. To do so, I took advantage of two particular methods that have been developed over the last decade, optogenetics and pharmacogenetics. Both are targeted, non-invasive circuit manipulation techniques that allow for the activation or

silencing of individual neurons in a particular brain region in awake and behaving animals. First, I down-regulated activity in either MEC or RSC while recording the activity of border cells in the opposing brain region, and established that communication is unidirectional, with information flowing from the MEC to RSC but not vice versa. I then used optogenetics to confirm that specifically the MEC→RSC pathway is involved in the transfer of border information. Finally, I used information theory metrics to show how border information between both brain regions is different in terms of their relationship with the animal's behaviour.

RESULTS

INHIBITION OF MEC INPUT DISRUPTS BORDER CODING IN RSC BUT NOT VICE VERSA

The first goal was to establish whether there is any communication occurring between border cells in MEC and RSC. This pathway is known to have direct and bi-directional anatomical connections (Jones and Witter, 2007; Ohara et al., 2018; Sugar et al., 2011), but no previous studies have looked at functional connectivity between both regions. To study their interactions, an AAV was used that encoded Designer Receptors Exclusively Activated by Designer Drugs (DREADDs), G protein-coupled receptors that are activated by a bioavailable compound (clozapine-N-oxide; CNO) (Armbruster et al., 2007; Urban and Roth, 2015). The AAV construct (AAV8-hSyn-hM4Di-mCherry) expressed inhibitory receptors hM4Di in transfected neurons, which elicit a G protein inward-rectifying potassium channel (GIRK) response upon activation that attenuates neuronal activity and neurotransmitter release (Armbruster et al., 2007). While the agonist CNO has been shown to specifically target DREADDs, it can undergo metabolic transformation to clozapine which has affinity with many other receptors in the brain, most notably nearly all endogenous subtypes of the serotonin (5-HT) receptor (Roth et al., 2004; Yadav et al., 2011). So instead of CNO, the alternative Agonist-21 (11-(1-piperazinyl)-5H-dibenzo[b,e][1,4] diazepine) was used to selectively activate DREADDs with fewer off-targets (Thompson et al., 2018).

The virus was first injected in bilateral MEC, together with the implantation of a 28-tetrode microdrive in the right RSC to record neural activity (**Figure 21A,B**). A volume of 1000 nL was sufficient to diffuse and transfect neurons across most of the MEC region (**Figure 21C**). Recording experiments began several weeks after virus injection to allow enough time for cells to express DREADDs. In order to verify success of the

manipulation, several additional tetrodes were placed nearby the virus injection site. During the experiment, Agonist-21 was administered to the animals subcutaneously, and after passing through the blood-brain barrier was able to activate DREADDs 20 mins after the injection (**Figure 21D**). As a result, 59% (26/44) of neurons were affected by the manipulation, showing disrupted activity and reducing their spikes rates to $47.2 \pm 5.5\%$ (mean \pm S.E.M.) of baseline firing (**Figure 21D**).

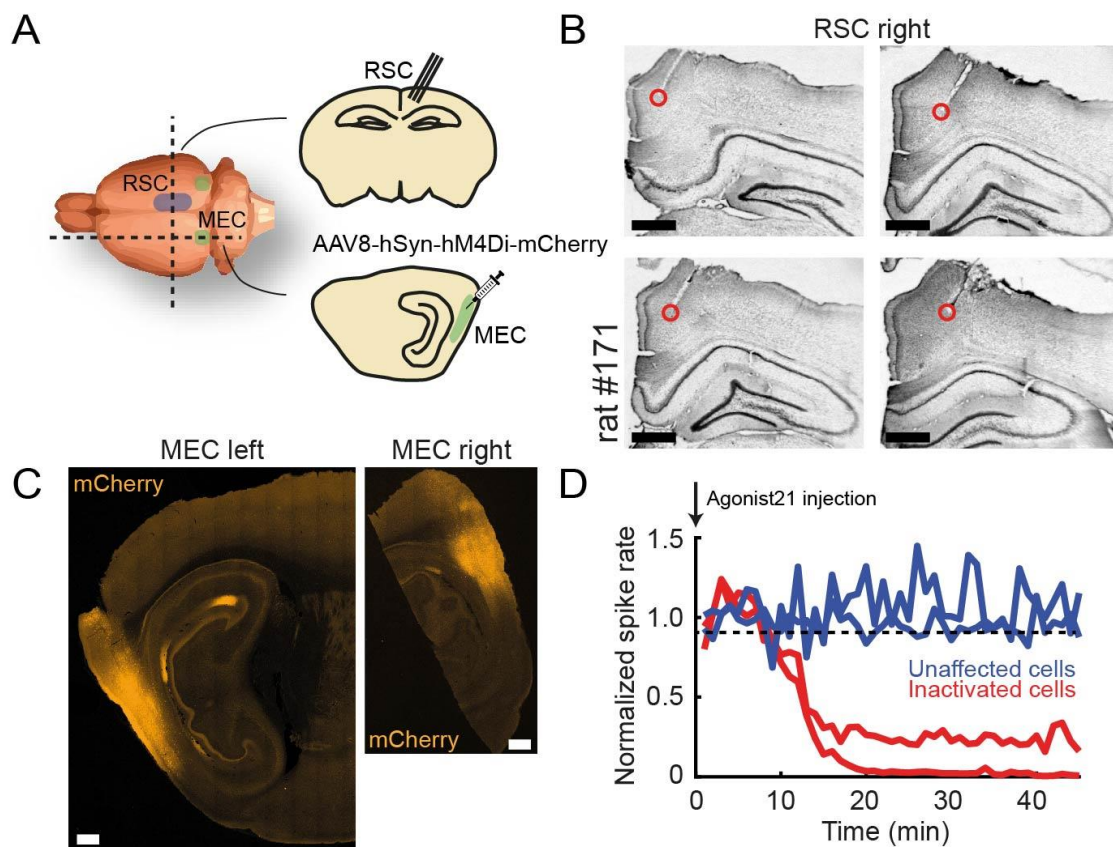


Figure 21. Inhibiting neural activity in MEC using chemogenetics.

(A) An AAV encoding inhibitory DREADDs hM4Di was injected into MEC, while a microdrive with tetrodes was implanted in RSC to record neural activity. (B) Nissl-stained coronal sections of the right RSC showing tetrode tracts and recording locations. Red circles indicate the final position of the tetrode. Scale bar, 1 mm. (C) Sagittal sections of left and right MEC showing the bilateral virus injection sites, with mCherry as a fluorescent marker in the virus construct. Scale bar, 1 mm. (D) Several additional tetrodes were placed nearby the virus injection site to confirm activity manipulation. Shown are activity traces of transfected cells (red; $p < 0.05$, Wilcoxon ranksum test for spike rate changes between 0–10 min and 30–40 min) and unaffected cells (blue) after subcutaneous administration of Agonist-21 (DREADDs agonist), with the down-regulation of activity to below 50% of baseline firing after 20 min.

In order to study the effects of MEC inhibition on RSC cell firing, first a recording session was performed to measure firing properties of RSC border cells under normal conditions, where animals were free to forage an open-field arena. Then, animals were injected with Agonist-21 subcutaneously, followed by 30 mins of waiting time for the drug to take effect. Finally, another recording session was made, now with the down-regulation of neural activity in MEC. It is known that cell activity in MEC is related to movement of the animal, in particular running speed that is encoded in the activity of ‘speed cells’ which are characterised by a positive, linear response to running speed (Kropff et al., 2015). But in the manipulated session, animals did not show any abnormal navigation behaviour, as they continued to move around the arena without changes in their running speed profiles ($p > 0.05$; Friedman test; **Figure 22A**). However, inhibition of activity in MEC did affect cell firing in RSC, where a subset of RSC border cells had reduced spatial selectivity and disrupted boundary tuning (examples shown in **Figure 22B**).

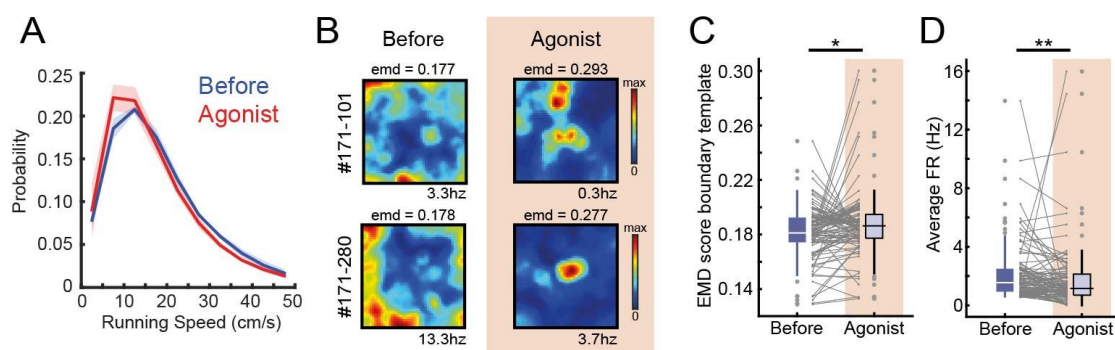


Figure 22. Sharp boundary tuning of RSC border cells is disrupted upon inhibition of MEC.

(A) Administration of Agonist-21 and the subsequent reduction in MEC cell firing had no effect on the animal’s running speed during free foraging of the arena. (B) Two example RSC border cells that were affected by MEC inhibition and lost their spatial tuning. (C-D) Across the population, border cells in RSC exhibited increased EMD scores as well as lower firing rates after inhibition of MEC. Grey lines indicate individual neurons. * $p < 0.05$, ** $p < 0.01$, Wilcoxon signed-rank test

The population of border cells had reduced border tuning that manifested in an overall increase in EMD scores (before: EMD score = 0.181 ± 0.002 , after: EMD score = 0.186 ± 0.003 ; Wilcoxon signed-rank test: $z = -2.40$, $p=0.016$; $n = 102$ border cells; **Figure 22C**), while their overall firing rates were also reduced (before: FR = 1.52 ± 0.20 Hz, after: FR = 1.12 ± 0.24 Hz, Wilcoxon signed-rank test: $z = 3.15$, $p=0.0016$; **Figure 22D**).

After observing that MEC inhibition affects border tuning in RSC, the next question was whether the opposite effect also holds true. Does border cell firing in MEC depend on RSC input in a similar manner? To answer this question, the following reversed experiment was performed, where the same AAV construct was injected into bilateral RSC, while a microdrive with 28 tetrodes was placed in MEC, split evenly between the left and right hemisphere (**Figure 23A-C**). Tetrodes near the virus injection site again confirmed that the administration of Agonist-21 successfully inhibited cells in MEC transfected with the virus, where 70% (14/20) of the MEC cells decreased their spiking rate to $53.0 \pm 6.4\%$ of baseline firing (**Figure 23D**). Unlike the previous manipulation however, RSC inhibition had no immediate effect on border cell firing in RSC, with no significant changes in their border tuning (before: border score = 0.53 ± 0.013 , after: border score = 0.53 ± 0.01 ; Wilcoxon signed-rank test: $z = 0.56$, $p=0.57$; $n = 83$ border cells; **Figure 23E,F**), nor a change in their overall firing rates (before: FR = 1.33 ± 0.11 Hz, after: FR = 1.27 ± 0.12 Hz; Wilcoxon signed-rank test: $z = -0.31$, $p=0.76$; **Figure 23G**).

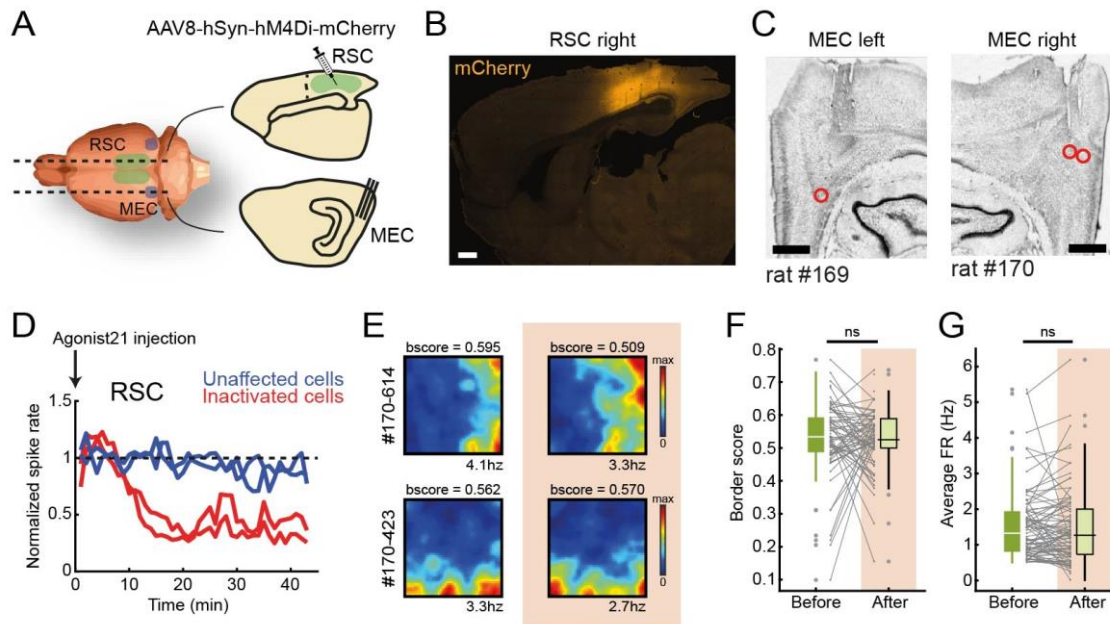


Figure 23. Reverse manipulation experiment, inhibiting activity in MEC while recording from RSC border cells.

(A) Electrophysiological recordings were performed in MEC, while DREADDs were expressed in bilateral RSC (B) Sagittal section of RSC showing spread of the virus across most of RSC, covering both dorsal and ventral parts. (C) Sagittal Nissl-stained sections of left and right MEC with tetrode tracts, with red circles highlighting the final tetrode positions. (D) Tetrodes placed near the virus injection site confirmed successful inhibition of affected cells 15-20 min after subcutaneous administration of Agonist-21. (E) Two example MEC border cells that were unaffected by inhibition of RSC. (F-G) Border cells in MEC did not show any significant qualitative changes in border tuning or firing rates after RSC inhibition. Grey lines indicate individual cells. Wilcoxon signed-rank test.

These DREADD-manipulation experiments suggest that MEC signals are involved in the transfer of spatial information to border cells in RSC, while this does not seem to be the case in the opposite direction. However, it's possible that MEC inhibition had only an indirect effect on RSC activity, for example, by reducing inputs to other communication partners of RSC such as the subiculum (Roy et al., 2017). To account for this possibility, two additional experiments were performed that directly target the MEC-RSC pathway, using optogenetic methods.

This technique relies on photoreceptors in the cell membrane, first discovered as the protein bacteriorhodopsin in the Halobacteria (Oesterhelt and Stoeckenius, 1973), which express light-activatable proton-pumps that pump protons across the cell membrane in the presence of light. The optogenetic approach is to modify an AAV to genetically encode light-gated proton channels, typically channelrhodopsin-2, and express them in neurons by injecting the virus construct into the relevant brain area (Nagel et al., 2003).

For the purpose of this experiment, two inhibitory variants of optogenetics were used to silence, rather than activate, the MEC-RSC pathway. First, an AAV was injected into MEC that encoded inhibitory Halorhodopsin chloride pumps (eNpHR3.0), which is a light-gated transmembrane ion pump for chloride ions that hyperpolarizes the cell membrane upon activation (Zhang et al., 2007). These inhibitory ion pumps are then expressed throughout the neuronal compartments of transfected cells in MEC, and by intracellular anterograde transport this includes the axons that terminate in RSC (**Figure 24A**). An optrode was then implanted into RSC, which allows for electrophysiological recordings of border cell activity using tetrodes, combined with an optic fibre to deliver light where cells are recorded to specifically inhibit axon terminals of RSC-projecting neurons in MEC (**Figure 24A**). The second approach was to inject a retrograde AAV construct into RSC, which encoded red-shifted Cruxhalorhodopsin chloride pumps (Jaws) that are expressed at the cell body located in MEC due to retrograde intracellular transport (Chuong et al., 2014; Tervo et al., 2016). This was combined with the placement of an optical fibre at the dorsal edge of MEC, which could be used to deliver light and inhibit activity of cells that project to RSC (**Figure 24B**). A 64-channel silicon probe was further implanted in RSC to simultaneously record the activity of border cells.

During the experiment, activation of laser light while the animal explored the arena led to a subsequent disruption of border coding in RSC, as cells lost specificity of firing near the edges and formed firing fields in the centre of the arena (**Figure 24C,D**). This resulted in an increase in EMD dissimilarity scores across the population, both for axon-terminal inhibition (Boundary EMD score: laser OFF1, 0.187 ± 0.003 , laser ON, 0.203 ± 0.003 , laser OFF2, 0.190 ± 0.005 ; Friedman test: $X^2(2)=6.9$, $p=0.032$; Post-hoc Wilcoxon signed-rank test: OFF1-ON, $z = -3.45$, $p=5.7 \times 10^{-4}$, OFF1-OFF2, $z = -1.55$, $p=0.12$; Bonferroni-corrected $\alpha = 0.025$; $n = 34$ border cells; **Figure 24E,F**), and cell-body inhibition (Boundary EMD score: laser OFF1, 0.184 ± 0.002 , laser ON, 0.192 ± 0.002 , laser OFF2, 0.189 ± 0.002 ; Friedman test: $X^2(2)=24.5$, $p=4.7 \times 10^{-6}$; Post-hoc Wilcoxon signed-rank test: OFF1-ON, $z = -4.97$, $p=6.7 \times 10^{-7}$, OFF1-OFF2, $z = -4.11$, $p=4.0 \times 10^{-5}$; Bonferroni-corrected $\alpha = 0.025$; $n = 141$ border cells; **Figure 24E,F**) that partially recovered after turning laser light off.

For border cell classification, neurons were allowed to have average firing rates below the rate threshold of 0.5 Hz in the manipulated session, as a reduction in spiking rate indicates disrupted coding. In order to confirm that increased EMD scores during MEC inhibition were not driven by spurious rate maps of low-firing cells, the EMD analysis was repeated after excluding all cells with an average firing rate below 0.5 Hz in the laser ON session (axon-terminal inhibition, identical results with 34/34 cells; cell-body inhibition, Boundary EMD score: laser OFF1, 0.183 ± 0.002 , laser ON, 0.192 ± 0.002 , laser OFF2, 0.189 ± 0.002 ; Friedman test: $X^2(2)=26.9$, $p=1.4 \times 10^{-6}$; Post-hoc Wilcoxon signed-rank test: OFF1-ON, $z = -5.26$, $p=1.4 \times 10^{-7}$, OFF1-OFF2, $z = -4.51$, $p=6.6 \times 10^{-6}$; Bonferroni-corrected $\alpha = 0.025$; $n = 138/141$ border cells), but results were very similar.

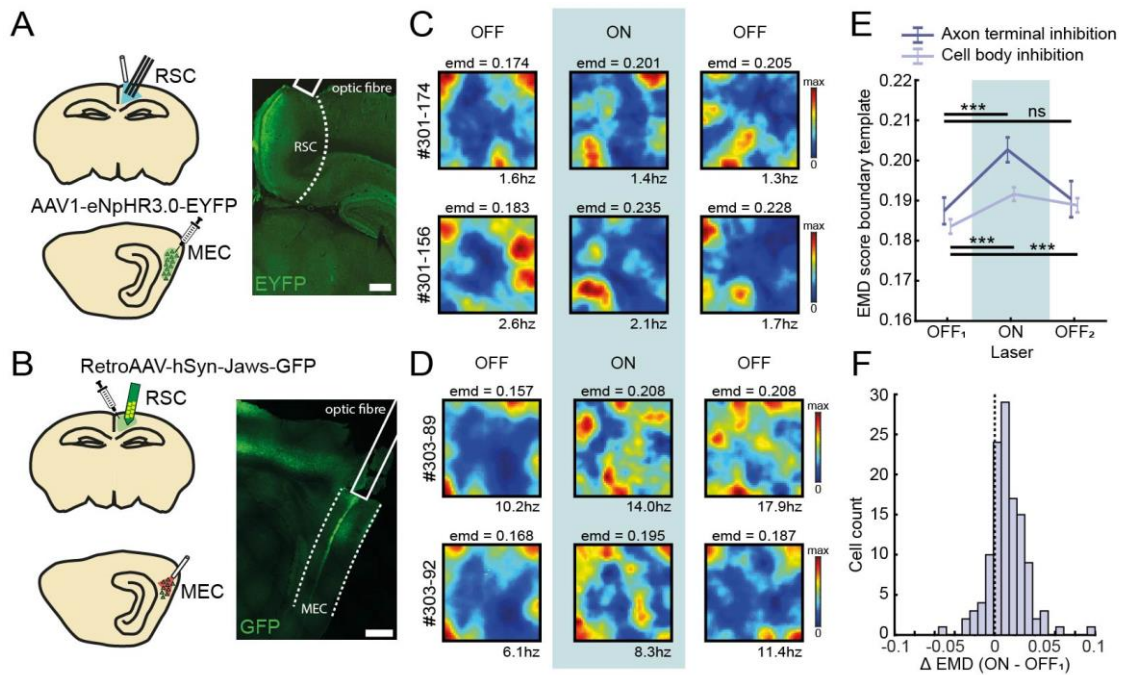


Figure 24. Pathway-specific inhibition of MEC input to RSC using optogenetics. (A) An anterograde AAV construct encoding inhibitory Halorhodopsin channels was injected into MEC, while an optrode with tetrodes and optic fibre was implanted in RSC to inhibit MEC axon terminals. Coronal section shows axons terminate mostly in the superficial layers close to the midline. Scale bar, 1 mm. (B) A retrograde AAV encoding red-shifted inhibitory Crux-halorhodopsin (Jaws) channels was injected into RSC together with the implantation of a 64-channel silicon-probe, while an optic fibre was placed at the dorsal edge of MEC for the silencing of cells that project to RSC. Histology shows the expression of the virus in neurons located in deep layers of MEC. Scale bar, 1 mm. (C) Spatial rate maps of two example border cells in RSC that show disrupted border tuning during local inhibition of MEC input. (D) Two example border cells in RSC that lose their spatial selectivity after cell-body inhibition of neurons in MEC that project to RSC. (E) RSC border cells showed disrupted border tuning on a population-level, resulting in higher EMD scores as a direct result of MEC inhibition in both types of manipulations. (F) Distribution of changes in EMD scores for RSC border cells between rate maps of the first laser OFF and ON session. *** $p < 0.001$, Wilcoxon signed-rank test

Unlike the DREADD-mediated manipulation however, RSC border cells did not change their overall firing rates, but only the spatial selectivity of these spikes (Laser ON: normalized FR = 0.94 ± 0.04 , Wilcoxon signed-rank test: $z = 1.68$, $p = 0.09$; laser OFF2: normalized FR = 0.96 ± 0.04 , Wilcoxon signed-rank test: $z = -1.80$, $p = 0.07$; **Figure 24A**). Additional

analyses of the animal's behaviour showed that the manipulation was specific to cell firing, but had no observable effects on navigation behaviour, with no changes in their profiles of running speed, head-direction or distance to the nearest boundary (**Figure 25B-D**).

Inhibition of the MEC-RSC pathway had considerable post-synaptic effects on border cells in RSC. But this pathway could be important also for encoding other spatial variables, given the presence of spatially-stable cells and head-direction in both RSC and MEC (**Figure 19B,F**). In contrast to the effects for border cells, the manipulation did not lead to any measurable changes in the firing properties of head-direction cells, as they continued firing normally during MEC input inhibition (Average FR: laser OFF1, 1.86 ± 0.53 , laser ON, 1.68 ± 0.61 , laser OFF2, 1.91 ± 0.62 ; Friedman test: $X^2(2)=0.17$, $p=0.92$; $n = 47$ HD cells; **Figure 25F**), with similar mean vector lengths (MVL: laser OFF1, 0.29 ± 0.03 , laser ON, 0.26 ± 0.03 , laser OFF2, 0.28 ± 0.03 ; Friedman test: $X^2(2)=6.64$, $p=0.036$; Post-hoc Wilcoxon signed-rank test: OFF1-ON, $z = 2.17$, $p=0.030$, OFF1-OFF2, $z = 1.92$, $p=0.055$; Bonferroni-corrected $\alpha = 0.025$; **Figure 25G**) and without a shift in their preferred direction (Shift in preferred direction: laser OFF1-ON, 0.056 ± 0.06 ; Wilcoxon signed-rank test: $z = 0.95$, $p=0.34$; laser OFF1-OFF2, -0.005 ± 0.07 ; Wilcoxon ranksum test: $z = 0.20$, $p=0.84$; Bonferroni-corrected $\alpha = 0.025$; **Figure 25H**). This would indicate that the head-direction signal in RSC is likely provided by brain regions other than MEC, for example, the anterodorsal thalamic nucleus (Mitchell et al., 2018). A different picture emerged for the spatially-stable cells, which were classified based on significantly high correlations between spatial rate maps of sessions without

laser light. In the presence of laser light, and with the inhibition of MEC input, these cells showed a drop in their spatial correlations (spatial correlations: laser OFF1-OFF2, $r = 0.59 \pm 0.02$, laser OFF1-ON, $r = 0.44 \pm 0.03$; Wilcoxon signed-rank test: $z = 5.87$, $p = 4.5 \times 10^{-9}$; $n = 83$ spatial cells; **Figure 25E**), suggesting that their spatial selectivity is contingent on information coming from MEC.

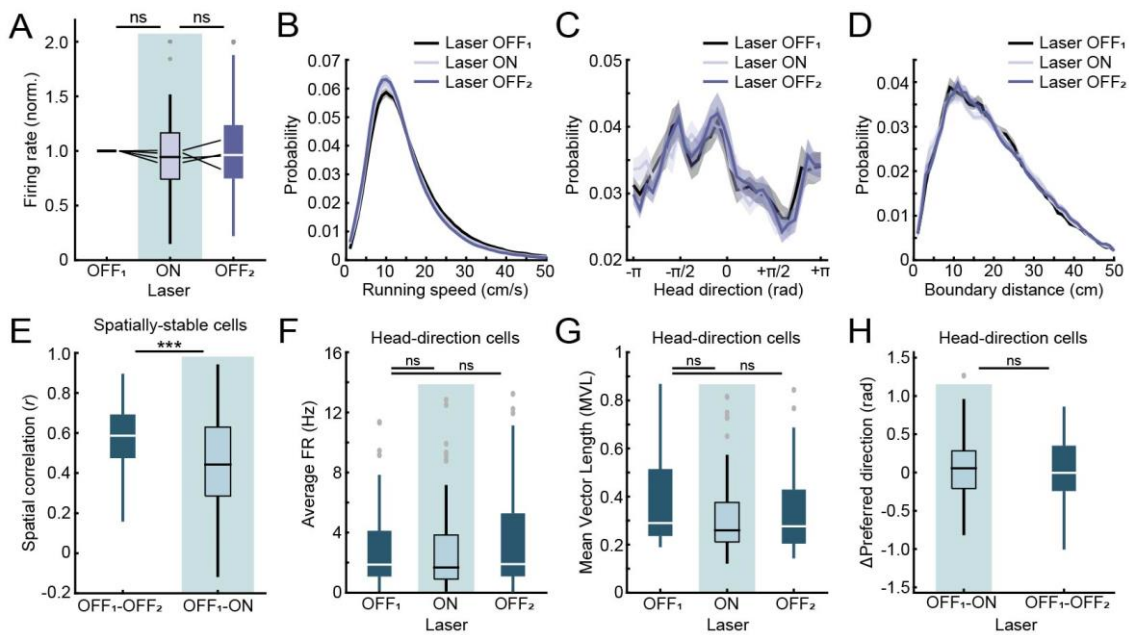


Figure 25. Additional effects of optogenetic inhibition of MEC.

(A) Distribution of overall firing rates of RSC border cells during and after the manipulation. (B-D) Behavioural profiles of the animal's running speed (B), head-direction (C) and distance to any boundary (D) during the experimental sessions. (E) Spatial correlations of spatially-stable cells in RSC ($n = 83$ spatial cells), classified with spatial correlations between rate maps of both laser OFF sessions above the 99th percentile of a shuffled distribution that were not border cells. (F-H) Tuning properties of head-direction cells in RSC. *** $p < 0.001$, Wilcoxon signed-rank test

It's important to note that one potential issue with optogenetic techniques is that light is delivered through an optic fibre connected to high-intensity lasers, and this illumination invariably generates heat inside the brain tissue (Owen et al., 2019). Many biological processes are heat-sensitive and their efficacy or function can change depending on changes in temperature (Yizhar et al., 2011). In order to account for the potential confound of circuit manipulation that is solely caused by the light application method, and not input-specific inhibition, an additional control experiment was performed under the same conditions as the original optogenetic experiments, but without opsin expression (**Figure 26A**). Recording of RSC border cells in the absence of inhibitory opsin expression showed stable firing patterns for border cells near all boundaries of the environment (**Figure 26B,C**), before, during and after the application of laser light, with no changes for the neurons in their EMD scores (Boundary EMD score: laser OFF₁, 0.173 ± 0.002 , laser ON₁, 0.176 ± 0.003 , laser ON₂, 0.174 ± 0.004 , laser OFF₂, 0.170 ± 0.001 ; Friedman test: $X^2(3)=5.44$, $p=0.14$; $n = 33$ border cells; **Figure 26E**) or overall firing rates (FR: laser OFF₁, 2.95 ± 0.72 , laser ON₁, 2.43 ± 0.75 , laser ON₂, 2.39 ± 0.88 , laser OFF₂, 2.78 ± 0.68 ; Friedman test: $X^2(3)=2.64$, $p=0.45$; **Figure 26D**). This result confirms that the impairment of boundary tuning in RSC during laser application is indeed specific to the silencing of MEC inputs.

Altogether these manipulation results confirm that both RSC and MEC are involved in a broader border coding network, where border representations in RSC are dependent on direct inputs from MEC but not vice versa.

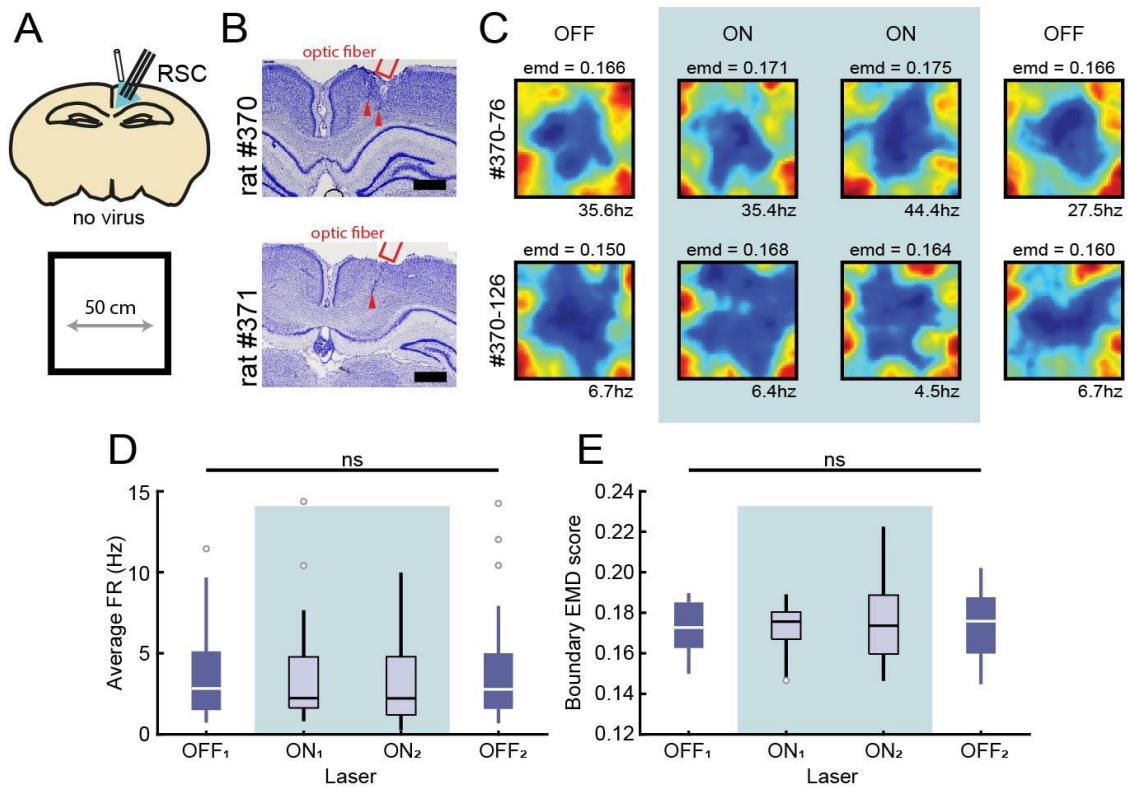


Figure 26. Control experiment for optogenetic-mediated manipulations to address the tissue heating confound.

(A) In order to account for non-specific manipulation effects such as tissue heating, no inhibitory opsins were expressed for two control animals while exposing the recorded neurons to laser light as animals navigated an open field arena. (B) Nissl-stained coronal sections showing recording locations of the tetrodes in RSC. (C) Spatial rate maps of two example neurons that were unaffected by exposure to laser light, and maintained their sharp boundary tuning near the edges. (D) Across the population, border cells did not increase or decrease their firing during the laser application. (E) Border cells also retained their spatial selectivity with no changes in EMD scores. Friedman test

RSC BORDER CODING IS MORE LOCAL AND CORRELATED WITH THE ANIMAL'S FUTURE MOTION

The previous results have shown that MEC input is necessary to maintain sharp border tuning in RSC. However, border cells in both regions do not encode boundary information in the same manner, where border cells in MEC have different firing properties than those in RSC. For example, border cells in MEC are allocentric in nature, and generally fire whenever the animal is close to only one or two walls of the arena, but remain silent nearby the other borders (**Figure 27A**, bottom). Conversely, many border cells in RSC have an egocentric direction component, and cell firing occurs alongside all of the available walls (**Figure 27A**, top).

This brings up the question what kind of information is transferred from MEC to RSC that is necessary for RSC border cells to generate their activity. To address this issue, I applied a set of spike information analyses to data of border cells from both anatomical regions in order to compare the content and nature of spatial information present in their spiking activity in respect to the animal's behaviour.

A comparison of properties of the firing fields from all recorded neurons showed that RSC border cells indeed show low variability when comparing fields between the available walls, as opposed to high variance for MEC cells (variance between average FR near each wall: RSC, $CV = 0.103 \pm 0.004$, MEC, $CV = 0.458 \pm 0.02$; Wilcoxon ranksum test: $z = -13.25$, $p = 4.6 \times 10^{-40}$; **Figure 27B**), confirming the allocentric spatial selectivity in MEC but not RSC. Border cells in MEC further showed stronger firing when walls were in the cell's receptive field, with higher field peak firing rates (RSC: FR = 4.02 ± 0.53 Hz, MEC: FR = 5.30 ± 0.47 Hz, Wilcoxon ranksum test: $z = 2.79$,

$p=0.0053$; **Figure 27C**). When comparing their directional selectivity, RSC border cells that showed significant directional tuning were nearly all tuned only for egocentric boundary-direction, but not allocentric head-direction (**Figure 27D**). In case of MEC, the complete opposite was observed, where border cells that showed any direction tuning predominantly had conjunctive selectivity for allocentric head-direction, but not boundary-direction (**Figure 27D**). However, both groups of border cells had nearly identical distributions for their preferred distance tuning (**Figure 20D**, **Figure 27E**).

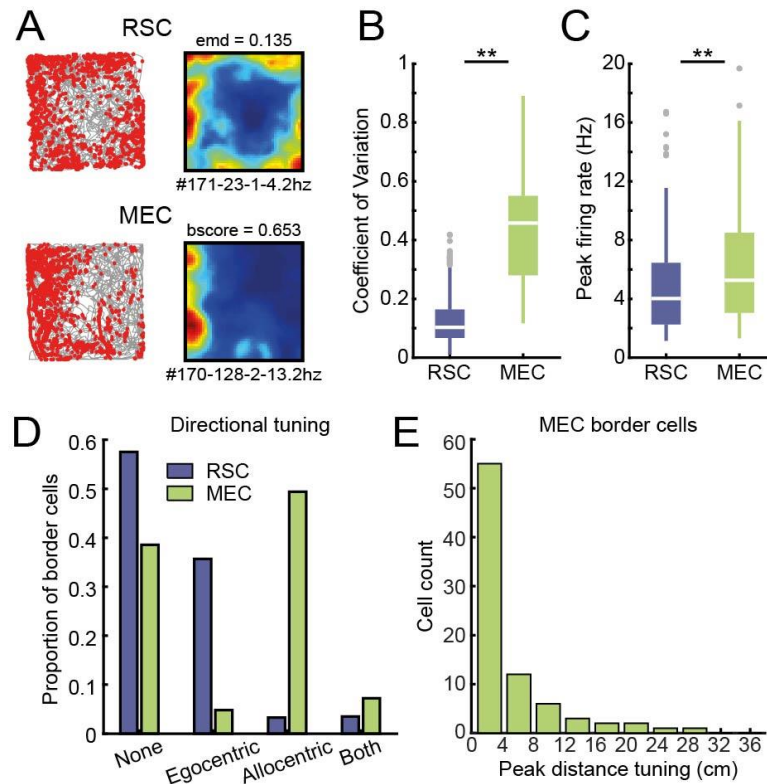


Figure 27. Firing field and border tuning analyses of border cells in MEC and RSC. (A) Spike trajectory plots (left) and spatial rate maps (right) of typical border cells recorded in RSC and MEC. (B) Coefficient of variation (CV) between average firing rates alongside each wall for RSC and MEC border cells. (C) Peak firing rates in the spatial rate map fields of border cells. (D) Proportion of border cells in RSC and MEC that had significant directional tuning to allocentric head-direction or egocentric boundary-direction. (E) Distribution of peak distance tuning for MEC border cells. ** $p<0.01$, Wilcoxon ranksum test

The next step was to investigate how much distance information was present in the spiking activity of border cells. A support vector machine (SVM) classifier used the population spiking activity of all border cells recorded simultaneously in either brain region to decode the animal's distance away from the wall in 10 cm distance bins. This decoder performed with high accuracy when using spiking activity from cells in MEC or RSC in the lower distance range ($p < 0.05$ for 0–20 cm, compared with a chance level of 20%; **Figure 28A**). However, decoding performance from RSC activity dropped to chance-level in the higher distance range ($p > 0.05$ for 30–50 cm; **Figure 28A**), suggesting RSC border cells mainly encode local information, which matches firing properties of RSC cells which have preferred distance tuning up to 20 cm away from the wall (**Figure 20D**).

Conversely, MEC computes distance information that extends well towards the centre of the arena, with decoding performance above chance-level until the maximum range of 50 cm ($p < 0.05$ for 0–50 cm; **Figure 28A**). Even though MEC border cells fire maximally at the edge of the arena, the correlation between population vectors of activity decayed faster over neighbouring distance bins for cells in MEC, particularly when the animal was more than 20 cm away from the wall (**Figure 28B,C**). This suggests more heterogeneity in firing across the population of MEC border cells at this farther distance, which allows the population to better distinguish wall distance, giving increased decoding performance.

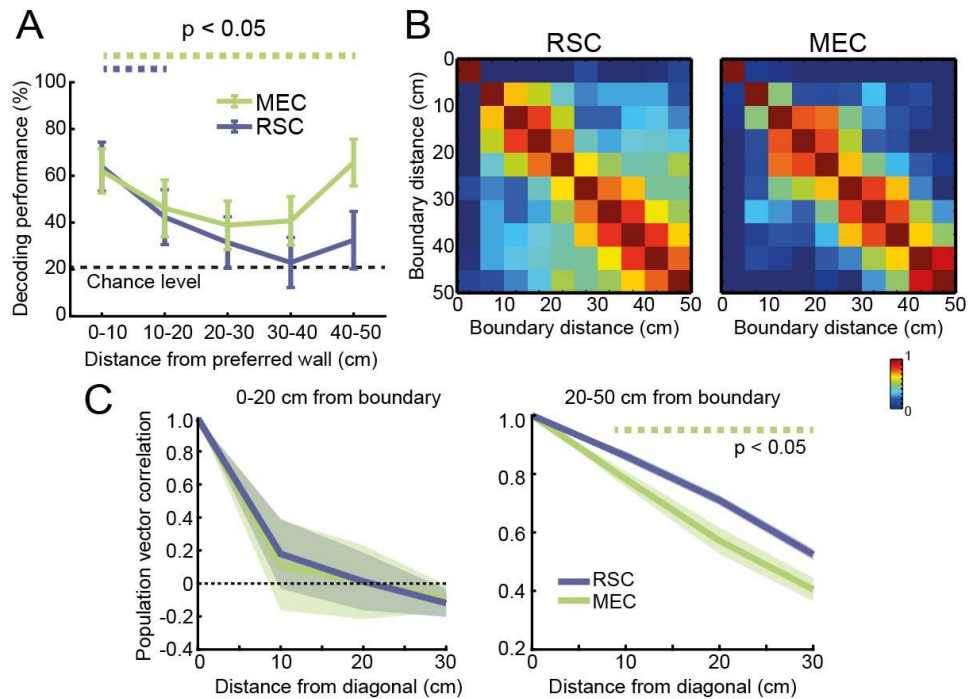


Figure 28. Decoding the animal's distance from a wall using population spiking activity. (A) A support vector machine (SVM) classifier was used to decode the animal's distance towards the nearest wall based on spiking activity of all simultaneously recorded border cells. Local distance information was present in both regions, but extended further into the centre of the arena only in MEC. (B) Population vector correlation of firings rates, binned according to the wall distance for border cells in RSC and MEC. (C) Decay of vector correlations from the diagonal in the proximity (left) and farther wall-distance range (right). Wilcoxon ranksum test

Finally, to explore whether border cell activity has any behavioural correlates I analysed the relationship between cell firing and the animal's behaviour. This was done by decomposing behavioural position variables from 2D coordinates into trajectory information, taking 100 ms time bins around each timepoint to calculate the animal's movement direction and distance travelled on lateral and forward axes (**Figure 29A**). Combining this motion information with the timings of cell spiking makes for egocentric motion maps that capture firing rate as a function of the animal's movement (Ito et al., 2015; Whitlock et al., 2012).

After generating self-motion rate maps for border cells in RSC, no obvious patterns could initially be observed. However, performing time-

lagged analyses by shifting spike-timings either ahead or backwards in time relative to motion data revealed that RSC border cells fired prospective to motion (example shown in **Figure 29B**). Using a metric from Shannon's information theory to summarise the amount of information present in motion maps (Shannon, 1948; Skaggs et al., 1996), the population of border cells had maximal amount of information present when spike-timings were shifted earlier in time ($p < 0.05$ for the time-lag range of -300 to -50 ms compared to shuffled data; **Figure 29C, top**). By contrast, no such shift was observed for retrospective or prospective lags for MEC border cells (**Figure 29C, bottom**), showing that any spike correlations of border cells with prospective motion are not simply due to behavioural restrictions near walls.

When aligning the animal's changes in movement direction using the cell's spike timings, animal's displayed consistent turning behaviour 200 ms after cell firing of RSC neurons (**Figure 29D, top**). The direction of turning was dependent on the hemisphere where the border cell was recorded, such that neurons fired prospective of ipsilateral turns (i.e., cell firing of neurons in right RSC preceded turns towards the right; **Figure 29D, top**). No prospective or retrospective correlates were observed for border cells in MEC (**Figure 29D, bottom**). Although this difference between border cells from both regions shows this correlate does not arise naturally from biased behaviour near borders, I further simulated a set of synthetic neurons based on real behavioural data (**Figure 29E**). The resulting spike-triggered turning data showed no clear time-lagged correlations between cell firing near boundaries and the following turning behaviour (**Figure 29F**).

Taken together, these results show there is a relationship between border cell firing and the animal's next motion, but only in RSC. This supports the idea that RSC and MEC encode different aspects of border representations, where spatial input from MEC is used to compute information that is needed for the animal's next actions.

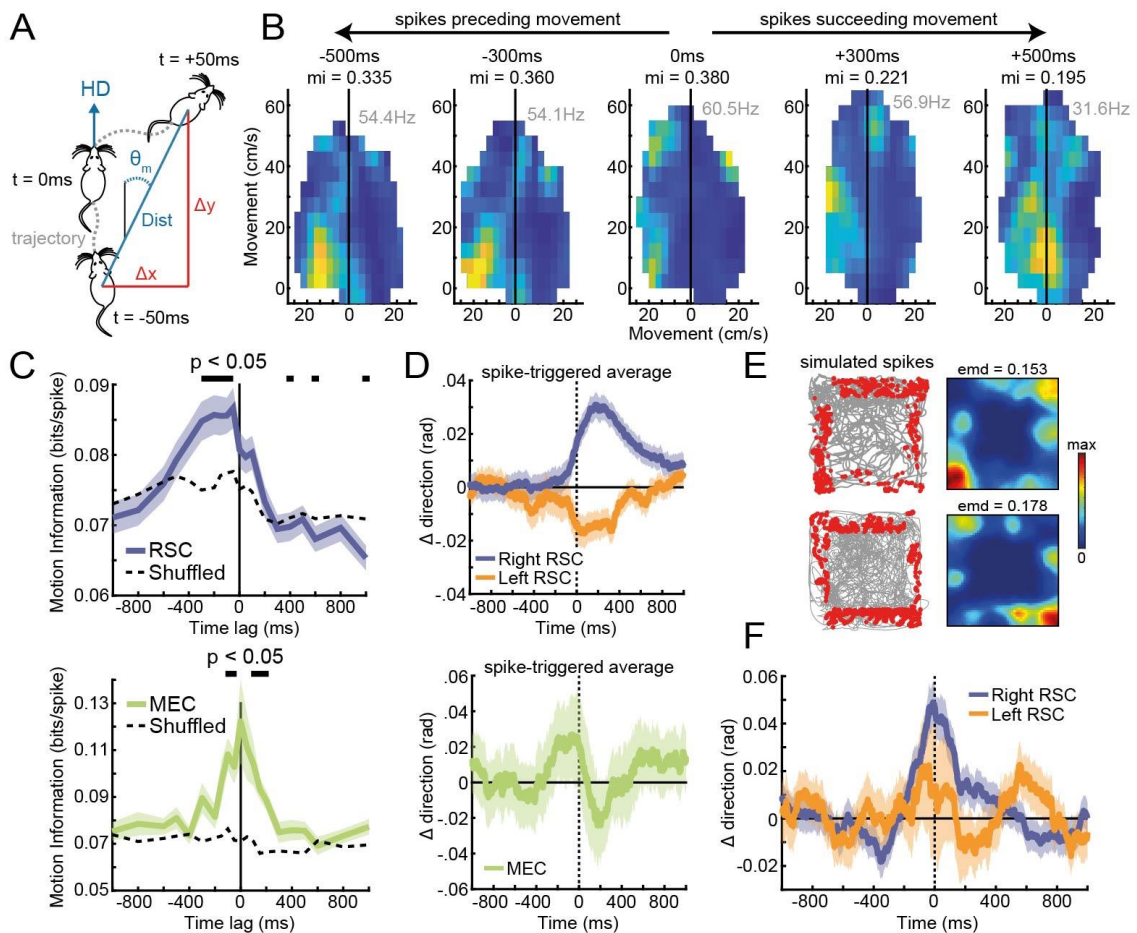


Figure 29. Correlations between border cell firing and the animal's trajectory.

(A) Self-motion maps were computed based on short trajectories of the animal, giving firing rate as a function of lateral and frontal displacements (Δx and Δy , respectively). At each timepoint, 100 ms time bins were used to calculate the animal's distance travelled (Dist), and its self-centred moving direction (θ_m) relative to the forward head-direction. (B) Example self-motion maps of an RSC border cell with spike times shifted in time relative to the animal's motion data. A firing field emerged on left turns when spikes were shifted -300 to -500 ms before motion. (C) The amount of information present in motion maps for RSC (top) and MEC (bottom) border cells. (D) Spike-triggered average of changes in movement direction – calculated as the difference in movement direction in 250 ms time bins where positive values indicate right turns – for cells in RSC (top) and MEC (bottom). (E) Simulated spiking data using real behavioural position variables. Spikes were generated based on a non-uniform Poisson distribution and selected from time points where the animal was both located between 5 and 20 cm distance of a boundary (randomly selected for each cell), and had a specific orientation toward the wall. Shown are examples of trajectory spike plots and their associated spatial rate maps of two simulated cells. (F) Spike-triggered average of changes in moving direction using simulated spiking data, with behaviour coming from sessions where cells were recording in left or right RSC. * $p < 0.05$, t-test

DISCUSSION

The brain performs an incredibly large number of functions at the same time, and each process depends on a coordinated effort across many neurons that are often spread across multiple brain regions. For example, when we examine the brain's involvement in encoding direction information of the body, captured by head-direction cells, we find many reports on modulation of cell activity after physical rotation of the body across the brain (reviewed in Taube, 2007). These head-direction cells have been recorded in at least 7 different anatomical regions, including the mammillary body, two thalamic nuclei, the postsubiculum, entorhinal cortex, hippocampus and also retrosplenial cortex. But it's likely that each set of head-direction cells has a specific role within the network that contributes certain information to the overall function.

On a superficial and phenomenological level, we learn only a limited amount from experiments that describe firing properties of these cells as a function of the animal's behaviour. Instead, adding lesion studies to probe associated functional losses, anatomical tracing studies for structural connectivity, and functional manipulation experiments to establish circuit interactions allows us to dissect the entire network and establish the role of each individual part. In case of the head-direction circuit, this approach has revealed that there are at least three sensory pathways involved on the input side that together update the global direction signal, with information coming from the vestibular organ, signal copies from the motor system, and the flow of visual information from the visual system (Taube, 2007).

For border cells in the brain, the work in this thesis is the third description of a functional cell type that encodes boundary information. One important issue then is to understand the overlap and differences between these classes in order to uncover their individual contributions to spatial coding. The focus of this chapter was on two of the three regions involved, border cells in RSC and border cells in MEC. Pharmacogenetic inactivation of either brain region has shown that signals from MEC were required for accurate boundary representations in RSC, but this effect only holds true in one direction. The optogenetic inactivation experiments further showed that this disruption is specific to the direct MEC→RSC pathway, and is not caused by a third mediating brain region.

This result is surprising, because the directionality of this effect seems to contradict the interpretation presented in several recent papers on egocentric representation in the neocortex (Alexander et al., 2020; Hinman et al., 2019; LaChance et al., 2019; Wang et al., 2018). These reports ascribe egocentric encoding of features of the environment in the cortex to a sensory domain, and propose that they result from early thalamic and cortical processing of sensory signals. Such an interpretation relies on a dominant computational model of egocentric-allothetic transformation in the brain (Bicanski and Burgess, 2018; Byrne et al., 2007), which proposes that egocentric sensory signals are used to compute allocentric spatial representation in the parahippocampal brain areas. In other words, egocentric border representations in the RSC are predominantly on the input side of the computational process.

Yet if this interpretation holds true, there should have been a measurable effect of RSC inactivation on MEC border coding. Instead, my results suggest the opposite, that egocentric boundary computations in RSC depend on allocentric signals from MEC. Following the same model diagram (Figure 4), this would imply that the Retrosplenial cortex's involvement is rather on the output side of the process, where allocentric spatial computations are used to generate egocentric information in RSC, which can then be passed on to downstream targets for action plans that are anchored to the body. This is consistent with results presented in the final figure, which show that border cells are indeed correlated with the behaviour of the animal such that cell activity precedes specific movements of a trajectory.

Chapter V

Conclusions & future perspectives

CONCLUSIONS

Navigation behaviour is critical for survival, and the brain has dedicated many of its resources to the processing of spatial information. These spatial computations are well-studied, and decades of research have resulted in a large number of functional cell types that are involved in spatial coding. Despite having a good understanding of this functional circuitry, in particular for the encoding of position information, one remaining open question is still to what extent these different cell types depend on external contextual information, and how they integrate distance and direction information to distal landmarks.

The goal of this thesis was to address this question, starting with the Retrosplenial Cortex as the most likely candidate to participate in the processing of position information of landmarks and other notable distal features of the environment. The road of discovery throughout this work passed three distinct stages in the project, discussed separately in each result chapter.

Initial electrophysiological recordings of single cells in the RSC during free exploration behaviour of the animal revealed a new functional class of neurons in RSC, the border cell. With results presented in *Chapter II*, activity of border cells in the Retrosplenial cortex was characterized by high firing rates near all boundaries of the arena that were available to the animal. Sensory behavioural experiments revealed that this activity persisted in the absence of direct visual or somatosensory detection, and was furthermore specific to walls but not objects.

It soon became apparent that distance to the wall was not the only modulating factor for border cells, shown in *Chapter III*. Remapping activity from allocentric position coordinates to self-centred boundary coordinates revealed that many neurons had conjunctive selectivity for the direction of the wall relative to the animal's head-direction. This egocentric direction information was resistant to the physical rotation of the arena, demonstrating its independence from the internal global direction signal in the brain.

As the RSC forms anatomical connections with many brain regions that encode spatial information, like the hippocampus and parahippocampal areas, *Chapter IV* addressed how the RSC fits into this functional network, and forms a wider border coding circuit with the medial entorhinal cortex. Pharmacogenetic- and optogenetic-mediated inhibition experiments showed that the inter-dependence between both brain regions occurred only in one direction, as MEC signals were needed for precise border coding in RSC but not vice versa.

Prominent standing theories on RSC function all suggest that the RSC contributes to spatial cognition, but there remain some controversies on its exact role across spatial domains (Mitchell et al., 2018; Vann et al., 2009). It's clear that both human patients and rodents with lesions in RSC exhibited severe impairment in navigation ability (Takahashi et al., 1997; Vann et al., 2009). And an fMRI study found that RSC is particularly engaged in representing permanent landmarks in the environment (Auger et al., 2012), complimented by calcium-imaging recordings in mice that showed that landmark coding depends on supra-linear integration of visual and motor inputs in a virtual-reality setting (Fischer et al., 2020). These findings are

consistent with the results described in this thesis, in the sense that borders can serve as permanent landmarks in an open field area, especially when no other local cues are present. However, both previous studies stress the importance of visual detection of the landmark as the main driving input pathway, which is inconsistent from the darkness recordings in *Chapter III* which found no effect on border tuning in RSC.

On the other hand, previous recording studies in rodents have identified several types of spatially-tuned cells in RSC, such as head-direction cells, place cells, cells that represent geometric features of the environment, and now also border cells (Alexander and Nitz, 2015; Cho and Sharp, 2001; Mao et al., 2017). Because of the existence of these spatially-tuned cells, combined with its structural connectivity with the rest of the brain, the RSC is considered an ideal brain region to implement the transformation of spatial representations between egocentric and allocentric coordinate systems (Bicanski and Burgess, 2018; Byrne et al., 2007; Mitchell et al., 2018). This transformation is an essential computational step for navigation, because many spatial representations are anchored to external features of the environment (i.e., in allocentric coordinates), but the world is experienced through sensory organs in a self-referenced (i.e., egocentric) manner.

The results presented in this thesis are consistent with the idea of translational computations to be performed in RSC, because of the presence of both allocentric place and head-direction cells in combination with egocentric border cells that encode both distance and direction information. But one major question that remains is how these egocentric representations are generated. As discussed earlier, previous studies

proposed egocentric tuning in RSC and related structures to result from the egocentric nature of sensory input, which after transformation can be relayed to allocentric down-stream targets (Alexander et al., 2020; LaChance et al., 2019). But this notion is unlikely given several of my key findings. Sensory behavioural experiments have shown that border cell activity persists in the absence of direct visual or whisker-mediated detection of the wall, while RSC border cells furthermore distinguish walls from objects, unlike whisker-responsive wells in the barrel cortex. This result implies that border cell activity can be generated even without unimodal sensory input, shedding doubt on the sensory interpretation.

Neural manipulation experiments further revealed that the down-regulation of activity in bilateral RSC had no measurable effect on border cells in MEC, which is its direct downstream neighbour. This pathway would be one of two major candidates to provide egocentric spatial input to the MTL system, with the other being the Subiculum as a tertiary structure, but border information does not appear to flow from RSC to MEC. Instead, my results suggest the opposite, and favour the idea that RSC border cells are driven by spatial cells with allocentric tuning in MEC. This view is consistent with the previously discussed theoretical circuit model (Byrne et al., 2007), in which information about allocentric boundary locations is integrated with head-direction signals to form egocentric border representations. One important finding to support this interpretation was that the cue rotation of the arena affected the direction tuning of head-direction cells but not border cells, but also caused a rotation of the spatially-tuned cells in RSC. This means that position and direction encoding in RSC must be bound together, rotating in unison during the environmental manipulations.

Although the sensory explanation for egocentric tuning seems unlikely, it was the most promising initial interpretation of the direction selectivity results presented in *Chapter III*. One prominent feature of this tuning was the high consistency observed across neurons in the same animal, and thus recorded in the same hemisphere. More data across both hemispheres further confirmed the strong hemispheric-bias in preferred directions. So, what causes this bias if not the lateralized sensory processing in the brain?

My proposition is that it is the manifestation of the animal's immediate action in respect to the arena, as it is consistently running either parallel to or away from the walls. We know that movement commands are lateralized in the brain, and follow along the left-right body axis in each respective hemisphere (Fritsch and Hitzig, 2009; Kim et al., 1993). Collision detection and avoidance are fundamental roles of sensory-motor systems for many species of animals (Fotowat and Gabbiani, 2011), and rodents also need to detect boundaries to avoid hitting walls or falling off edges. The boundary information in RSC may therefore be used for computations in down-stream brain regions to control the animal's next movement relative to these walls. The RSC provides inputs to brain areas necessary for motor control and initiation, such as premotor and motor cortices, cingulate cortex, as well as the dorsal striatum (Guo et al., 2015; Jones et al., 2005; Yamawaki et al., 2016), although the exact function of these pathways is not yet established. A recent recording study on the dorsomedial striatum furthermore identified a type of neuron that fire near environmental borders similar to RSC border cells. However, their egocentric tuning is largely dependent on the animal's movement direction (Hinman et al., 2019), rather than head-direction as in RSC (Alexander et al., 2020).

But the idea of RSC's involvement in action planning goes beyond just structural connectivity. The final results presented in this thesis demonstrated for the first time that neural activity in the RSC is indeed related to movements of the animal, with significant correlations between cell firing and the subsequently taken trajectory. Notably, this activity was prospective in nature, and border cell activity preceded the following turns by roughly 300 ms. This lag in time could mean that the brain performs several additional computations with this border information in downstream receivers such as the striatum, before it converges into a direct motor action. Turning behaviour generally occurred in the ipsilateral direction of the recorded hemisphere, while direction selectivity was present in contralateral space. This would imply that border cells in the right hemisphere are active whenever the wall is positioned on the left hemifield in proximal space, and the subsequent action is to take a right turn away from the wall towards the centre of the arena. This lateralized coding scheme may thus help associate RSC boundary coding with the next appropriate action. Taken together, this supports the idea that the RSC plays a critical role in spatial cognition by allowing the animal to use walls as prominent landmarks to navigate the room.

Chapter VI

Methods & Analyses

The methods described in the following chapter have been published previously in *eLife* under the citation below.

van Wijngaarden, J. B. G., Babl, S. S., & Ito, H. T. (2020). Entorhinal-retrosplenial circuits for allocentric-egocentric transformation of boundary coding. *Elife*, 9, e59816. DOI: 10.7554/eLife.59816

SUBJECTS

All experiments were approved by the local authorities (RP Darmstadt, protocol F126/1009) in concordance with the European Convention for the Protection of Vertebrate Animals used for Experimental and Other Scientific Purposes. Subjects were 19 male Long-Evans rats weighing 400 to 550 g (aged 3–5 months) at the start of the experiment. Rats were housed individually in Plexiglass cages (45 × 35 × 40 cm; Tecniplast GR1800) and maintained a reversed 12 hr light-dark cycle, with behavioural experiments performed during the dark phase. Animals were mildly food-restricted with unlimited access to water and kept at 85–90% of their free-feeding body-weight throughout the experiment.

For recording experiments in *Chapter II* and *Chapter III*, eight rats had tetrodes located unilaterally in RSC, either in the left (four rats) or right (four rats) hemisphere. One rat had a 64-channel silicon probe (Buzsaki64-sp; Neuronexus) implanted directly into the barrel field of the right primary somatosensory cortex (S1bf). Four rats were injected with an AAV encoding inhibitory DREADDs bilaterally in either MEC or RSC, combined with a tetrode drive in MEC or RSC in the right hemisphere. For optogenetic inactivation experiments, two rats were injected with a retroAAV (Tervo et al., 2016) expressing inhibitory Cruxhalorhodopsin chloride pumps (Jaws) (Chuong et al., 2014) in the right RSC together with the implantation of a 64-channel silicon probe (Buzsaki64-sp), while an optic fibre was positioned above MEC. Finally, two more rats were injected with an AAV expressing inhibitory Halorhodopsin chloride pumps (eNpHR3.0) (Zhang et al., 2007) in the right MEC, while eight tetrodes and an optic fibre were implanted together in the right RSC. No statistical method was used to predetermine sample size, although the number of animals used here is similar to previous work.

SURGERY, VIRUS INJECTION, AND DRIVE IMPLANTATION

Anaesthesia was induced by isoflurane (5% induction concentration, 0.5–2% maintenance adjusted according to physiological monitoring). For analgesia, Buprenovet (Buprenorphine, 0.06 mg/mL; WdT) was administered by subcutaneous injection, followed by local intracutaneous application of either Bupivacain (Bupivacain hydrochloride, 0.5 mg/mL; Jenapharm) or Ropivacain (Ropivacain hydrochloride, 2 mg/mL; Fresenius Kabi) into the scalp. Rats were subsequently placed in a Kopf stereotaxic frame, and an incision was made in the scalp to expose the skull. After horizontal alignment, several holes were drilled into the skull to place anchor screws, and craniotomies were made for microdrive implantation. The microdrive was fixed to the anchor screws with dental cement, while two screws above the cerebellum were connected to the electrode's ground. All tetrodes were then positioned at 920 μm depth from the cortical surface. All animals received analgesics (Metacam, 2 mg/mL Meloxicam; Boehringer Ingelheim) and antibiotics (Baytril, 25 mg/mL Enrofloxacin; Bayer) for at least 5 d post-surgery.

For tetrode recordings, rats were unilaterally implanted with a hyperdrive that contained 28 individually adjustable tetrodes made from 17 μm polyimide-coated platinum-iridium (90–10%; California Fine Wire; plated with gold to impedances below 150 k Ω at 1 kHz). The tetrode bundle consisted of 30-gauge stainless steel cannula, soldered together in a 14 \times 2 rectangular shape for recordings of the entire RSC, 7 \times 4 for anterior RSC, or two squared bundles for bilateral MEC. For RSC, tetrodes were implanted alongside the anteroposterior axis, starting at (AP) -2.5 mm posterior from bregma until -4 mm to -6.5 mm, (ML) 0.8 mm lateral from the midline,

(DV) 1.0 mm below the dura, and at a 25° angle in a coronal plane pointing to the midline in order to get underneath the superior sagittal sinus. For MEC, tetrodes were implanted at 4.5 mm lateral of the midline, 0.2 mm anterior to the transverse sinus, at an angle of 15 degrees in a sagittal plane with the tips pointing to the anterior direction. Experiments began at least 1-week post-surgery to allow the animals to recover.

For DREADDs experiments, an AAV8-hSyn-hM4Di-mCherry (a gift from Bryan Roth; Addgene viral prep # 44362-AAV8) was injected with an infusion rate of 100 nL/min using a 10 µL NanoFil syringe and a 33-gauge bevelled metal needle (World Precision Instruments). After the injection was completed, the needle was left in place for 10 min. The virus was injected at two sites for each bilateral MEC (500 nL each at the depth of 2.5 mm and 3.5 mm from the cortical surface, 4.5 mm lateral to the midline, 0.2 mm anterior to the transverse sinus at an angle of 20° in a sagittal plane with the needle pointing to the anterior direction), or four sites along the anteroposterior axis for each bilateral RSC (500 nL each at AP 2.5, 3.5, 4.5, 5.5 mm, 0.8 mm lateral to the midline, at an angle of 25° in a coronal plane pointing to the midline). The flow was controlled with a Micro4 microsyringe pump controller. A small microdrive (Axona Ltd) connected to four-wire tetrodes was additionally implanted nearby the injection site to evaluate the effects of the manipulation. Virus injection was performed in the same surgery as electrode implantation, and recordings began at least 3 weeks post-surgery to allow time for the virus to express.

For optogenetic silencing of MEC terminals in RSC, an AAV1-hSyn-eNpHR3.0-EYFP (a gift from Karl Deisseroth; Addgene viral prep # 26972-AAV1) was injected into right MEC with the same procedure as the

DREADDs experiments; injection location was 4.0 mm lateral to the midline, 0.2 mm anterior to the transverse sinus pointing 20° in the anterior direction, with two sites at 2.5 mm and 3.5 mm depths from the cortical surface (500 nL volume each). For optogenetic inhibition of MEC cells projecting to RSC, an AAV-retro-hSyn-Jaws-GFP (a gift from Edward Boyden; Addgene viral prep # 65014-AAVrg) was injected into right RSC at four sites (AP 2.5, 3.5, 4.5, and 5.5 mm, 0.8 mm lateral of the midline and pointing 25° to the midline; 500 nL volume each). Electrode and optic fibre implantation were performed 1 week following virus injection, and experiments began at least 3 weeks post-surgery.

SPIKE SORTING AND CELL CLASSIFICATION

All main analyses and data processing steps were performed in MatLab (MathWorks). Neural signals were acquired and amplified using two 64-channel RHD2164 headstages (Intan technologies), combined with an OpenEphys acquisition system, sampling data at 15 kHz. Neuronal spikes were detected by passing a digitally band-pass filtered LFP (0.6–6 kHz) through the 'Kilosort' algorithm to isolate individual spikes and assign them to separate clusters based on waveform properties (<https://github.com/cortex-lab/KiloSort>) (Pachitariu et al., 2016). Clusters were manually checked and adjusted in autocorrelograms and for waveform characteristics in principal component space to obtain well-isolated single units, discarding any multi-unit or noise clusters. Tetrodes were moved a minimum distance of 80 µm between recording days to find a new set of neurons for the next recording session.

RSC BORDER CELLS

I applied a novel template-matching procedure to classify RSC neurons as border cells using the Earth Mover's Distance (EMD), a distance metric from the mathematical theory of optimal transport (Hitchcock, 1941; Rubner et al., 1998). First, the animal's spatial position occupancy was divided into 4×4 cm spatial bins, and the firing rate in each position bin was calculated by dividing the number of spikes with the amount of time spent there. The resulting rate map was smoothed by applying a 2D Gaussian filter (width of 1 bin), and converted to a probability distribution by taking unit weight. I then calculated the Earth Mover's Distance relative to a 'boundary template' using a MatLab implementation of the fastEMD algorithm (<https://github.com/dkoslicki/EMDeBruijn>) (Pele and Werman, 2008, 2009). This boundary template consisted of a 25×25 matrix with each bin's value set to 0, except the outer ring bins with a value of 1, smoothed with the same Gaussian kernel and converted to unit weight. Several additional templates were constructed to assess the effects of behavioural manipulation, adding additional weight in the location of placed objects/walls (**Figure 10E**, **Figure 11E**). The EMD distance between a rate map and a template represents the minimal cost that must be paid to transform one distribution into another, with values ranging between zero (identical maps) and one (maximal difference), and is thus a normalized metric of dissimilarity (Grossberger et al., 2018).

MEC BORDER CELLS

To compare classification results with a related metric, I computed the original border score for each cell (Solstad et al., 2008). First, a cell's

firing field was estimated by isolating a continuous region of at least 200 cm² and a maximum of 70% of the arena surface where the firing rate was above 30% of the peak firing rate. This was an iterative search until all fields with the above criteria were identified. Next, the border score, b , was computed for each wall separately:

$$b = \frac{c_m - d_m}{c_m + d_m} \quad (\text{Eq. 2})$$

where c_m was defined as the maximum coverage of any single field over the wall and d_m the mean firing distance, calculated as the average distance to the nearest wall over all bins covered by the field. This was done separately for each of the four walls out of which the maximum score was selected. Cells recorded in MEC were classified as border cells whenever their border score was above the threshold of 0.5 (corresponding to the 99.3th percentile of scores generated from randomly time-shifted spikes) for either of the two recorded sessions, and had an average firing rate of at least 0.5 Hz.

HEAD-DIRECTION CELLS

The rat's head-direction was calculated based on the relative x/y-position of two light-emitting diodes (LEDs), corrected for an offset in the placement of the LEDs relative to the animal's true head-direction. For each cell, the mean vector length (MVL) and direction (MVD) was calculated by computing the circular mean and direction from a vector that contained the head-direction of the animal at spike timings in unit space. A cell was classified as a head-direction cell when its MVL was greater than the 95th

percentile of a null distribution obtained by thousand-fold Monte Carlo simulations with randomly time-shifted spike trains.

BORDER RATE MAPS

Locations of walls were estimated based on the most extreme values of the position of the animal. The animal's distance to the wall was computed for each of the four walls separately by taking the difference between the wall's location and the animal's position in the respective x or y-dimension, and selecting the lowest value at each time point. The direction of this wall relative to the animal's direction was computed by calculating the angle difference between the animal's true heading direction and a vector pointing directly toward the wall (e.g., relative to an angle of 0° for the east wall, 90° for the north wall). Because 0° corresponds with the 'East' side in angular polar plots, this data was further shifted by 90° to align the front of the animal with the 'North' part in border maps (see **Figure 17**) to improve visual interpretation of the results.

Firing rate in body-centric border coordinates was calculated by dividing the animal's occupancy in these coordinates into 4 cm distance bins and 20° angle bins. The number of spikes in each bin was then divided by the time spent there, further smoothed using a 2-D Gaussian kernel (one bin width), similar to how spatial rate maps are computed. A cell's preferred direction and distance was obtained by finding the bin with maximal firing rate and selecting the bin's corresponding distance and angle values. For visualization purposes only, this matrix was transformed into a circular diagram shown in **Figure 17** to **Figure 19**.

To establish the directional tuning of a cell, the wall-direction angle at the time of each spike was taken whenever the animal was located within 20 cm distance of a wall, from which a mean vector length was calculated. This MVL was then compared to a thousand-fold shuffled distribution, where each iteration produced an MVL value using randomly time-shifted spike timings (similar to head-direction cell classification). If the real MVL exceeded the 95th percentile of this shuffled distribution in all regular sessions, it was considered significantly tuned to wall direction.

SELF-MOTION MAPS

First, the animal's movement direction was computed at each time point, using position changes in a 100 ms segment of the preceding and succeeding 50 ms, and calculating the angle of movement by taking the arctangent of the difference in x/y-position. The movement directions were then aligned with the animal's forward head-direction, giving moment-to-moment changes in the animal's movement directions from a self-centred perspective (Ito et al., 2015; Whitlock et al., 2012). The distance travelled in this time bin captures the distance from the origin in self-motion maps, while clockwise or counter-clockwise movements are reflected in shifts over the x-axis. Self-motion data was binned into 3 cm/s bins, and rate maps were computed by dividing the number of spikes by time spent in each bin (**Figure 29**). For time-lagged analyses, shifted self-motion maps were generated by shifting spike-timing step-wise between -1000 and +1000 ms earlier or later relative to self-motion data. For each time lag, an additional shuffled distribution was computed by shifting the spike-timings a random amount of time, at least 4 s forward, with the excess wrapped around to the beginning, and taking the average over 10 iterations.

From these self-motion rate maps, the total amount of self-motion information could be calculated as:

$$information = \sum_{i=1}^N p_i \frac{\lambda_i}{\lambda} \log_2 \frac{\lambda_i}{\lambda} \quad (\text{Eq. 3})$$

with $i = 1, \dots, N$ motion bins, p_i the probability of occupancy in bin i , λ_i the mean firing rate for bin i , and λ the overall mean firing rate of the neuron (Skaggs et al., 1996).

DECODING ANALYSIS

For decoding of wall distance from the activity of border cells in RSC and MEC, the optimal wall with maximum coverage by firing fields was chosen for individual cells (the same procedure as used in border score calculations) (Solstad et al., 2008). To determine the optimal head-direction to the selected wall for individual border cells, I searched for a range of head-directions (360-degree range in 5-degree steps) that gave the maximum mean firing rate of the cell when the animal was within 20 cm of the wall. I then focused on neural activity when the animal was at this optimal head-direction and in the range of wall distances from 0 to 50 cm at 10 cm steps (five ranges in total), but excluding timepoints where the animal was within 25 cm of other walls to avoid their potential influence. All of the incidents when the animal was in each of the five wall-distance ranges were equally divided into 20 segments in time, and mean firing rates of individual border cells in the 20 segments were assembled across recording sessions.

To implement a decoding analysis, 20 cells were randomly chosen, and the order of 20 segments was randomly shuffled for each cell, such that the data in each segment is a collection of firing rates from 20 border cells across various time points of behaviours when the animal was in a particular distance range to the wall. Ensemble firing rates of border cells in one of the segments were selected as a test dataset, and the rest of the data were used to train a support vector machine (using a MATLAB package LibSVM with a linear function) (Chang and Lin, 2011). Trained weights were then applied to the activity of border cells in the test dataset to estimate the animal's distance to the wall, which was repeated for all segments to be tested (leave-one-out cross-validation), giving a representative decoding performance for the selected population of cells. This procedure was repeated for different cell pairs for 1000 times to estimate a statistical distribution of decoding performance (bootstrap resampling method).

BEHAVIOURAL METHODS

Data was collected over a total of 30–120 min per day while rats foraged for food (chocolate cereal) in a squared open field arena, either 50 × 50 cm, 100 × 100 cm, or 120 × 120 cm in size. Each session consisted of 10–15 min of free exploration in the arena, separated by 5 min of resting time on a pedestal. No curtains surrounded the recording arena, with the exception of the rotation and darkness experiments where all distal cues were blocked completely. The surface of the arena was elevated 50 cm above the ground, and was enclosed by three black and one white wall with a 50 cm height that were positioned with consistent orientation in the room for all animals. The experimental set-up was extensively cleaned with a 70%

ethanol solution in between every recording session to eliminate any odours.

Behavioural manipulation experiments always followed the same protocol of A-B-B-A', where A is a regular session, and the manipulation was performed in B. This allowed for a recovery phase after the manipulation in the final session A'. The only exception was the drop-edge experiment (**Figure 14**) where the animal had limited motivation; so to ensure good coverage of the arena I reduced the protocol to A-B-A'. All changes to the maze were made in between the first and second session while the animal was resting on a pedestal. For the added wall manipulation (**Figure 10**), an additional black wall (50 cm length × 50 cm height × 1 cm width) was placed in the maze, protruding from one outer wall at half-length toward the centre. For the added object manipulation (**Figure 11**) either a circular, non-climbable aluminium object (10 cm diameter × 50 cm height) or circular climbable object (10 cm diameter × 10 cm height) was placed in the centre, or off-centre 40 cm away from the north and west walls.

For the DREADDs-mediated manipulation experiments, animals were injected with agonist-21 (DREADDs agonist 21 dihydrochloride, 3.52 mg/mL [10 mM]; Hellobio) subcutaneously after the first recording session, followed by at least 30 min waiting time to allow the drug to reach the brain and take effect before starting the next recording session. For the experiments using optogenetic methods, laser light was turned on continuously for the duration of the middle session (5 min, with laser power of 20 mW at the fibre tip), after which the animals had at least 5 min of recovery time on the pedestal before starting the final behavioural session. A green laser (532 nm; Shanghai Laser and Optics Century, China) was used

to activate eNpHR3.0, while a red laser (632 nm; Shanghai Laser and Optics Century, China) was used to activate red-shifted opsins.

The animal's position and head-direction were obtained by tracking two LEDs on the headstage at 25 Hz and recording under dim light conditions. For darkness sessions, I switched to an infra-red OptiTrack camera system (Natural Points Inc) under the assumption that rats have limited vision in the higher wavelengths, with cone sensitivity tapering off rapidly above 600–650 nm (Jacobs et al., 2001). Six Flex three cameras were positioned 2 m above the arena surface on a ceiling mount, at a 45–60° angle pointing downwards, that used infra-red illumination (peak spectral emission at 850 nm) to track the location of three reflective markers in an asymmetric frame attached to the headstage. Position and direction data were acquired and processed using Motive 2.0 software. To ensure no visible light was present for the animals, all lights were turned off and small light sources in the room such as computer and sensor lights were taped off, while the arena was enclosed by a thick, black curtain. A room lamp was turned on for dimly light conditions until 10 s before the start of the recording, and turned on again during the inter-trial interval duration of 5 min. During recording, I remained stationary and silent near the arena throughout the recording while scattering food pellets.

HISTOLOGICAL PROCEDURES

Once the experiment was completed, animals were deeply anesthetized by sodium pentobarbital and perfused intracardially with saline, followed by 10% formalin solution. Brains were extracted and fixed in formalin for at least 72 hr at 6° C temperature. Frozen coronal sections

were cut (50 μm) and stained using cresyl violet and mounted on glass slides. Electrode tips were identified by comparison across adjacent sections, with the location of recorded cells estimated by backward measurement from the most ventral tip of the tetrode tracks.

STATISTICAL PROCEDURES

All statistical tests were two-sided and non-parametric unless stated otherwise. Error bars in all figures represent the standard error of the mean (SEM). All values mentioned in the text are medians \pm SEM.

Chapter VII

Supplementary Information

LITERATURE CITED

- Alexander, A.S., and Nitz, D. a (2015). Retrosplenial cortex maps the conjunction of internal and external spaces. *Nat. Neurosci.* *18*, 1143–1151.
- Alexander, A.S., Carstensen, L.C., Hinman, J.R., Raudies, F., Chapman, G.W., and Hasselmo, M.E. (2020). Egocentric boundary vector tuning of the retrosplenial cortex. *Sci. Adv.* *6*, eaaz2322.
- Andersen, R.A., Essick, G.K., and Siegel, R.M. (1985). Encoding of spatial location by posterior parietal neurons. *Science* *230*, 456–458.
- Arieli, A., Sterkin, A., Grinvald, A., and Aertsen, A. (1996). Dynamics of ongoing activity: Explanation of the large variability in evoked cortical responses. *Science* (80-.). *273*, 1868–1871.
- Armbruster, B.N., Li, X., Pausch, M.H., Herlitze, S., and Roth, B.L. (2007). Evolving the lock to fit the key to create a family of G protein-coupled receptors potently activated by an inert ligand. *Proc. Natl. Acad. Sci. U. S. A.* *104*, 5163–5168.
- Auger, S.D., Mullally, S.L., and Maguire, E.A. (2012). Retrosplenial cortex codes for permanent landmarks. *PLoS One* *7*, e43620.
- Barry, C., Lever, C., Hayman, R., Hartley, T., Burton, S., O’Keefe, J., Jeffery, K., and Burgess, N. (2006). The boundary vector cell model of place cell firing and spatial memory. *Rev. Neurosci.* *17*, 71–97.
- Bicanski, A., and Burgess, N. (2018). A neural-level model of spatial memory and imagery. *Elife* *7*, 77–80.
- Bossema, I. (1979). Jays and Oaks: an Eco-Ethological Study of a Symbiosis. *Behaviour* *70*, 1–116.
- Brown, E.N., Frank, L.M., Tang, D., Quirk, M.C., and Wilson, M.A. (1998). A statistical paradigm for neural spike train decoding applied to position prediction from ensemble firing patterns of rat hippocampal place cells. *J. Neurosci.* *18*, 7411–7425.
- Byrne, P., Becker, S., and Burgess, N. (2007). Remembering the past and imagining the future: A neural model of spatial memory and imagery. *Psychol. Rev.* *114*, 340–375.
- Carandini, M. (2004). Amplification of trial-to-trial response variability by neurons in visual cortex. *PLoS Biol.* *2*.
- Chang, C.C., and Lin, C.J. (2011). LIBSVM: A Library for support vector machines. *ACM Trans. Intell. Syst. Technol.* *2*.
- Chen, L.L., Lin, L.H., Green, E.J., Barnes, C.A., and McNaughton, B.L. (1994). Head-direction cells in the rat posterior cortex. I. Anatomical distribution and behavioral modulation. *Exp. Brain Res.* *101*, 8–23.

-
- Cho, J., and Sharp, P.E. (2001). Head direction, place, and movement correlates for cells in the rat retrosplenial cortex. *Behav. Neurosci.* *115*, 3–25.
- Chuong, A.S., Miri, M.L., Busskamp, V., Matthews, G.A.C., Acker, L.C., Sørensen, A.T., Young, A., Klapoetke, N.C., Henninger, M.A., Kodandaramaiah, S.B., et al. (2014). Noninvasive optical inhibition with a red-shifted microbial rhodopsin. *Nat. Neurosci.* *17*, 1123–1129.
- Clark, B.J., Simmons, C.M., Berkowitz, L.E., and Wilber, A.A. (2018). The retrosplenial-parietal network and reference frame coordination for spatial navigation. *Behav. Neurosci.* *132*, 416–429.
- Cowie, R.J., Krebs, J.R., and Sherry, D.F. (1981). Food storing by marsh tits. *Anim. Behav.* *29*, 1252–1259.
- Darwin, C. (1859). *On the origin of species by means of natural selection, or the preservation of favoured races in the struggle for life* (London,: J. Murray).
- Ding, S.L. (2013). Comparative anatomy of the prosubiculum, subiculum, presubiculum, postsubiculum, and parasubiculum in human, monkey, and rodent. *J. Comp. Neurol.* *521*, 4145–4162.
- Ekstrom, A.D., Arnold, A.E.G.F., and Iaria, G. (2014). A critical review of the allocentric spatial representation and its neural underpinnings: toward a network-based perspective. *Front. Hum. Neurosci.* *8*, 803.
- Equence, C.E.S., Iology, T.O.B., The, C., and Consortium, S. (1998). Genome sequence of the nematode *C. elegans*: A platform for investigating biology. *Science* (80-.). *282*, 2012–2018.
- Fischer, L.F., Mojica Soto-Albors, R., Buck, F., and Harnett, M.T. (2020). Representation of visual landmarks in retrosplenial cortex. *Elife* *9*, 1–25.
- Flanders, M., Tillery, S.I.H., and Soechting, J.F. (1992). Early stages in a sensorimotor transformation. *Behav. Brain Sci.* *15*, 309–320.
- Fogassi, L., and Luppino, G. (2005). Motor functions of the parietal lobe. *Curr. Opin. Neurobiol.* *15*, 626–631.
- Fotowat, H., and Gabbiani, F. (2011). Collision Detection as a Model for Sensory-Motor Integration. *Annu. Rev. Neurosci.* *34*, 1–19.
- Fritsch, G., and Hitzig, E. (2009). Electric excitability of the cerebrum (Über die elektrische Erregbarkeit des Grosshirns). *Epilepsy Behav.* *15*, 123–130.
- Georgopoulos, A.P. (1988). Neural integration of movement: role of motor cortex in reaching. *FASEB J.* *2*, 2849–2857.
- Gofman, X., Tocker, G., Weiss, S., Boccara, C.N., Lu, L., Moser, M.-B., Moser, E.I., Morris, G., and Derdikman, D. (2019). Dissociation between Postrhinal Cortex and Downstream Parahippocampal Regions in the Representation of Egocentric Boundaries. *Curr. Biol.* *27*, 2751–2757.

-
- Goris, R.L.T., Movshon, J.A., and Simoncelli, E.P. (2014). Partitioning neuronal variability. *Nat. Neurosci.* *17*, 858–865.
- Grant, R.A., Mitchinson, B., Fox, C.W., and Prescott, T.J. (2009). Active touch sensing in the rat: Anticipatory and regulatory control of whisker movements during surface exploration. *J. Neurophysiol.* *101*, 862–874.
- van Groen, T., and Wyss, J.M. (1990). Connections of the retrosplenial granular a cortex in the rat. *J. Comp. Neurol.* *300*, 593–606.
- van Groen, T., and Wyss, J.M. (1992). Connections of the retrosplenial dysgranular cortex in the rat. *J. Comp. Neurol.* *315*, 200–216.
- Van Groen, T., and Wyss, J.M. (2003). Connections of the retrosplenial granular b cortex in the rat. *J. Comp. Neurol.* *463*, 249–263.
- Grossberger, L., Battaglia, F.P., and Vinck, M. (2018). Unsupervised clustering of temporal patterns in high-dimensional neuronal ensembles using a novel dissimilarity measure. *PLoS Comput. Biol.* *14*, e1006283.
- Guo, Q., Wang, D., He, X., Feng, Q., Lin, R., Xu, F., Fu, L., and Luo, M. (2015). Whole-brain mapping of inputs to projection neurons and cholinergic interneurons in the dorsal striatum. *PLoS One* *10*, 1–15.
- Hafting, T., Fyhn, M., Molden, S., Moser, M.-B., and Moser, E.I. (2005). Microstructure of a spatial map in the entorhinal cortex. *Nature* *436*, 801–806.
- Hall, C.S. (1934). Emotional behavior in the rat. I. Defecation and urination as measures of individual differences in emotionality. *J. Comp. Psychol.* *18*, 385–403.
- Hardcastle, K., Ganguli, S., and Giocomo, L.M. (2015). Environmental Boundaries as an Error Correction Mechanism for Grid Cells. *Neuron* *86*, 827–839.
- Hardcastle, K., Maheswaranathan, N., Ganguli, S., and Giocomo, L.M. (2017). A Multiplexed, Heterogeneous, and Adaptive Code for Navigation in Medial Entorhinal Cortex. *Neuron* 1–13.
- Hartley, T., Burgess, N., Lever, C., Cacucci, F., and O’Keefe, J. (2000). Modeling place fields in terms of the cortical inputs to the hippocampus. *Hippocampus* *10*, 369–379.
- Hinman, J.R., Chapman, G.W., and Hasselmo, M.E. (2019). Neuronal representation of environmental boundaries in egocentric coordinates. *Nat. Commun.* *10*, 1–8.
- Hitchcock, F.L. (1941). The Distribution of a Product from Several Sources to Numerous Localities. *J. Math. Phys.* *20*, 224–230.
- Honda, Y., and Ishizuka, N. (2015). Topographic distribution of cortical projection cells in the rat subiculum. *Neurosci. Res.* *92*, 1–20.

-
- Hoydal, O.A., Skytoen, E.R., Andersson, S.O., Moser, M.-B., and Moser, E.I. (2019). Object-vector coding in the medial entorhinal cortex. *Nature* 568, 400–404.
- Ito, H.T., Zhang, S., Witter, M.P., Moser, E.I., and Moser, M. (2015). A prefrontal-thalamo-hippocampal circuit for goal-directed spatial navigation. *Nature* 522, 50–55.
- Jacob, P.-Y., Casali, G., Spieser, L., Page, H., Overington, D., and Jeffery, K. (2017). An independent, landmark-dominated head-direction signal in dysgranular retrosplenial cortex. *Nat. Neurosci.* 20, 173–175.
- Jacobs, G.H., Fenwick, J.A., and Williams, G.A. (2001). Cone-based vision of rats for ultraviolet and visible lights. *J. Exp. Biol.* 204, 2439–2446.
- Jones, B.F., and Witter, M.P. (2007). Cingulate cortex projections to the parahippocampal region and hippocampal formation in the rat. *Hippocampus* 17, 957–976.
- Jones, B.F., Groenewegen, H.J., and Witter, M.P. (2005). Intrinsic connections of the cingulate cortex in the rat suggest the existence of multiple functionally segregated networks. *Neuroscience* 133, 193–207.
- Keinath, A.T., Epstein, R.A., and Balasubramanian, V. (2018). Environmental deformations dynamically shift the grid cell spatial metric. *Elife* 7, 1–22.
- Kim, S.G., Ashe, J., Hendrich, K., Ellermann, J.M., Merkle, H., Ugurbil, K., and Georgopoulos, A.P. (1993). Functional magnetic resonance imaging of motor cortex: Hemispheric asymmetry and handedness. *Science* (80-.). 261, 615–617.
- Klatzky, R.L. (1998). Allocentric and Egocentric Spatial Representations: Definitions, Distinctions, and Interconnections. In *Spatial Cognition: An Interdisciplinary Approach to Representing and Processing Spatial Knowledge*, C. Freksa, C. Habel, and K.F. Wender, eds. (Berlin, Heidelberg: Springer Berlin Heidelberg), pp. 1–17.
- Kropff, E., Carmichael, J.E., Moser, M.-B., and Moser, E.I. (2015). Speed cells in the medial entorhinal cortex. *Nature* 523, 419–424.
- Krupic, J., Bauza, M., Burton, S., and O’Keefe, J. (2018). Local transformations of the hippocampal cognitive map. *Science* (80-.). 359, 1143–1146.
- LaChance, P.A., Todd, T.P., and Taube, J.S. (2019). A sense of space in postrhinal cortex. *Science* 365.
- Lever, C., Burton, S., Jeewajee, A., O’Keefe, J., and Burgess, N. (2009). Boundary vector cells in the subiculum of the hippocampal formation. *J. Neurosci.* 29, 9771–9777.
- Loomis, J.M., Da Silva, J.A., Fujita, N., and Fukusima, S.S. (1992). Visual Space Perception and Visually Directed Action. *J. Exp. Psychol. Hum. Percept. Perform.* 18, 906–921.

-
- Maguire, E.A. (2001). The retrosplenial contribution to human navigation: A review of lesion and neuroimaging findings. *Scand. J. Psychol.* *42*, 225–238.
- Mao, D., Kandler, S., McNaughton, B.L., and Bonin, V. (2017). Sparse orthogonal population representation of spatial context in the retrosplenial cortex. *Nat. Commun.* *8*, 243.
- McNaughton, B.L., Battaglia, F.P., Jensen, O., Moser, E.I., and Moser, M.-B. (2006). Path integration and the neural basis of the “cognitive map”. *Nat. Rev. Neurosci.* *7*, 663–678.
- Mitchell, A.S., Czajkowski, R., Zhang, N., Jeffery, K., and Nelson, A.J.D. (2018). Retrosplenial cortex and its role in spatial cognition. *Brain Neurosci. Adv.* *2*, 2398212818757098.
- Morris, R.G.M. (1981). Spatial localization does not require the presence of local cues. *Learn. Motiv.* *12*, 239–260.
- Moser, E.I., Kropff, E., and Moser, M.B. (2008). Place cells, grid cells, and the brain’s spatial representation system. *Annu. Rev. Neurosci.* *31*, 69–89.
- Muller, R.U., and Kubie, J.L. (1987). The Effects of Changes in the Environment Hippocampal Cells on the Spatial Firing of. *New York* *7*, 1951–1968.
- Nagel, G., Szellas, T., Huhn, W., Kateriya, S., Adeishvili, N., Berthold, P., Ollig, D., Hegemann, P., and Bamberg, E. (2003). Channelrhodopsin-2, a directly light-gated cation-selective membrane channel. *Proc. Natl. Acad. Sci. U. S. A.* *100*, 13940–13945.
- O’Keefe, J., and Burgess, N. (1996a). Geometric determinants of the place fields of hippocampal neurons. *Nature* *381*, 425–428.
- O’Keefe, J., and Burgess, N. (1996b). Geometric determinants of the place fields of hippocampal neurons. *Nature* *381*, 425–428.
- O’Keefe, J., and Dostrovsky, J. (1971). The hippocampus as a spatial map. Preliminary evidence from unit activity in the freely-moving rat. *Brain Res.* *34*, 171–175.
- O’Keefe, J., and Nadel, L. (1978). *The Hippocampus as a Cognitive Map* (Oxford University Press).
- Oesterhelt, D., and Stoeckenius, W. (1973). Functions of a new photoreceptor membrane. *Proc. Natl. Acad. Sci. U. S. A.* *70*, 2853–2857.
- Ohara, S., Onodera, M., Simonsen, O.W., Yoshino, R., Hioki, H., Iijima, T., Tsutsui, K.-I., and Witter, M.P. (2018). Intrinsic Projections of Layer Vb Neurons to Layers Va, III, and II in the Lateral and Medial Entorhinal Cortex of the Rat. *Cell Rep.* *24*, 107–116.
- Owen, S.F., Liu, M.H., and Kreitzer, A.C. (2019). Thermal constraints on in vivo optogenetic manipulations. *Nat. Neurosci.* *22*, 1061–1065.

-
- Pachitariu, M., Steinmetz, N., Kadir, S., Carandini, M., and Harris, K.D. (2016). Kilosort: realtime spike-sorting for extracellular electrophysiology with hundreds of channels. *BioRxiv* 061481.
- Passarelli, L., Rosa, M.G.P., Bakola, S., Gamberini, M., Worthy, K.H., Fattori, P., and Galletti, C. (2018). Uniformity and diversity of cortical projections to precuneate areas in the macaque monkey: What defines area PGM? *Cereb. Cortex* *28*, 1700–1717.
- Pele, O., and Werman, M. (2008). A Linear Time Histogram Metric for Improved SIFT Matching. In *Computer Vision -- ECCV 2008*, D. Forsyth, P. Torr, and A. Zisserman, eds. (Berlin, Heidelberg: Springer Berlin Heidelberg), pp. 495–508.
- Pele, O., and Werman, M. (2009). Fast and robust Earth Mover's Distances. In *2009 IEEE 12th International Conference on Computer Vision*, (IEEE), pp. 460–467.
- Pouget, A., and Snyder, L.H. (2000). Computational approaches to sensorimotor transformations. *Nat. Neurosci.* *3*, 1192–1198.
- Raudies, F., and Hasselmo, M.E. (2012). Modeling boundary vector cell firing given optic flow as a cue. *PLoS Comput. Biol.* *8*, e1002553.
- Redish, A.D., and Touretzky, D.S. (1997). Cognitive maps beyond the hippocampus. *Hippocampus* *7*, 15–35.
- Roth, B.L., Sheffler, D.J., and Kroeze, W.K. (2004). Mood Disorders and Schizophrenia. *Nat. Rev. Drug Discov.* *3*, 353–359.
- Roy, D.S., Kitamura, T., Okuyama, T., Ogawa, S.K., Sun, C., Obata, Y., Yoshiki, A., and Tonegawa, S. (2017). Distinct Neural Circuits for the Formation and Retrieval of Episodic Memories. *Cell* *170*, 1000-1012.e19.
- Rubner, Y., Tomasi, C., and Guibas, L.J. (1998). A metric for distributions with applications to image databases. In *Sixth International Conference on Computer Vision (IEEE Cat. No.98CH36271)*, (Narosa Publishing House), pp. 59–66.
- Schmitzer-Torbert, N., Jackson, J., Henze, D., Harris, K., and Redish, A.D. (2005). Quantitative measures of cluster quality for use in extracellular recordings. *Neuroscience* *131*, 1–11.
- Shadlen, M.N., and Newsome, W.T. (1994). Noise, neural codes and cortical organization. *Curr. Opin. Neurobiol.* *4*, 569–579.
- Shannon, C.E. (1948). *A Mathematical Theory of Communication*. *Bell Syst. Tech. J.* *27*, 379–423.
- Shettleworth, S.J., and Krebs, J.R. (1982). How marsh tits find their hoards: the roles of site preference and spatial memory. *J. Exp. Psychol. Anim. Behav. Process.* *8*, 354–375.
- Shtonda, B.B., and Avery, L. (2006). Dietary choice behavior in *Caenorhabditis elegans*. *J. Exp. Biol.* *209*, 89–102.

-
- Skaggs, W.E., McNaughton, B.L., Wilson, M.A., and Barnes, C.A. (1996). Theta phase precession in hippocampal neuronal populations and the compression of temporal sequences. *Hippocampus* *6*, 149–172.
- Smith, C.C., and Reichman, O.J. (1984). The Evolution of Food Caching by Birds and Mammals. *Annu. Rev. Ecol. Syst.* *15*, 329–351.
- Snyder, L.H., Batista, A.P., and Andersen, R.A. (2000). Intention-related activity in the posterior parietal cortex: A review. *Vision Res.* *40*, 1433–1441.
- Solstad, T., Boccara, C.N., Kropff, E., Moser, M.-B., and Moser, E.I. (2008). Representation of geometric borders in the entorhinal cortex. *Science* *322*, 1865–1868.
- Squire, L.R., Stark, C.E.L., and Clark, R.E. (2004). The Medial Temporal Lobe. *Annu. Rev. Neurosci.* *27*, 279–306.
- Stewart, S., Jeewajee, A., Wills, T.J., Burgess, N., and Lever, C. (2014). Boundary coding in the rat subiculum. *Philos. Trans. R. Soc. Lond. B. Biol. Sci.* *369*, 20120514.
- Sugar, J., Witter, M.P., van Strien, N.M., and Cappaert, N.L.M. (2011). The retrosplenial cortex: intrinsic connectivity and connections with the (para)hippocampal region in the rat. An interactive connectome. *Front. Neuroinform.* *5*, 7.
- Takahashi, N., Kawamura, M., Shiota, J., Kasahata, N., and Hirayama, K. (1997). Pure topographic disorientation due to right retrosplenial lesion. *Neurology* *49*, 464–469.
- Taube, J.S. (1998). Head direction cells and the neurophysiological basis for a sense of direction. *Prog. Neurobiol.* *55*, 225–256.
- Taube, J.S. (2007). The head direction signal: Origins and sensory-motor integration. *Annu. Rev. Neurosci.* *30*, 181–207.
- Taube, J.S., Muller, R.U., and Ranck, J.B. (1990). Head-direction cells recorded from the postsubiculum in freely moving rats. I. Description and quantitative analysis. *J. Neurosci.* *10*, 420–435.
- Tervo, D.G.R., Hwang, B.Y., Viswanathan, S., Gaj, T., Lavzin, M., Ritola, K.D., Lindo, S., Michael, S., Kuleshova, E., Ojala, D., et al. (2016). A Designer AAV Variant Permits Efficient Retrograde Access to Projection Neurons. *Neuron* *92*, 372–382.
- Thompson, K.J., Khajehali, E., Bradley, S.J., Navarrete, J.S., Huang, X.P., Slocum, S., Jin, J., Liu, J., Xiong, Y., Olsen, R.H.J., et al. (2018). DREADD Agonist 21 Is an Effective Agonist for Muscarinic-Based DREADDs in Vitro and in Vivo. *ACS Pharmacol. Transl. Sci.* *1*, 61–72.
- Tolman, E.C., Ritchie, B.F., and Kalish, D. (1946). Studies in spatial learning. I. Orientation and the short-cut. *J. Exp. Psychol.* *36*, 13–24.
- Tomko, G.J., and Crapper, D.R. (1974). Neuronal variability: non-stationary responses to identical visual stimuli. *Brain Res.* *79*, 405–418.

-
- Touretzky, D.S., and Redish, A.D. (1996). Theory of rodent navigation based on interacting representations of space. *Hippocampus* 6, 247–270.
- Urban, D.J., and Roth, B.L. (2015). DREADDs (designer receptors exclusively activated by designer drugs): Chemogenetic tools with therapeutic utility. *Annu. Rev. Pharmacol. Toxicol.* 55, 399–417.
- Valle, F.P. (1970). Effects of strain, sex, and illumination on open-field behavior of rats. *Am. J. Psychol.* 83, 103–111.
- Vann, S.D., Aggleton, J.P., and Maguire, E.A. (2009). What does the retrosplenial cortex do? *Nat. Rev. Neurosci.* 10, 792–802.
- Vogt, B.A., and Miller, M.W. (1983). Cortical connections between rat cingulate cortex and visual, motor, and postsubicular cortices. *J. Comp. Neurol.* 216, 192–210.
- Walsh, R.N., and Cummins, R.A. (1976). The open-field test: A critical review. *Psychol. Bull.* 83, 482–504.
- Wang, C., Chen, X., Lee, H., Deshmukh, S.S., Yoganarasimha, D., Savelli, F., and Knierim, J.J. (2018). Egocentric coding of external items in the lateral entorhinal cortex. *Science* 362, 945–949.
- White, J.G., Southgate, E., Thomson, J.N., and Brenner, S. (1986). The structure of the nervous system of the nematode *Caenorhabditis elegans*. *Philos. Trans. R. Soc. London. B, Biol. Sci.* 314, 1–340.
- Whitlock, J.R., Pfuhl, G., Dagslott, N., Moser, M.-B., and Moser, E.I. (2012). Functional split between parietal and entorhinal cortices in the rat. *Neuron* 73, 789–802.
- Wilson, M.A., and McNaughton, B.L. (1993). Dynamics of the hippocampal ensemble code for space. *Science* (80-.). 261, 1055–1058.
- Yadav, P.N., Abbas, A.I., Farrell, M.S., Setola, V., Sciaky, N., Huang, X.P., Kroeze, W.K., Crawford, L.K., Piel, D.A., Keiser, M.J., et al. (2011). The presynaptic component of the serotonergic system is required for clozapine's efficacy. *Neuropsychopharmacology* 36, 638–651.
- Yamawaki, N., Radulovic, J., and Shepherd, G.M.G. (2016). A Corticocortical Circuit Directly Links Retrosplenial Cortex to M2 in the Mouse. *J. Neurosci.* 36, 9365–9374.
- Yizhar, O., Fenno, L.E., Davidson, T.J., Mogri, M., and Deisseroth, K. (2011). Optogenetics in Neural Systems. *Neuron* 71, 9–34.
- Zhang, F., Wang, L.-P., Brauner, M., Liewald, J.F., Kay, K., Watzke, N., Wood, P.G., Bamberg, E., Nagel, G., Gottschalk, A., et al. (2007). Multimodal fast optical interrogation of neural circuitry. *Nature* 446, 633–639.

LIST OF FIGURES

Figure 1. Depiction of animal species that are iconic for navigation behaviour in the wild.....	18
Figure 2. The medial temporal lobe is a key circuit involved in spatial cognition	20
Figure 3. Anatomical location of the retrosplenial cortex.....	22
Figure 4. Schematic of a computational model that implements information transformation.....	25
Figure 5. Response profiles of border cells in RSC.....	34
Figure 6. Border cell classification using the Earth Mover’s Distance	35
Figure 7. Classification results using the EMD and border score metrics	37
Figure 8. RSC border cell population characteristics.....	38
Figure 9. The dissociation between the animal’s running speed and activity around borders	39
Figure 10. Single cell and population activity of border cells around an added wall	41
Figure 11. Single cell and population activity of border cells around objects.....	43
Figure 12. RSC border cell firing under novel conditions and different arena shapes	45
Figure 13. Border coding is maintained in darkness	47
Figure 14. Border coding is maintained the absence of physical walls	48
Figure 15. Control experiment to assess the role of somatosensory information in computing border information	49

Figure 16. Control experiment to compare boundary coding in RSC with somatosensory coding in SI1bf.....	51
Figure 17. Egocentric direction tuning of RSC border cells.....	60
Figure 18. Neuron cluster properties along all behavioural axes.....	61
Figure 19. Egocentric direction tuning of RSC border cells functions independent of global head-direction signals.....	63
Figure 20. Directional and distance tuning properties of RSC border cells.....	66
Figure 21. Inhibiting neural activity in MEC using chemogenetics	77
Figure 22. Sharp boundary tuning of RSC border cells is disrupted upon inhibition of MEC	78
Figure 23. Reverse manipulation experiment, inhibiting activity in MEC while recording from RSC border cells	80
Figure 24. Pathway-specific inhibition of MEC input to RSC using optogenetics	83
Figure 25. Additional effects of optogenetic inhibition of MEC.....	85
Figure 26. Control experiment for optogenetic-mediated manipulations to address the tissue heating confound	87
Figure 27. Firing field and border tuning analyses of border cells in MEC and RSC.....	89
Figure 28. Decoding the animal's distance from a wall using population spiking activity	91
Figure 29. Correlations between border cell firing and the animal's trajectory	93

ABBREVIATIONS USED

2D	2-Dimensional
5-HT	5-Hydroxytryptamin
AAV	Adeno-associated virus
ACC	Anterior cingulate cortex
AP	Anterior-posterior
BVC	Boundary vector cell
CNO	Clozapine N-oxide
CV	Coefficient of variation
DREADDs	Designer receptors exclusively activated by designer drugs
DV	Dorsal-ventral
EMD	Earth mover's distance
fMRI	Functional magnetic resonance imaging
FR	Firing rate
GFP	Green fluorescent protein
GIRK	G protein-coupled inwardly-rectifying potassium channels
HD	Head-direction
ID	Isolation distance
LED	Light-emitting diode
LFP	Local field potential
MEC	Medial entorhinal cortex
ML	Medial-lateral
MTL	Medial temporal lobe

MVD	Mean vector direction
MVL	Mean vector length
PF	Place field
Rdg	Dysgranular area 30 of the retrosplenial cortex
Rga	Granular area 29a of the retrosplenial cortex
Rgb	Granular area 29b of the retrosplenial cortex
ROI	Region-of-interest
RSC	Retrosplenial cortex
Slbf	Primary somatosensory cortex, barrel field
SEM	Standard error of the mean
SVD	Single vector decomposition
SVM	Support vector machine

CURRICULUM VITAE

Joeri BG van Wijngaarden

Date and place of birth: September 13th 1988, Rotterdam, Netherlands
Nationality: Dutch
Home address: Ginnheimerstr. 22, 60487, Frankfurt am Main (DE)
Work address: Max Planck Institute for Brain Research
Max-von-laue-str. 4, 60438, Frankfurt am Main (DE)
Phone: +31 6 4108 5015
Email: joerivanwijngaarden@gmail.com

EDUCATION & TRAINING

Ph.D. in Neuroscience | Max Planck Institute for Brain Research 2017-2021

- ❖ Ph.D. thesis on “Using Walls to Navigate the Room: Egocentric Representations of Borders for Spatial Navigation” under supervision of Dr. Hiroshi Ito
- ❖ Funded by the European Research Council (ERC)
- ❖ Projects include tetrode electrophysiology in awake, behaving rats, DREADD inhibition of neural circuits, and complex behavioural training

Research Master Psychology | University of Amsterdam 2012-2015

- ❖ Major in Brain & Cognition | Minors in Methods & Developmental Psychology
- ❖ Grade average: 8.3/10
- ❖ Distinctive classification: With Merit
- ❖ Thesis: “*The Emergence of Thalamocortical Dysrhythmia after Acute Ischaemic Stroke*” under supervision of Dr. Mike X. Cohen (grade 9/10)

Bachelor Psychology | University of Amsterdam 2007-2011

- ❖ Major in Clinical Developmental Psychology
- ❖ Grade average: 7.6/10
- ❖ Thesis: “*Automatic Cognitive Information Processing: The Attentional, Interpretation, and Memory-Bias in Anxious Youth*” under supervision of Prof. Dr. Pier J.M. Prins (grade 8/10)

Highschool VWO | Comenius College, Netherlands 2000-2006

PROFESSIONAL EXPERIENCE

Research Assistant | Universitat Pompeu Fabra, Spain 2015-2016 (1 fte)

- ❖ SPECS laboratory, supervision of Dr. Paul F.M.J. Verschure
- ❖ Projects included human intracranial EEG analysis, computational spiking models of brain circuits, and clinical trials with hemi-neglect patients

Technical Assistant | University of Amsterdam 2014-2015 (0.3 fte)

- ❖ ADAPT laboratory, supervision of Prof. Dr. Reinout W.H.J. Wiers

PUBLICATIONS

Papers

- ❖ **van Wijngaarden JBG**, Babl SS, Ito HT (2020). Entorhinal-retrosplenial circuits for allocentric-egocentric transformation of boundary coding. *Elife*, 9, e59816. *Doi:10.7554/eLife.59816*
- ❖ **van Wijngaarden JBG**, Zucca R, Finnigan S, & Verschure PFMJ (2016). The Development of Thalamocortical Dysrhythmia After Acute Ischaemic Stroke: A Combined Experimental and Theoretical Study. *PLoS Comput Biol* 12(8): e1005048. *doi:10.1371/journal.pcbi.1005048*
- ❖ Wen S, Larsen H, Boffo M, Grasman RPPP, Pronk T, **van Wijngaarden JBG**, & Wiers RW (2020). Combining Web-Based Attentional Bias Modification and Approach Bias Modification as a Self-Help Smoking Intervention for Adult Smokers Seeking Online Help: Double-Blind Randomized Controlled Trial. *JMIR mental health*, 7(5): e16342. *doi:10.2196/16342*
- ❖ Puigbò J-Y, **van Wijngaarden JBG**, Low SC, & Verschure PFMJ (2016). Synaptogenesis: Constraining Synaptic Plasticity Based on a Distance Rule. *In: 25th International Conference on Artificial Neural Networks (ICANN; vol. 9886, pp. 28-35). Springer International Publishing.*
- ❖ Low SC, **van Wijngaarden JBG**, & Verschure PFMJ (2016). Modelling the Effect of Cognitive Load on Eye Saccades and Reportability: The Validation Gate. *In: Conference on Biomimetic and Biohybrid Systems (pp. 459-466). Springer International Publishing.*

ACHIEVEMENTS

Research Fellow | International Max Planck Research School
One-year funding for a fellowship at the MPI for Brain Research: a competitive educational program part of the IMPRS for Neural Circuits

Best Student Project 2015 | BCBT Summer School
Project: "Modelling Temporal Lobe Epilepsy using the BrainX³"

SUMMER SCHOOLS

NSAS | Advanced course on Neural Circuit Dynamics
2019 Venice, Italy
Duration: 1 week

TENSS | Transylvanian Exp. Neuroscience Summer School
2017 Pike Lake, Romania
Duration: 3 weeks

CSN | Summer School on Neurotechniques
2015 Padova, Italy
Duration: 1 week

BCBT | Brain & Technology Summer School
2015 Barcelona, Spain
Duration: 2 weeks
